# Modeling, Design and Analysis of Micro-Scale Rankine-Based Systems

by
Ling Cui

Bachelor of Engineering, Beijing University of Aeronautics and Astronautics, 2001

Submitted to the Department of Aeronautics and Astronautics
in partial fulfillment of the degree of

MASTER OF SCIENCE
at the

MASSACHUSETTS INSTITUTE OF TECHNOLOGY



October 2003



Author _____
Ling Cui
Department of Aeronautics and Astronautics
November 2003

Certified by _____
Professor John G. Brisson
Professor of Department of Mechanical Engineering
Thesis Supervisor

Accepted by _____
Professor Edward M. Greitzer
H. N. Slater Professor of Aeronautics and Astronautics
Chairman, Committee on Graduate Students

**Modeling, Design and Analysis of Micro-scale Rankine-Based Systems**

**by**

**Ling Cui**

# Abstract

This thesis presents the modeling and design of two major types of micro Rankine-cycle-based machines: a single-Rankine-based power system and a waste-heat-driven cooler. As part of the Massachusetts Institute of Technology (MIT) Micro Engine Project, these projected machines can be combined with the MIT micro gas turbine engines to improve their overall performance.

The models were based on the conventional heat transfer and fluid mechanics correlations. And the state-of-the-art turbomachinery technologies and fabrication capability were taken into consideration in the designing of these devices. The results show that the single-Rankine bottoming power system could provide as high as 37-watt power when it is combined with a micro gas turbine engine, given a one square inch footprint and 50% turbomachinery efficiency. The waste-heat-driven cooler, or the heat pump, could provide air-conditioning and condensed water when it is combined to a micro gas turbine engine. Within a footprint of 7 cm by 7 cm, it could generate a 25-watt total cooling power. The amount of effective cooling (air-conditioning) power and condensed water is highly dependent on the ambient temperature and humidity.

Micro heat exchanger designs for the above Rankine machines were also delineated in this thesis. The traditional fin-type heat exchanger and a new low-pressure-drop hole-type heat exchanger were discussed. All of these heat exchangers are within the realm of the state-of-the-art fabrication capabilities. At the end of the thesis, the challenges of bringing these micro Rankine machines into reality were also discussed and some possible solutions were proposed.

This work broadens the variety of the micro power systems. It is not intended to be framed in a single specific device, but rather, it presents the measures and expanse of the micro-Rankine-machine designs.

**Thesis Supervisor: John G. Brisson**

**Title: Professor of Mechanical Engineering**

## Acknowledgements

My graduate research experience at MIT would not have been so delightful and this thesis would not have been reached this extent and depth without the direction and help from Professor Brisson. He directed me through my most difficult period at MIT, which was the start of my study here. I want to express my most sincere and heartfelt thanks to him. Besides, I want to extend my gratitude to other Gas Turbine Lab professors and my colleagues who helped me in my research, study and added so many colors in my life. I also want to thank my dearest dad and mom, who always give me full support and trust—thank you all.

# Table of Contents

# List of Figures

## List of Figures (continued)

## List of Figures (continued)

## List of Tables

## List of Tables (continued)

## List of Symbols

$a$ [m]—heat exchanger channel height

$A_c$ [$m^2$]—cross-sectional area of a channel in the heat exchanger

$b$ [m]— heat exchanger channel width

$c$—constant determined by the heat exchanger channel geometry in laminar flows

$C_p$ [J/kg· K]—specific heat

$d$ [m]— heat exchanger wall/fin thickness

$D_h$ [m]—hydraulic diameter of the heat exchanger channels

$f$—friction factor

$g$ [$m/s^2$]—gravitational acceleration

$h$ [J/kg]—specific enthalpy

$h_{fg}$ [J/kg]—latent heat

*HTHEX*—High Temperature Heat Exchanger

$L$ [m]—length of the heat exchanger channels

*LTHEX*—Low Temperature Heat Exchanger

$\dot{m}$ [kg/s]—mass flow rate

$n$—number of heat exchanger channels

$N$—number of heat exchanger stacks (layers of silicon wafers)

*NTU*—number of heat transfer units

$P$ [Pa]—pressure

$\Delta P$ [Pa]—pressure drop

$Q$ [J]—heat transfer

$\dot{Q}_{HTHEX}$ [W]—heat transfer rate of the high temperature heat exchanger

## List of Symbols (continued)

$\dot{Q}_{LTHEX}$ [W]—heat transfer rate of the low temperature heat exchanger

$r$ [m]—radius

$Re$—Reynolds number

$s$ [J/kg· K]—specific entropy

$t$ [m]—thickness of the base

$T$ [K]—temperature

$u$ [m/s]—velocity

$UA$ [W/K]—product of heat transfer area and heat transfer coefficient between the fluids and the heat transfer surfaces

$\dot{W}_{blower}$ [W]—work consumption rate of the blower

$\dot{W}_{net}$ [W]—net work output rate of the cycle

$\dot{W}_{pump}$ [W]—work consumption rate of the pump

$\dot{W}_{turbine}$ [W]—work output rate of the turbine

$\beta$— coefficient of performance (of a refrigeration cycle)

$\varepsilon$—heat exchanger effectiveness

$\eta$—turbomachinery efficiencies

$\eta_{thermal}$—thermal efficiency of the cycle

$\mu$ [Pa· s]—viscosity

$\rho$ [kg/m$^3$]—density

$\sigma$ [N/m]—surface tension

# Chapter 1 Introduction

In the past few decades, small-scale battery-powered electronic devices such as computers, handheld global positioning receivers and mobile phones have been successfully marketed. The length of time that these devices can be operated between battery chargings is an important market feature and has driven the development of commercial high energy density batteries. The use of electronics in the military has also mushroomed in the past decade with a concomitant need for a long-life portable power source. Micro-scale power generators using a high-energy-density hydrocarbon-based fuel show promise for fulfilling the need for a long-life portable power source [1].

Using Micro-Electro-Mechanical System (MEMS) technologies, the MIT micro engine group has been developing centimeter-scale power systems. The emphasis of the efforts has been on two power systems, namely a micro gas turbine engine and a micro rocket engine. Turbomachinery efficiencies are relatively low in the micro scale, typically between 30% and 70%. Nevertheless, calculations show that these devices could produce and deliver 10 to 100 W of power with a device volume less than a cubic centimeter [2].

The Rankine cycle is another power cycle that should be considered as a micro-scale prime mover. An advantage of the Rankine cycle over the gas turbine cycle is a high tolerance of low turbomachinery efficiency. The Rankine cycle can be used as a stand-alone prime mover or it can be used as a bottoming cycle to a gas turbine engine.

In this work, the virtues and foibles of the Rankine cycle as a micro scale prime mover and as a micro scale cooler are explored in detail. It will be shown that these devices are typically larger than the gas-turbine prime mover. This may not be an issue for electric generator applications since the overall size of the device is generally dominated by the size of the electric machinery.

All of the capabilities and technologies assumed in this work have been developed as part of the micro engine project at Massachusetts Institute of Technology (MIT). For this reason, the subsequent section is an overview of the base design for a micro-gas turbine. This is followed by a discussion of the Rankine cycle, the objectives for this study and, finally, the overall organization of this thesis.

## *1.1 Brief overview of Micro-gas turbine Engine*

Figure 1.1 is a cross-sectional view of a $H_2$ micro gas turbine demonstration engine (the "demo" engine). Figure 1.2 is a 3-D cutaway of the demo engine.

This demo engine consists of six silicon wafers bonded together. The rotor, shown as the crosshatched part in Figure 1.1 and the dark part in Figure 1.2, is the only moving part in the engine. The rotor has compressor blades etched into its top surface and turbine blades etched into its lower surface as shown in Figure 1.1 and Figure 1.2. In operation ambient air enters the engine through the inlet port, see Figure 1.1, and is compressed by the compressor. The pressurized air travels towards the combustor where it is mixed with fuel ($H_2$) and combusted. The hot air then goes through the turbine and is exhausted out the exhaust port. The power generated by the turbine drives the compressor and can provide shaft power for a generator. As an aside, there is no airflow through the "starting air in" port in the steady state operation of the engine. Pressurized air applied to the starting-air-in port is used to spin up the rotor prior to igniting the fuel in the combustor.

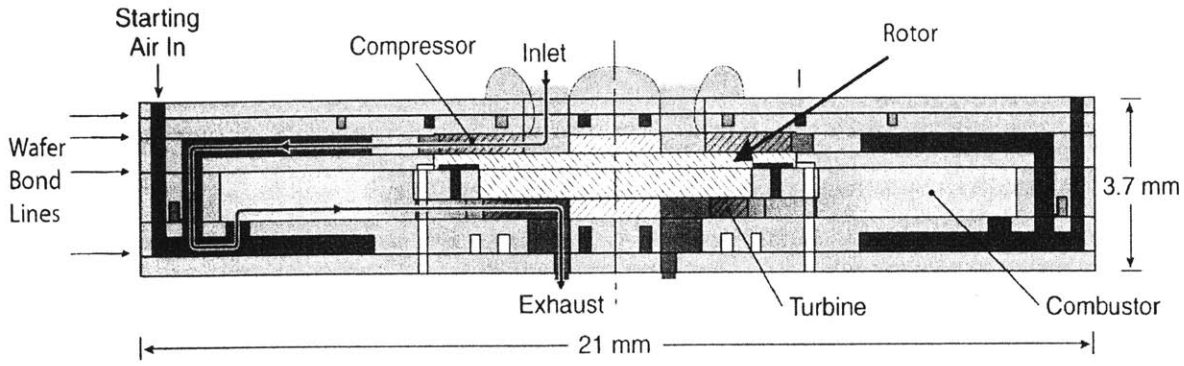


**Figure 1.1— $H_2$ demo engine cross-section diagram**

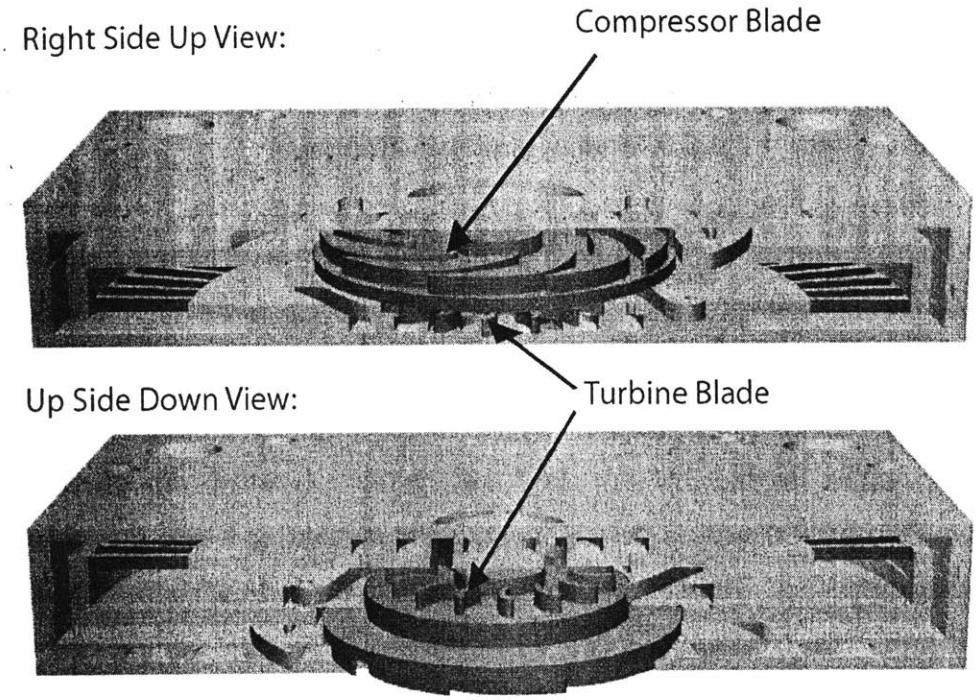


**Figure 1.2— $H_2$ demo engine 3-D cutaway**

## 1.2 Overview of the Rankine and Vapor compression Cycles

A block diagram for the Rankine power cycle is shown in Figure 1.3. The cycle consists of a boiler, a condenser, a pump and a power turbine (an expander). The corresponding Temperature-Entropy (T-s) diagram is shown in Figure 1.4. High-pressure water enters the boiler in state 1 where it is converted to superheated steam that exits the boiler in state 4. The superheated steam then enters the turbine where it is irreversibly expanded to state 5 (the reversible process is the dashed line to state 5R) in Figure 1.4. This low-pressure steam then enters the condenser where it is condensed to saturated liquid in state 7. The saturated liquid then enters the pump where it is pumped to the high pressure of state 1. (The reversible compression process is the dotted line to state 1R.) In an electric power application, the shaft power of the turbine is used to drive a generator as well as the feedpump. In general, the power turbine in the Rankine cycle generates many times the power required by the feedpump, which is unlike the gas-turbine (Brayton) cycle where the turbine and compressor powers can be comparable.

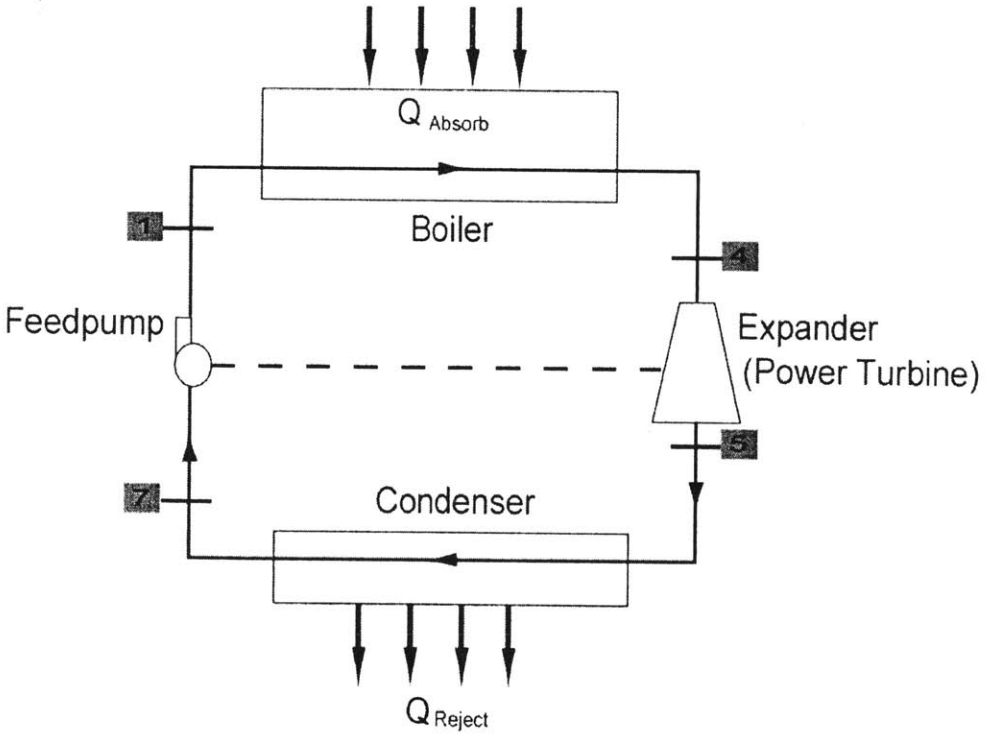


**Figure 1.3—A block diagram of the Rankine power cycle**

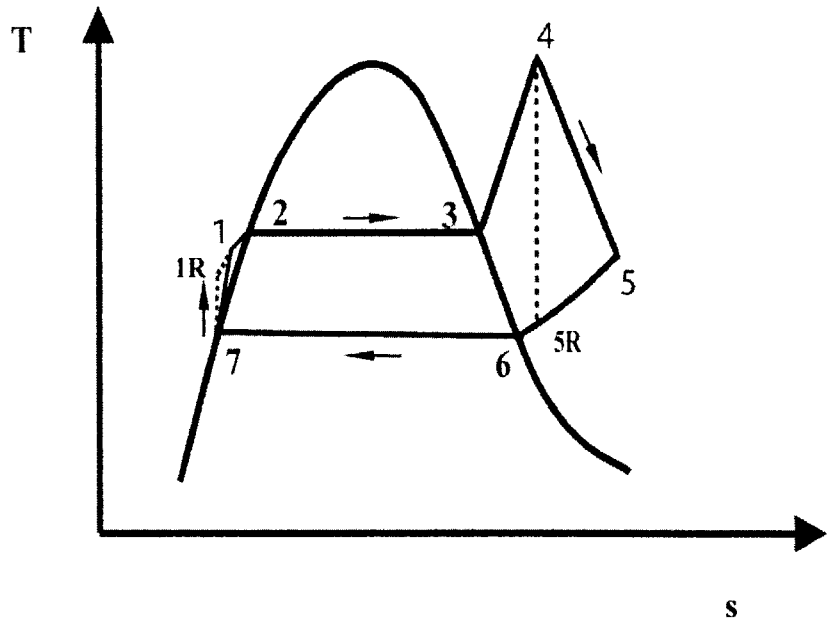


**Figure 1.4— A T-s diagram of the Rankine power cycle**

**The high-pressure liquid water is heated in a heat exchanger (point 1 to point 4) and travels through a power turbine (point 4 to point 5) generating shaft power. The working fluid is then condensed in another heat exchanger at a lower pressure (point 5 to point 7). At last, the fluid is pressurized from point 7 to point 1 by a feedpump. The dotted "7 - 1R" and "4 - 5R" paths in this figure indicate the reversible-process paths in the feedpump and turbine respectively.**

The reverse-Rankine cycle, usually referred to as the vapor compression cycle, is shown in the block and T-s diagram of Figure 1.5 and Figure 1.6. In this cycle, there is an evaporator and condenser that correspond to the reverse operation of a condenser and boiler respectively, in the power-producing Ranking cycle. The Rankine cycle turbine is now conceptually operated in reverse as a compressor in the vapor compression cycle. The Rankine cycle feedpump is replaced by a throttle valve in the vapor compression cycle (The benefits secured by using an expander, such as a turbine, instead of a throttle are not worth the added complexity to the machine). In the vapor compression cycle, high-pressure refrigerant vapor enters the condenser in state 1 where it is converted to a

saturated liquid that exits the condenser in state 2. The saturated liquid then enters the throttle where it is irreversibly expanded to state 3. This two-phase refrigerant then enters an evaporator where it is converted to a saturated vapor in state 4. The saturated vapor then enters the compressor where it is pressurized to the high pressure, state 1 (The reversible compression process is shown as the dotted line in Figure 1.6). The heat required for the low-temperature boiling process occurring in the evaporator can be used to provide cooling.

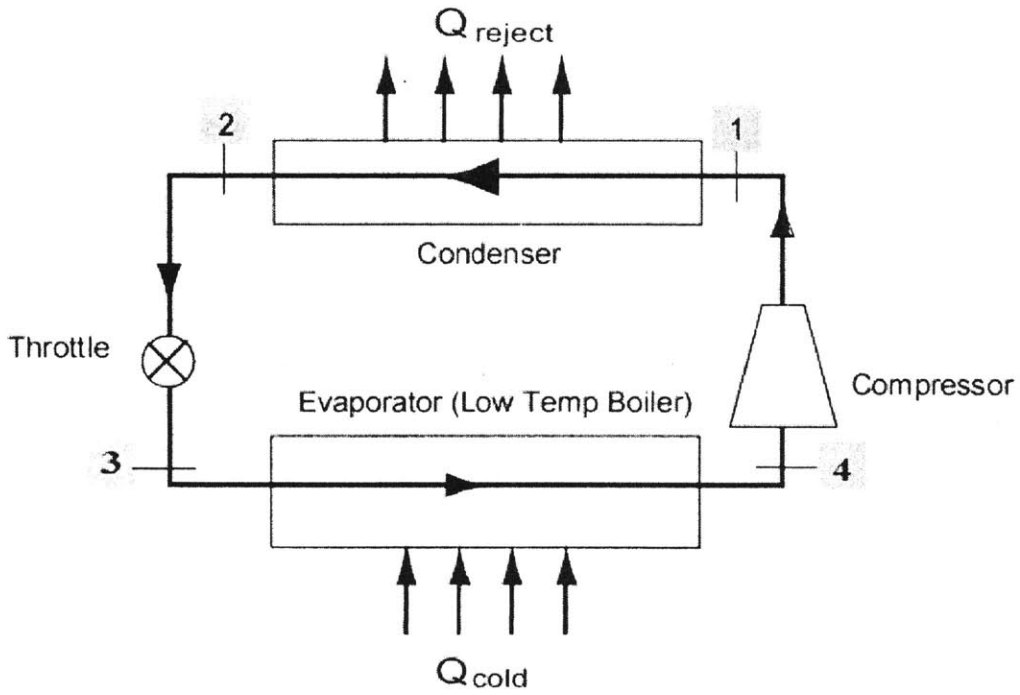


**Figure 1.5— A block diagram for the vapor compression cycle**

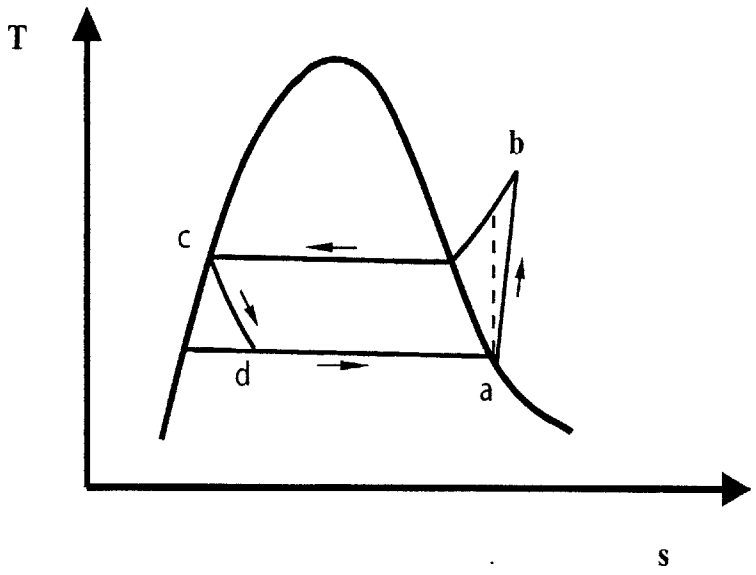


**Figure 1.6— A T-s diagram of the vapor compression cycle**

**The high-pressure refrigerant is condensed in a heat exchanger (point 1 to point 2) and travels through a throttle valve (point 2 to point 3) expanding to two-phase and the refrigerant is then evaporated in another heat exchanger at a lower pressure (point 3 to point 4). At last, the fluid is pressurized from point 4 to point 1. The dotted line in this figure indicates the reversible compression process.**

## *1.3 Motivation and Objectives of This Study*

The high-temperature exhaust gases of the micro gas turbine engine are a good energy source. In the MIT micro gas turbine engine, the typical exhaust gas temperature is between 750 K and 800 K. More specifically, the exhaust gas carries about 300 W of available energy. (This assumes an air mass flow rate of 1 g/s.) A Rankine bottoming cycle can be used to harvest some of this energy. A combining of the Rankine and Brayton cycles results in a net improvement of the overall thermal efficiency of the power system. To this end, the Rankine portion of a combined Brayton/Rankine cycle for the micro scale is modeled in this work. The calculations will indicate that the overall thermal efficiency of the system could be improved by at least 10% by adopting a Rankine-based bottoming machine.

In addition to power generation there are application that require cooling as well. A power-producing Rankine cycle can be combined with a vapor compression cycle to provide cooling. In a humid environment this waste-heat-driven cooler can provide water (by condensing the water out of the ambient air) as well as air-conditioning.

Figure 1.7 and Figure 1.8 are conceptual drawings of these two applications. In Figure 1.7, the Rankine cycle engine absorbs thermal energy from the micro gas turbine engine exhaust stream and discharges its waste heat into the ambient air. In that process it generates useful work. In Figure 1.8, the Rankine cycle engine on the left absorbs thermal energy from the gas turbine exhaust stream, and provides power to the vapor compression cycle on the right. Both the Rankine cycle and the vapor compression cycles reject heat to the ambient. The vapor compression cycle extracts thermal energy from an ambient air, cooling that air stream and condensing water from that air stream.

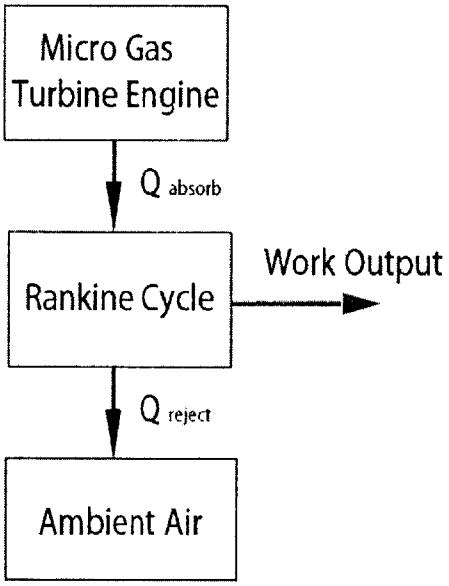


**Figure 1.7— Micro bottoming-cycle machine concept**
**The Rankine cycle absorbs energy from the micro gas turbine engine exhaust, and generates additional work output.**

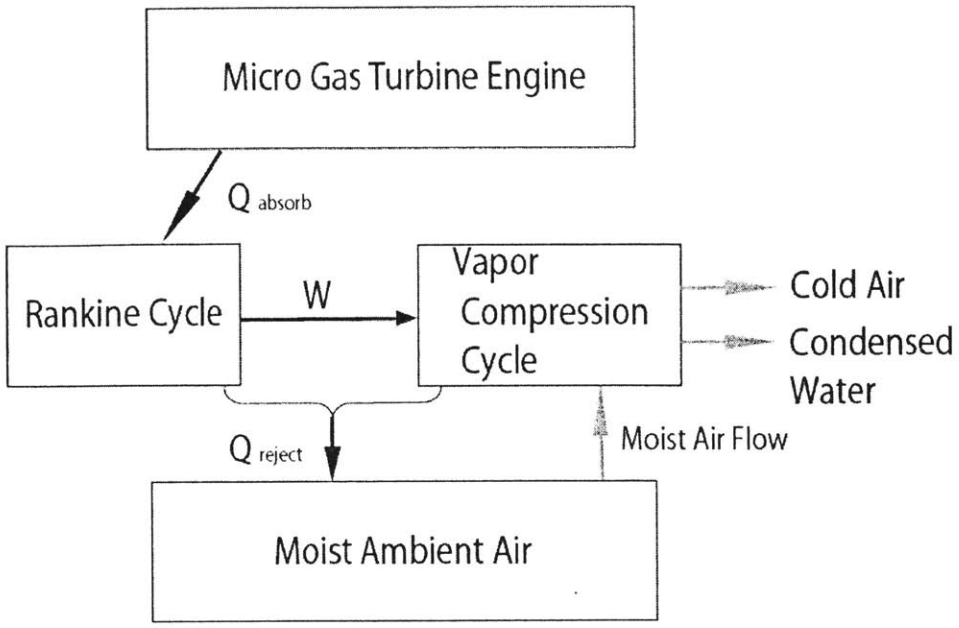


**Figure 1.8— Micro waste heat cooler concept**

**The Rankine power cycle on the left absorbs energy from the micro gas turbine engine exhaust, and provides the work generated to the vapor compression cycle on the right (a refrigeration cycle). Both cycles reject heat to the ambient to condense their respective working fluid. The refrigeration cycle also absorbs heat from an air stream taken from the ambient for generating cooling air and condensed water.**

These Rankine-cycle devices can work without the gas turbine engine by using a micro combustor to provide the hot air stream. Consequently, if the application does not require power generation the gas turbine portion of the system can be replaced by a combustor, reducing the overall system complexity.

It will be shown that the size of the Rankine device is set by the device's heat exchangers and that the overall performance of the Rankine device is strongly influenced by the performance of those heat exchangers. In response to these imperatives, this study examines several heat exchanger designs in detail.

The technology base chosen for this study is silicon-based MEMS technology. MEMS technology shows the most promise for realizing practical micro-scale Rankine machines. The choice of this has also allowed us to capitalize on the many innovations and achievements of the MIT micro-engine project. This includes the realization of high-speed turbomachinery components [2, 3] and heat exchangers in the micro scale [4]. In addition, the semi-conductor properties of silicon allow an easy integration of electronics and mechanics. Finally, the batch production of MEMS devices allows development to be within a reasonable time and cost.

Therefore, the goals of this study are to:

- Explore the feasibility of such micro Rankine-based systems;
- Estimate the potential performance of these devices;
- Explore micro-scale heat exchanger design and optimization;
- Define the technological barriers and challenges;
- Identify the improvements desired in the future.

## 1.4 Thesis Organization

This thesis can be divided into 6 major topics. Chapter 1 is the introduction, and Chapter 2 discusses the concept, modeling and performance analysis of the micro-bottoming-cycle machines. Chapter 3 provides a detailed discussion about the micro heat exchanger designs and optimization for the micro Rankine cycles and proposes a new low-pressure-drop heat exchanger design to be adopted in the micro waste heat driven cooler. Chapter 4 describes the concept, modeling, performance analysis and challenges of the micro waste heat cooler. And Chapter 5 updates the state-of-the-art micro turbomachinery development in the MIT micro engine group and states the different requirements of the micro Rankine machines. Chapter 5 also proposes scaling and turbomachinery structural arrangement for these micro Rankine devices. Chapter 6 is a summary of the study and as well as suggestions for future work.

# Chapter 2 Bottoming and Stand-Alone Rankine Cycle Modeling

This chapter introduces the theoretical approaches in both combining a Rankine-based machine with a micro gas turbine engine and using them as a stand-alone power device. The models discussed are based on Rankine-cycle principles. The modeling of the bottoming cycle is outlined at first and then the performance was optimized based on assumptions such as the current MIT micro gas turbine engine design, fabrication ability of MEMS devices and turbomachinery designs. The layout and fabrication concerns of the bottoming device are also discussed. After that, the performance of the stand-alone (single-cycle) Rankine machine is calculated. In most of the calculations in this chapter, steam ($H_2O$) was assumed as the working fluid; the pros and cons of introducing other working fluids into the current micro Rankine machine are explored at the end of this chapter by using quantitative and qualitative methods.

The discussion in this work is intended at a survey of the possibilities and limits of Rankine-based cycles in the micro scale. Consequently, this work will not settle on a single design, which will be application-sensitive, but rather establish general design criteria and examine tradeoffs for these cycles.

## 2.1 Bottoming Cycle Analysis

The modeling, structure, layout, and performance of a bottoming Rankine machine combined with a micro gas turbine engine to generate additional power and thus improve the overall efficiency and performance are introduced in the following sections.

### 2.1.1 Cycle and Modeling Overview

A simple Rankine cycle is shown in the T-s diagram of Figure 2.1, and a block diagram of the equipment for this cycle is shown in Figure 2.2. The numbers in the diagrams indicate the corresponding state points for the cycle.

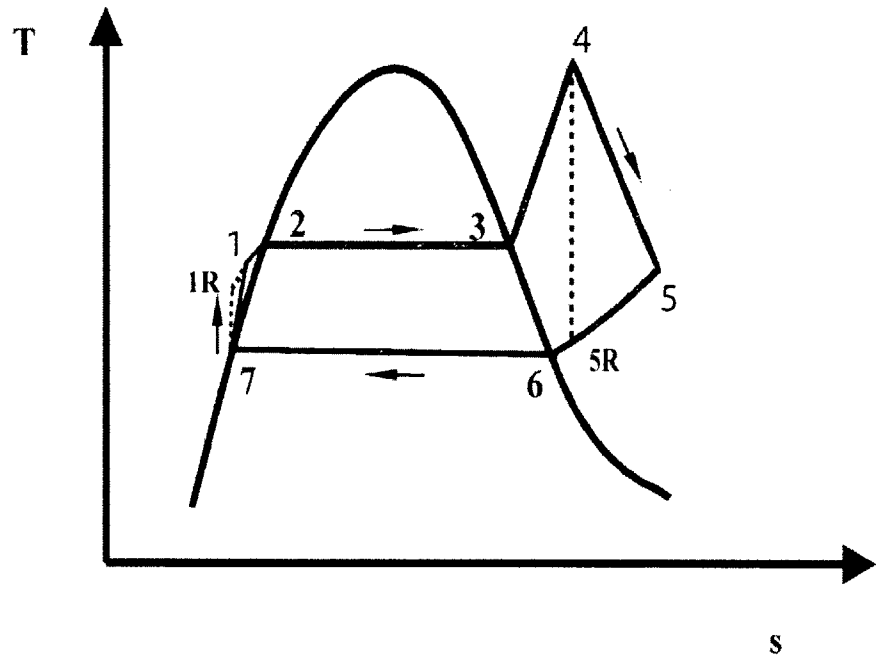


**Figure 2.1— A T-s diagram of the Rankine cycle**
**The dotted lines 7 to 1R and 4 to 5R indicate reversible/ideal compression and expansion processes respectively.**

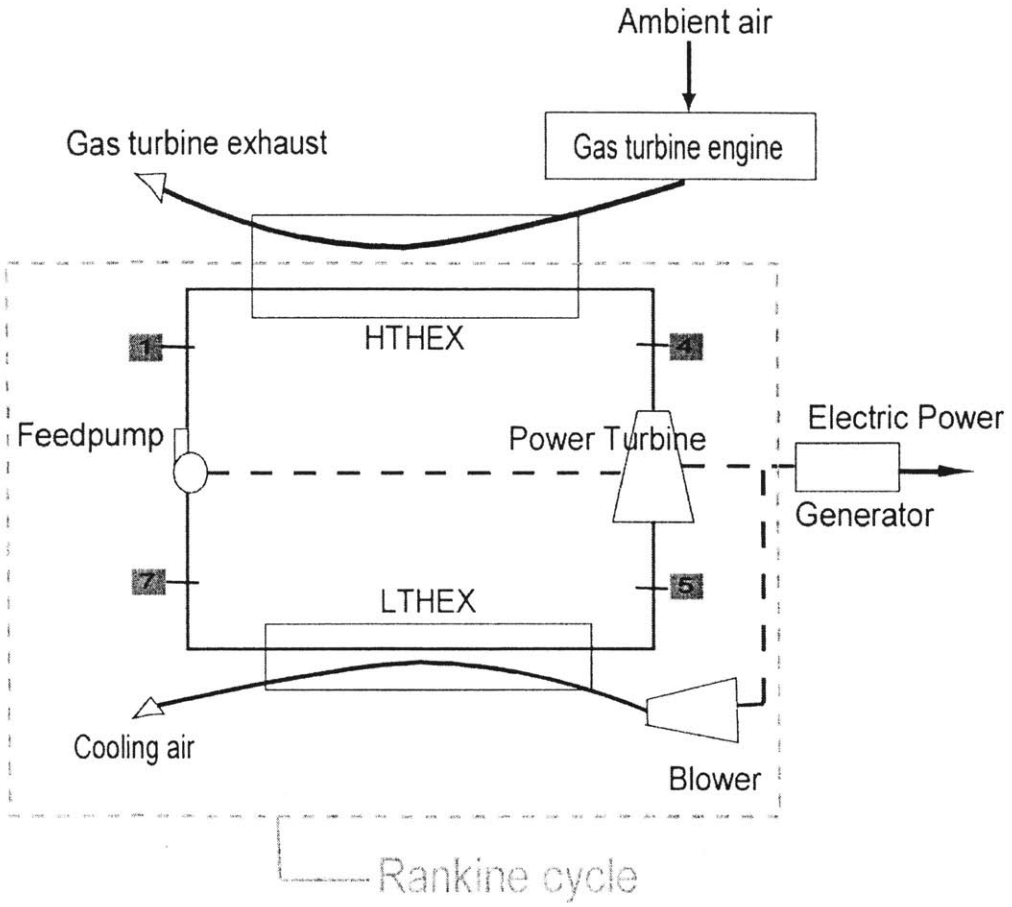


**Figure 2.2—Schematic diagram of a bottoming Rankine device**
**The dark dotted lines indicate mechanical connections between devices.**

Reiterating the discussion in Chapter 1, the liquid working fluid (water) exits the feedpump at a high pressure and a low temperature (state 1). The fluid then enters a high temperature heat exchanger (HTHEX) where it is warmed to saturated vapor (state 3) and finally becomes superheated vapor in State 4. The fluid then enters the turbine where it is expanded to a low pressure (state 5). This low-pressure fluid then enters the low temperature heat exchanger (LTHEX) where it is cooled (by what will be assumed here as an ambient air flow) to saturated vapor (state 6), and then condenses to saturated liquid (state 7). The liquid is then compressed to a high pressure (state 1) by the feed water pump.

In the Rankine micro engine, the evaporation process occurs in the high temperature heat exchanger. The hot micro-gas-turbine exhaust air stream will be passed through the HTHEX, as shown in Figure 2.2 (or directly from a micro combustor for a stand-alone device).

For most applications, the LTHEX will require a forced (as opposed to natural) airflow to keep this heat exchanger to a reasonable size. Consequently, a micro-scale Rankine-cycle prime mover will require a LTHEX blower (as shown in Figure 2.2). The power generated by the turbine can be divided into three parts: one is used to drive the feedpump, the second part is to power the blower, and the rest goes as the net output power of the whole cycle. In practice, the turbine will also need to drive an electric generator.

In sum, the Rankine micro power machine consists of five major parts: a low temperature heat exchanger, a high temperature heat exchanger, a steam turbine, a feedpump and a blower.

### 2.1.2 Schematic Layout and Design

A possible design for a combined micro gas turbine/Rankine-cycle prime mover is shown in Figure 2.3 and Figure 2.4. The device consists of four parts: a micro gas turbine engine, the Rankine cycle's HTHEX, feedpump/turbine/blower module, and the LTHEX.

In operation, the micro gas turbine exhausts hot air into the air passages of the HTHEX, as shown by the upper airflow line in Figure 2.3. The feedpump/turbine/blower module contains all the turbomachinery for the Rankine cycle and an electric generator. The turbine directly drives all of these components. The blower intakes cooling air from the ambient, driving it through the LTHEX air channels, and the flow paths are shown in Figure 2.3 and Figure 2.4. The HTHEX and the LTHEX are connected by connecting tubes that provide thermal isolation and allow the passage of the working fluid from one module to the other.

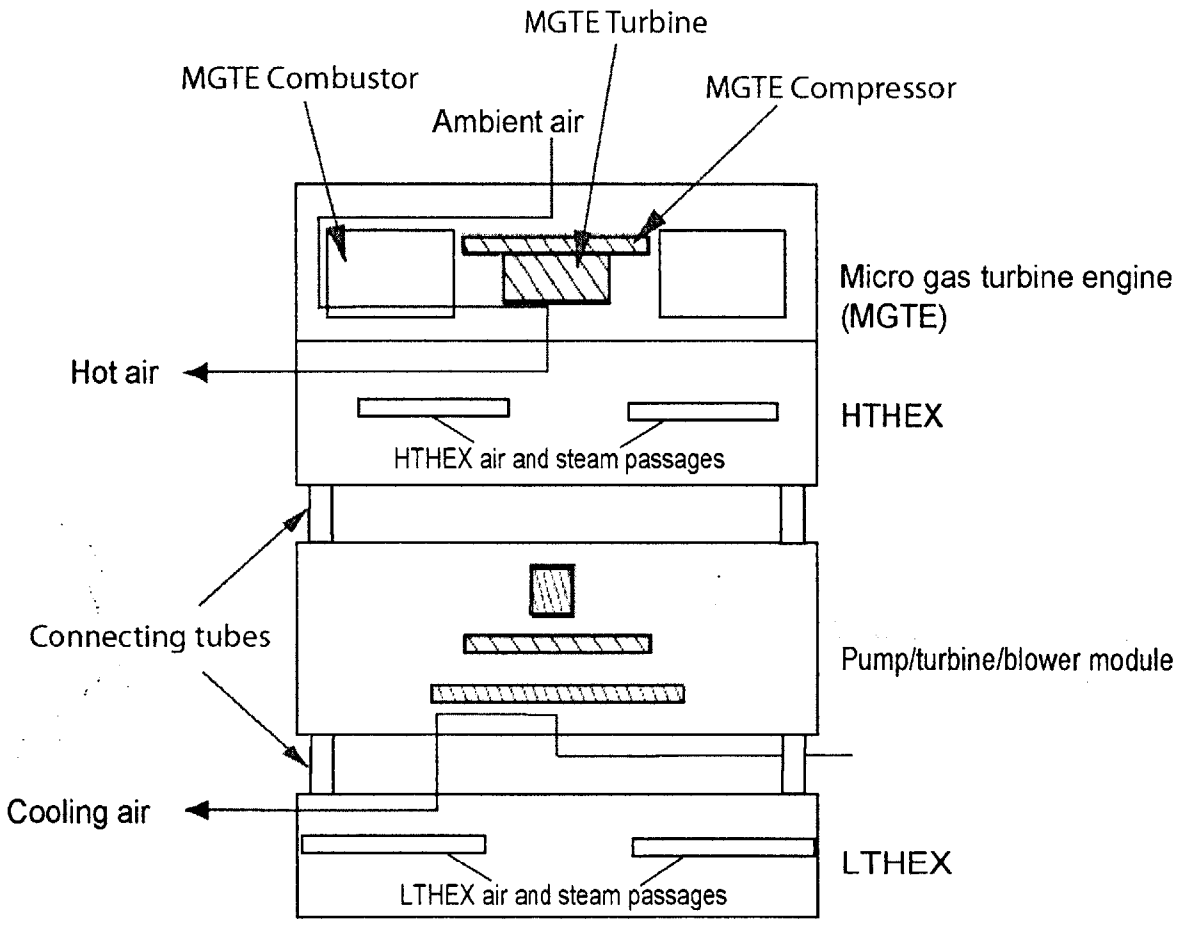


**Figure 2.3—Schematic modular design for the combined bottoming cycle**

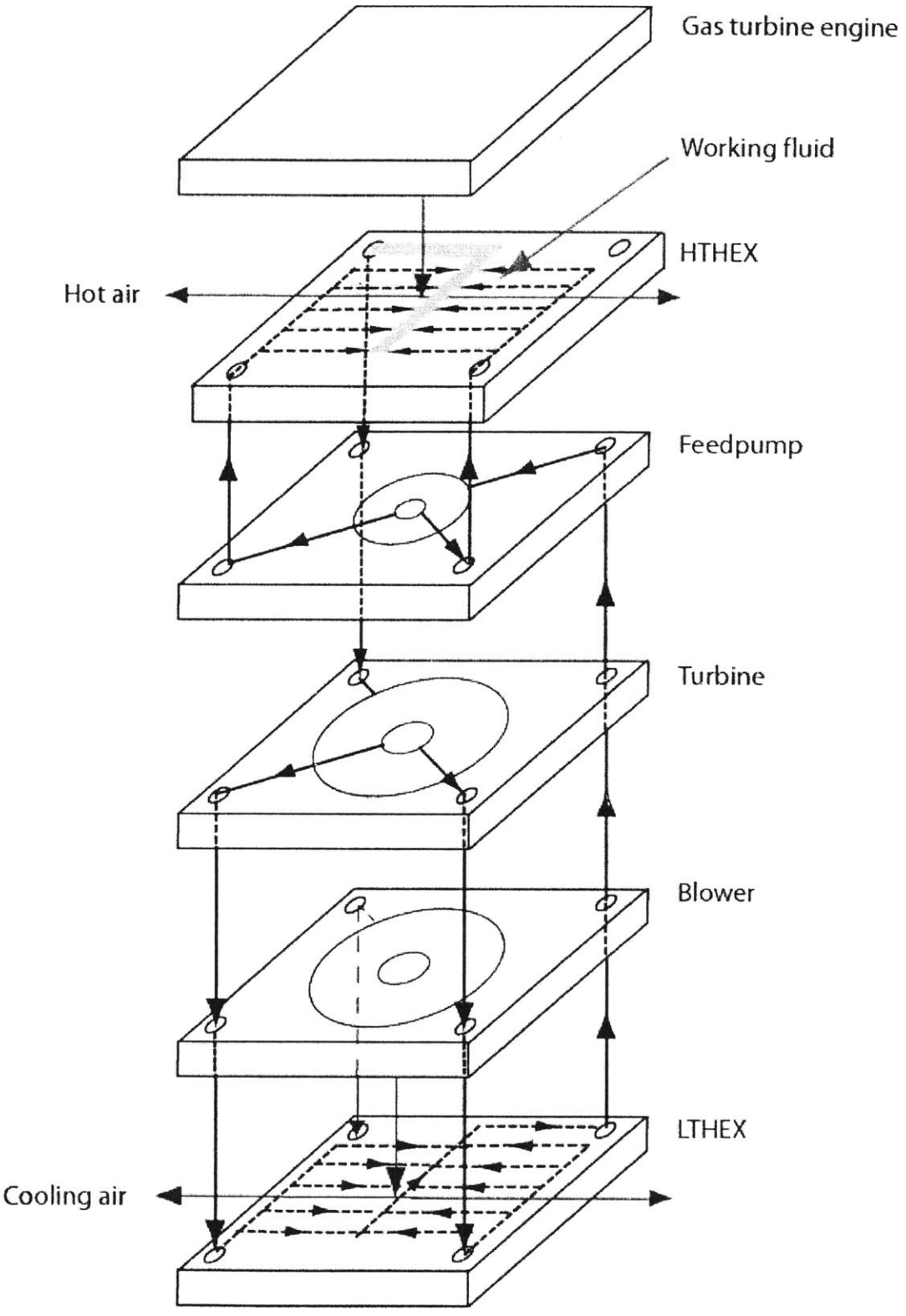


**Figure 2.4—Modular design flow paths of the combined bottoming cycle**

Heat exchanger design:

The heat exchangers are major components in this device. Figure 2.5 is a fin-type counter-flow heat exchanger design that can be applied to the LTHEX in the bottoming cycle. The heat exchanger designs are discussed in more detail in Chapter 3.

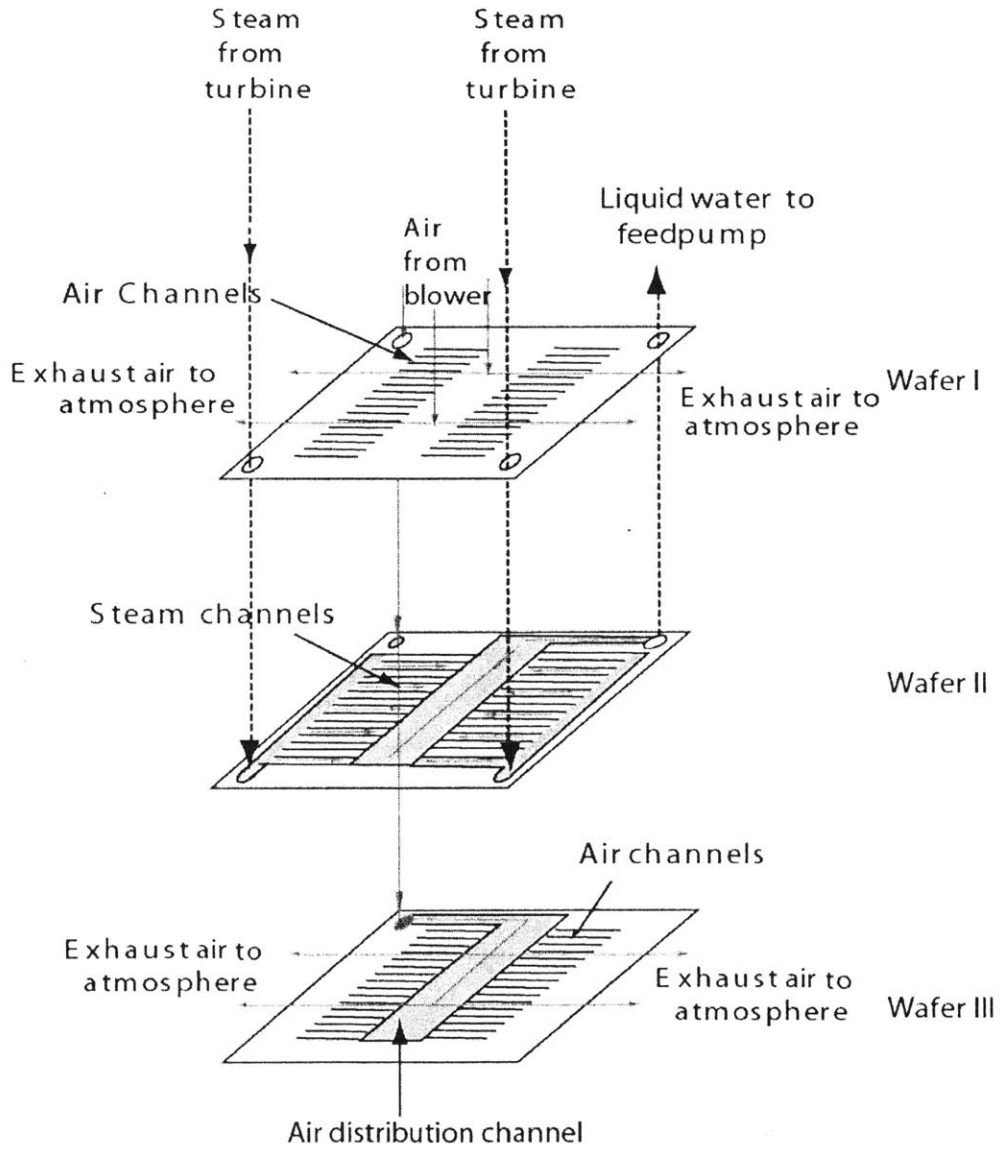


**Figure 2.5—Steam-air fin-type LTHEX flow paths**

The airflow throughout the LTHEX is seen in Figure 2.5. Ambient air is blown into wafer I and wafer III by the blower in the feedpump/turbine/blower module through connecting tubes. The air passes through the air distribution channels that are etched into the wafers and subsequently through heat transfer passages before it is exhausted to the atmosphere. The width of the distribution channels is kept large to minimize the distribution channel pressure drop and hence minimize flow misdistribution to the heat transfer passages.

The steam in the LTHEX enters from the steam turbine through another tube and is distributed to channels in Wafer II. The steam side of this heat exchanger has fewer channels than those on the airside. The low mass flow rate of the water (typically a tenth of the mass flow rate of the hot air in this machine) allows reasonable pressure drops for fewer passages shown in Figure 2.5. The high heat transfer coefficient for two-phase flow allows all the heat transfer passages for the steam to be on one wafer (vs. two for the air passages).

The HTHEX is also designed as a counter-flow heat exchanger, seen from Figure 2.6. This is because the exhaust gas from gas turbine engine is of relatively low temperature; therefore, effective use of its energy is the most important issue in HTHEX design. Seen from Figure 2.6, the HTHEX only has two silicon wafers: one for the hot air (gas turbine exhaust gas) and the other is for the working fluid. This is because of the lower volumetric flow rate of the hot air as well as the higher pressure drop tolerance (5 kPa in the HTHEX vs. 3 kPa in the LTHEX), based on the assumptions on the gas turbine exhaust gas and the calculations. In all the calculations that follow there is no work penalty assumed for the pressure drop across the HTHEX. The 5-kPa pressure drop across the HTHEX is assumed acceptable. It is assumed that the gas turbine or the combustor upstream of the HTHEX can provide the necessary pressure head to drive the flow through the HTHEX.

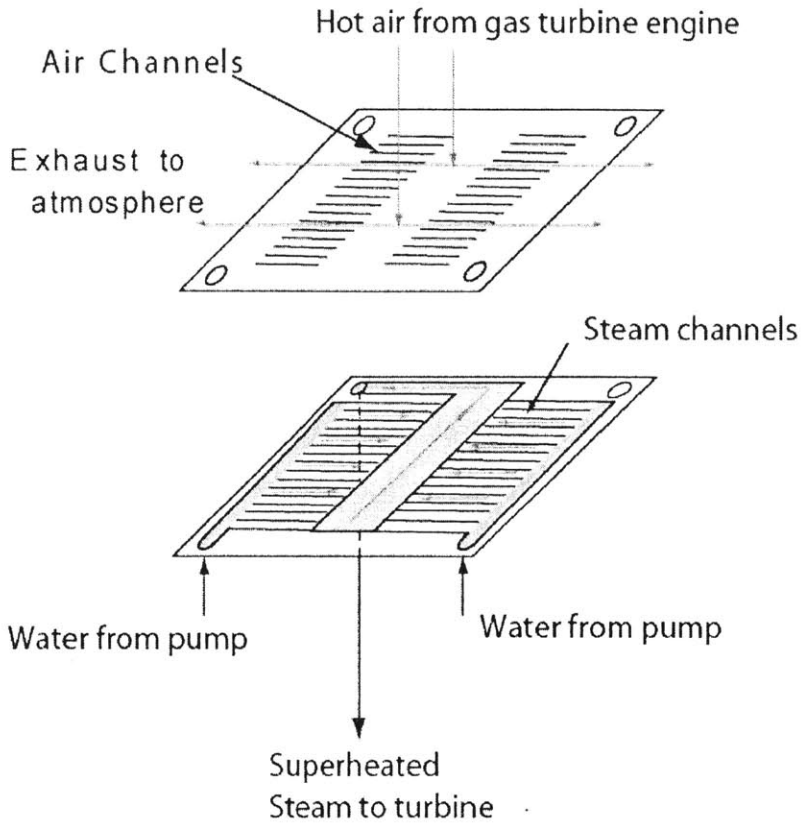


**Figure 2.6—Steam-air fin-type HTHEX flow paths**

In the heat exchanger design in this work, it is important to prevent leakage between the working fluid passages and the air passages, because both the loss of the steam and the air bubble in the water will result in the failure of the machine. Thus it is advantageous to keep the working fluid channels and the air channels in different wafers to minimize the length of potentially leaky silicon bonds with air on one side and steam on the other. In the MIT micro recuperator design [4] though, the channels of the two fluids (hot air and cold air) alternated one by one. This is because in the micro recuperator, a small amount of air-to-air leakage is tolerable.

Feasibility analysis of the design:

The design will have several fabrication challenges. First, the bottoming cycle design requires multi-wafer stacks that have more wafers than the current micro gas turbine engine. The HTHEX requires three layers of silicon wafers and the air channels etched into "Wafer I" are closed by the bottom of the gas turbine in the HTHEX, which means that it needs to be bonded directly to the gas turbine engine, as shown in Figure 2.3. In the case of the LTHEX, an additional cover layer must be bonded.

The number of the silicon wafers that can be bonded together depends on the thickness of the silicon wafers. Generally speaking, thin wafers are easier to bond than thick ones. The MIT micro gas turbine engines consisting of six-layer stacks have been successfully fabricated, with an average wafer thickness of about 0.5 mm. The thickest wafer (a combustor layer) is over 1 mm [5]. Given a reasonable HTHEX wafer thickness (less than 2 mm), it is a technically solvable problem to bond the HTHEX to the gas turbine engine, which would then be a nine-wafer stack. Table 2.1 shows the numbers of the wafer required for the MIT micro engine and components and estimated numbers of wafers to be used in the bottoming Rankine machine.

There will be four connecting tubes between each stack of the wafers, as shown in Figure 2.4. Kovar tubes have been successfully connected to many devices made for the MIT micro engine project. These include $\mu$-turbines, $\mu$-recuperators, and $\mu$-pumps, etc. We presume here that these processes can be used to connect the individual packages.

| MIT Micro engine | Number of wafers | Proposed Rankine micro engine | Estimated number of wafers |
|---|---|---|---|
| Gas turbine engine [2] | 6 | HTHEX | 2 |
| Micro turbopump [6] | 5 | HTHEX + G.T. engine | 2 + 6 = 8 |
| Micro blower [3] | 3 | LTHEX | 4 |
| Micro recuperator [4] | 3 | Turbomachinery module | 8~9 |

**Table 2.1—Comparison of the numbers of silicon wafers in micro engines**

### 2.1.3 Basic Assumptions and Modeling

Here we outline the assumptions and formulae used for modeling the combined cycle. We assume that the micro-Rankine cycle is operated in atmospheric air ($P = 10^5$ Pa) with an ambient temperature of 300 K. The air mass flow rates of the discharge of the micro gas turbine being developed at MIT are typically between 0.1 and 2 g/s with discharge temperatures between 770 K and 1000 K. Its discharge pressure was assumed 5 kPa higher than the ambient pressure, which does not substantially affect the operation of the gas turbine. The Rankine cycle models discussed here will assume the hot-air inlet conditions within these mass flow and temperature ranges. To be more specific, the superheat temperature of the working fluid in the HTHEX was assumed 20 K lower than the hot air entering the HTHEX.

In the micro-scale design, water was chosen as the working fluid in the calculation, because it has good thermophysical properties, is easily obtained, safe and stable, and water is the most widely used working fluid in the macro scale Rankine machines.

Assumptions about the components in the Rankine machine are also made. First, the walls (fins) in each layer of the LTHEX are isothermal. This is because that phase change of the working fluid is dominant in the LTHEX (details discussed in Chapter 3) and the conductivity of silicon is large (148 W/m K) compared to the thermal conductivity of the air (0.03 W/m K) [7]. Therefore, it is reasonable to assume that the thermal resistance of the LTHEX walls is negligible. Whereas in the HTHEX, the walls were not assumed isothermal, because the two-phase region of the steam is not dominant. Details about the isothermal LTHEX wall assumption are discussed further in Chapter 3. Second, interfaces between turbine, blower and pump are assumed adiabatic. In addition, minor losses in the heat exchangers are neglected.

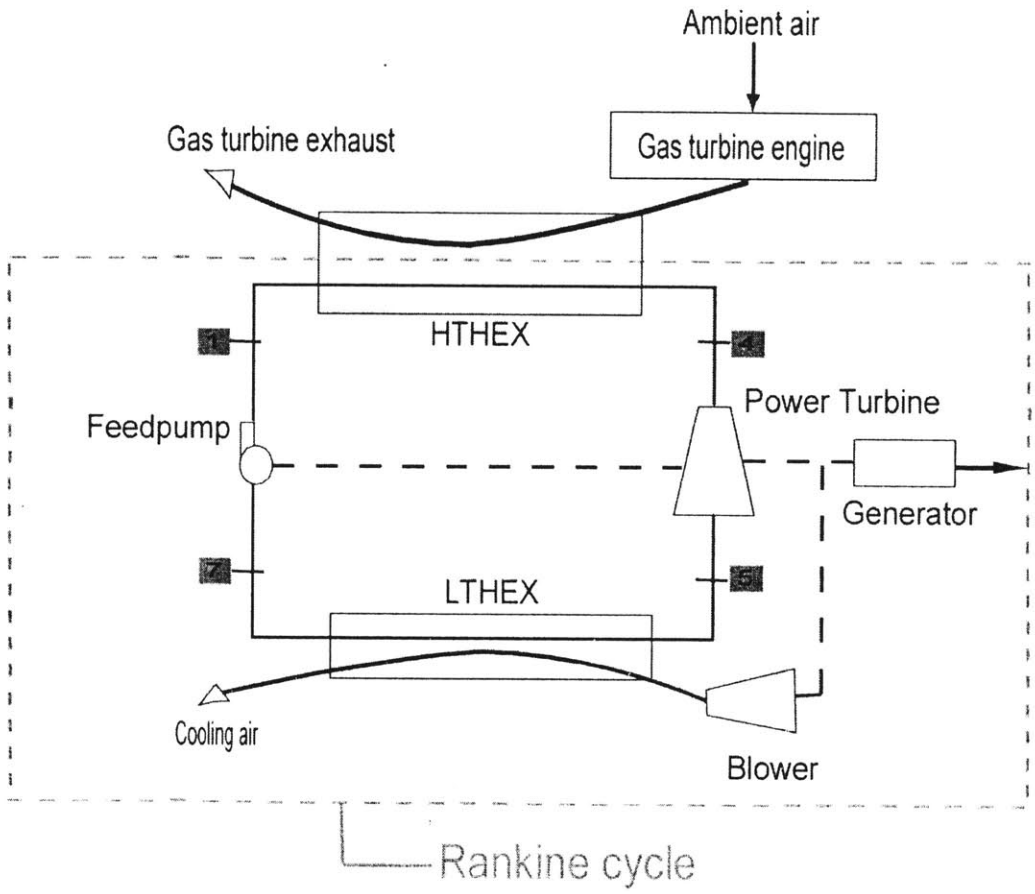


**Figure 2.7—Schematic diagram of a bottoming Rankine device**

A schematic diagram of the bottoming Rankine machine is shown again in Figure 2.7. The bottoming Rankine cycle performance is evaluated with its net (or useful) power output and cycle thermal efficiency, which can be defined as follows:

$$\dot{W}_{net} = \dot{W}_{turbine} - \dot{W}_{blower} \tag{2.1}$$

$$\eta_{thermal} = \frac{\dot{Q}_{HTHEX} - \dot{Q}_{LTHEX}}{\dot{Q}_{HTHEX}} \tag{2.2}$$

$$\dot{W}_{turbine} + \dot{W}_{pump} = \dot{Q}_{HTHEX} - \dot{Q}_{LTHEX} \tag{2.3}$$

$$\dot{W}_{pump} = \dot{m}_{H_2O} \times (h_1 - h_7) \tag{2.4}$$

$$\dot{W}_{blower} = \frac{\dot{m}_{coolingair} \times \Delta P_{coolingair}}{\rho_{air} \times \eta_{blower}} \tag{2.5}$$

$\dot{W}_{turbine}$ , $\dot{W}_{pump}$ , and $\dot{W}_{blower}$ are the work generation/consumption of turbomachinery respectively. $\eta_{thermal}$ is the thermal efficiency of the cycle, and $\dot{Q}_{HTHEX}$ (W) and $\dot{Q}_{LTHEX}$ (W) denote the heat transfer rate of the high temperature heat exchanger and the low temperature heat exchanger. $\dot{m}$ indicates mass flow rates; $h$ represents the enthalpy of the working fluid in the corresponding states, and $\Delta P_{cooling\ air}$ is the pressure drop of the cooling air over the LTHEX air channels. As per the state-of-the-art technology and the micro turbomachinery that M.I.T. micro engine group has been building, efficiencies of the turbomachinery components (turbine, pump, blower) are assumed to be 50% in the initial calculations.

The heat transfer rates of the heat exchangers can be obtained from their inlet and outlet enthalpy of the working fluid, which are functions of the design parameters (Equation (2.6) to (2.12) are from [7]):

$$\dot{Q}_{HTHEX} = \dot{m}_{H_2O} \times (h_4 - h_1) \tag{2.6}$$

$$\dot{Q}_{LTHEX} = \dot{m}_{H_2O} \times (h_5 - h_7) \tag{2.7}$$

The pressure drops along the air channels are one of the critical factors of the cycle performance. This is because $\dot{W}_{blower}$ is highly dependent on the pressure drop and from the calculation results, and the calculations show that the blower is a major consumer of the turbine power. The pressure drop on the airside can be obtained from the Equation (2.8):

$$\Delta P_{coolingair} = \frac{1}{2} \frac{L}{D_h} f \rho_{air} u^2 \tag{2.8}$$

where L is the length of the fins (channel walls in the direction of flow); $D_h$ is the hydraulic diameter of the channels; $u$ represents the velocity of the fluid, and $f$ is a friction factor corresponding to the value of Reynolds number and geometry of fluid channels.

Since the dimensions of the channel cross-section in this work are typically 0.1 mm by 1 mm or 2 mm, and the Reynolds numbers are always below 500. According to the examination by Jiang, et al., [8] and Mala and Li [9], the transition from laminar flow to turbulent flow may occur much earlier than in the macro scale (Re ~ 600). Under those standards, the flows in this work are still laminar in the heat exchangers. The friction factor is in defined as

$$f = \frac{c}{\mathrm{Re}} \tag{2.9}$$

where "$c$" is a constant which value is dependent on the aspect ratio of channels in heat exchangers. For example, if the height of the channel is 4 times of channel width, $c$ has a value of 73 [7]. Reynolds number is determined by both channel dimensions and air properties.

$$\mathrm{Re}_{D_h} = \frac{uD_h\rho}{\mu} \tag{2.10}$$

where $\mu$ is the viscosity of the fluid. Following the mass conservation law, the velocity "$u$" can be obtained as:

$$u = \frac{\dot{m}_{coolingair}}{n\rho A_c} \tag{2.11}$$

where $n$ is the number of air channels and $A_c$ is the cross sectional area of a channel.

One of the characteristics of these micro-scale heat exchangers is that the airflow in all of the micro heat exchangers is laminar. This is due to the small hydraulic diameter of the passage, the cycle limitations (turbomachinery efficiency and pressure ratio, etc.) and a necessarily low $\dot{W}_{blower}$ (in order to have net positive power output). From Equation (2.5), the power of the blower is determined by pressure drop, airflow rate and air properties. With fixed air properties, and $\dot{m}_{coolingair}$ is mainly determined by heat load of the heat exchanger. For a fixed channel aspect ratio (ratio of the channel height and channel width) the only way to reduce blower power is to increase the dimensions and/or the

number of the air channels. From the calculations, the velocity and Reynolds number are both small (in the order or 10 m/s and 100 respectively) when compared to macro-scale heat exchangers. Although turbulent flow is better than laminar flow with higher heat transfer coefficient, it is still unlikely to realize turbulent flow in this design due to the goal of minimizing blower power consumption.

The dimensional parameters of the heat exchangers are defined in Figure 2.8, which is a typical cutaway sketch of a layer of fin-type heat exchangers. The dimensional parameters of the channels are shown in the figure: a—channel height, b—channel width, d—wall/fin thickness, L—channel length and t—thickness of the base.

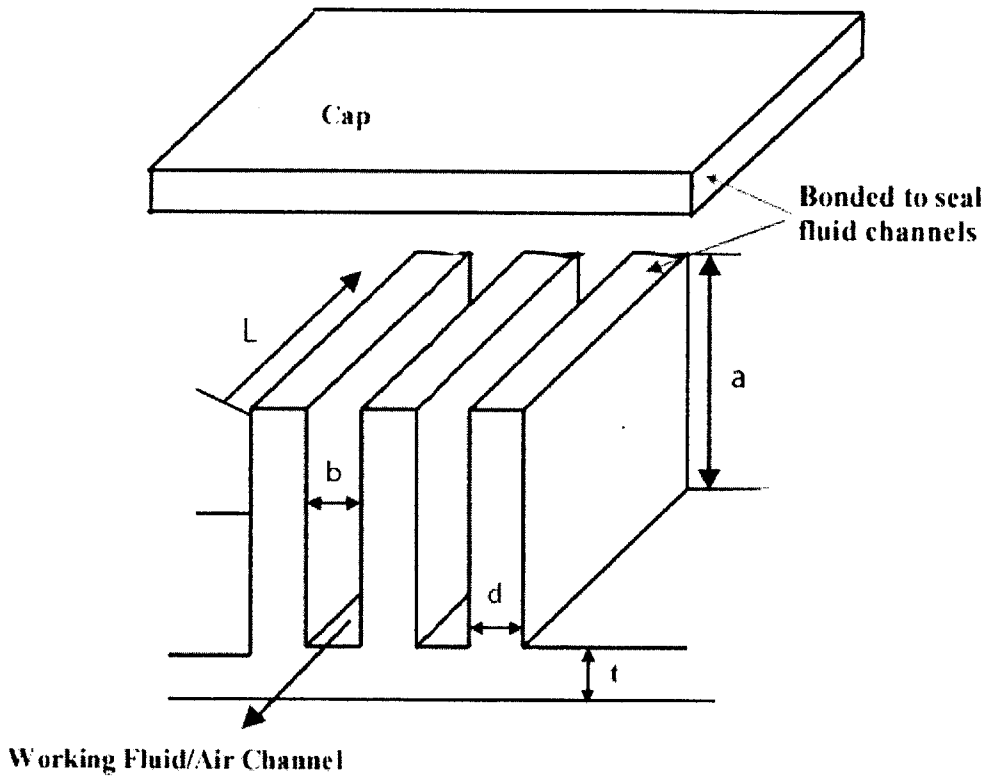


**Figure 2.8—Cutaway sketch of a fin-type heat exchanger**

The hydraulic diameter of the channels is:

$$D_h = \frac{4ab}{2(a+b)} \tag{2.12}$$

Substituting Equation (2.8) by (2.9) – (2.12),

$$\Delta P_{coolingair} = \frac{8\mu L \dot{m}_{coolingair}(a+b)^2}{n\rho a^3 b^3} \tag{2.13}$$

thus power consumption of the blower can be expressed as:

$$\dot{W}_{blower} = \frac{\dot{m}_{coolingair}^{\ 2}}{\eta_{blower}} \times \frac{8\mu L(a+b)^2}{n\rho^2 a^3 b^3} \tag{2.14}$$

Equation (2.13) and (2.14) shows that the pressure drop in the cooling air channels and the blower power consumption have a non-linear relation with the air channel width $b$ and height $a$. The bigger the product $ab$, the smaller the $\Delta P_{cooling\ air}$ and thus the $\dot{W}_{blower}$, with other parameters fixed. In addition, with the increase of channel dimensions $a$ and $b$, the useful heat transfer area increases as well, which will result in a smaller $\dot{m}_{coolingair}$ needed, which will also decrease the $\Delta P_{cooling\ air}$ and the $\dot{W}_{blower}$. More about fin-type heat exchanger designs will be discussed in Chapter 3.

### 2.1.4 Theoretical Results and Analysis

The goal of the calculations in this section is to estimate what the overall performance limitations of a small Rankine-cycle-based machine are. We will assume that this machine absorbs heat from and discharges heat to hot and cold air streams. The footprint of the device will be limited here to about a square inch. The first issue discussed here is a calculation for a reasonable estimate of the maximum power that can be generated from such a device given unlimited hot air supply in the HTHEX. This is followed by a calculation of the maximum power output for a restricted hot air mass flow rate through the HTHEX (0.1 g/s, one of a typical mass flow rates for the current MIT gas-turbine designs). The "optimum" cycles determined in the analysis described in the two previous sentences require very large pressure ratios across the power turbine. It is likely that initial Rankine turbine designs will be restricted to pressure ratios of 2 (due to cost and

complexity). Consequently, we continue the analysis in this section to determine the maximum power output of a Rankine cycle with a pressure ratio of 2 across the turbine. At the end of this section, improvement of the cycle power output by adopting a new LTHEX design. Performance is evaluated based on different assumptions on mass flow rates and heat exchanger geometry.

To find an "optimal" design for the Rankine machine with an unlimited hot air supply, the calculations start with a low temperature heat exchanger design (LTHEX). The condenser outlet temperature's effect on the cycle performance is studied by assuming a specific hot air inlet temperature and ambient air conditions. This then gives an optimal condenser operating temperature as a result of the tradeoff between the thermodynamic cycle efficiency and the blower power consumption.

More specifically, the inlet temperature for the hot air entering the HTHEX is 770 K. The HTHEX is assumed to be large enough so that the steam entering the power turbine has a temperature of 750 K. (In other words, the HTHEX is assumed to have a 20 K temperature defect at its hot end.) The pressure of the water/steam in the HTHEX is assumed to be 4 MPa. The geometry for the LTHEX is fixed with dimensions consistent with current fabrication limits (the LTHEX design must be "buildable"). These assumed dimensions are summarized in Table 2.2a. The start of the calculations requires the choosing of the condenser discharge temperature, $T_7$, and the mass flow rate of the steam in the Rankine cycle. With these assumptions, air mass flow rates through the heat exchangers and the work output of the cycle can be calculated using the relations discussed above.

For a given condenser discharge temperature, $T_7$, there is a steam mass flow rate which maximizes the net work output of the cycle. This optimum mass flow rate for a given $T_7$ can be found by plotting the results of the calculation described in the previous paragraph for several different steam mass flow rates at the fixed $T_7$. (The calculated net work output versus the steam mass flow rate is shown in Figure 2.9 for a condenser discharge temperature, $T_7$, of 420 K.) The results of a string of these optimum mass-flow

calculations for different condenser discharge temperatures are shown in the plot of the maximum net work of the cycle versus the condenser discharge temperature in Figure 2.10.

| | | | |
|---|---|---|---|
| Channel depth | 2 mm | Number of air channels | 480 |
| Channel length | 5 mm | Number of stacks (for cooling air) | 2 |
| Channel width | 100 μm | Sets of channels per stack | 2 |
| Fin thickness | 100 μm | Footprint | ~5.3 $cm^2$ |

**(a)**

| | | | |
|---|---|---|---|
| Channel depth | 2 mm | Number of air channels | 220 |
| Channel length | 5 mm | Number of stacks (for hot air) | 1 |
| Channel width | 100 μm | Sets of channels per stack | 2 |
| Fin thickness | 100 μm | Footprint | ~5 $cm^2$ |

**(b)**

**Table 2.2—Heat exchanger design for Figure 2.9 (a): LTHEX; (b): HTHEX**

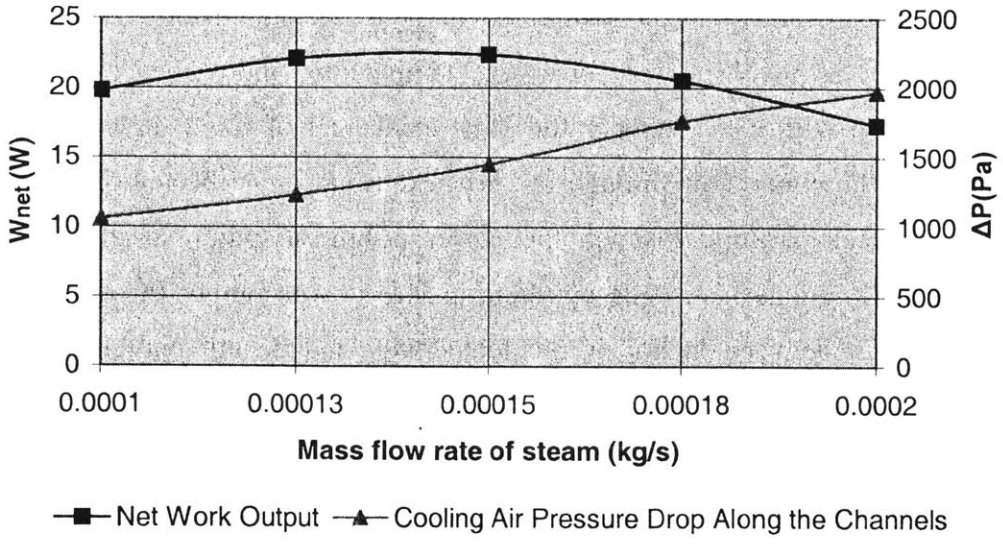


**Figure 2.9—Net work output & $\Delta P_{coolingair}$ in the LTHEX vs. working fluid mass flow rate with fixed saturation temperature (420 K) in the LTHEX**

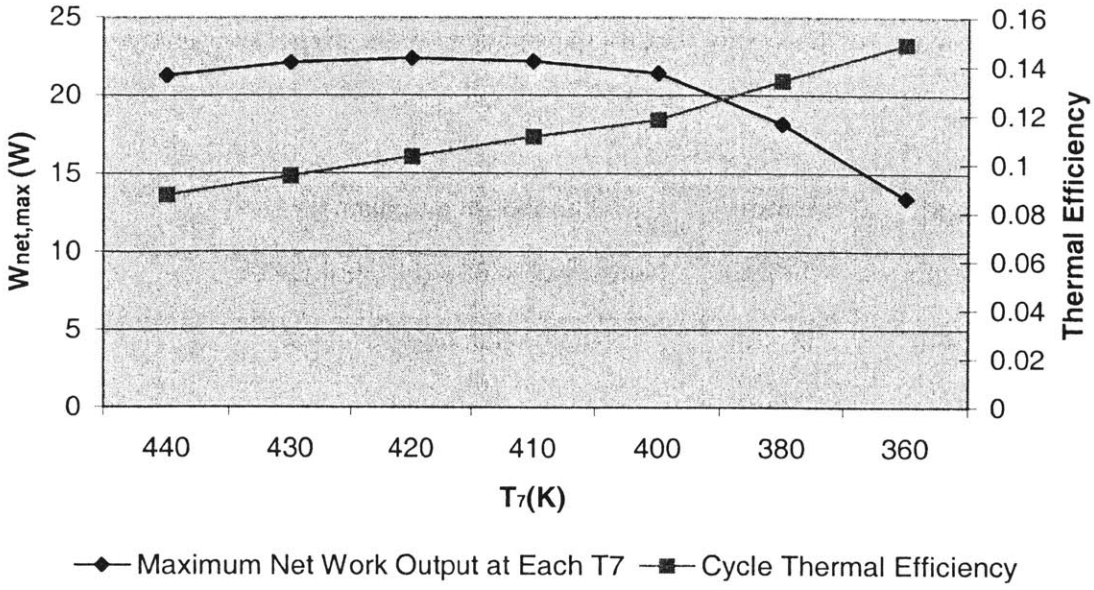


**Figure 2.10—Net work output and thermal efficiency as a function of LTHEX saturation temperature ($T_7$)**

There is an optimum in the net work output of 22.4 W when the condenser discharge temperature is 420 K. The optimum exists because of two competing effects. The thermodynamic efficiency improves as the temperature of the low temperature reservoir, essentially the condenser discharge temperature, is reduced. So from purely thermodynamic considerations, the condenser discharge temperature should be as low as possible. However as the condenser discharge temperature approaches the ambient temperature (300 K) with a low temperature heat exchanger of fixed dimensions, the mass flow rate of the cooling air through the heat exchanger must be increased. This increases the blower's parasitic load on the power turbine to pump air through the LTHEX. The result is that there is an optimum in the network output for a condenser discharge temperature between the hot air inlet temperature and the ambient temperature.

The corresponding HTHEX hot air mass flow rates that result from the calculations used to develop Figure 2.10 vary from 0.6 to 1.6 g/s and the corresponding water/steam circulation rates vary from 0.06 g/s to 0.17 g/s. The steam mass flow rate at $T_7 = 420$ K equals to 0.15 g/s. The corresponding thermodynamic efficiencies for the calculated cycles, shown in Figure 2.10 vary from 9% to 15 %.

The dimensions of a high temperature heat exchanger design that would deliver the thermal performance required for the optimized cycle ($T_7$ = 420 K) is cataloged in Table 2.2b. Table 2.2 makes it clear that the HTHEX is half the footprint of the LTHEX. Consequently, the size of the entire Rankine machine is dominated by LTHEX requirements.

Better performance and higher power outputs could be achieved with a larger LTHEX with the same one-square-inch footprint assumed above. This could be achieved by adding an additional layer to the stack of wafers that comprise the heat exchanger. In an attempt to analyze a realizable design, we have avoided doing this here. (There is an increasing difficulty of successfully fabricating the heat exchanger, as the number of wafers gets large.) An improved heat exchanger geometry that improves the performance of the Rankine device from 22 W to 41 W without the additional fabrication issues is discussed Chapter 3. Analysis with this improved heat exchanger will be discussed further later in this chapter.

The "optimum" 22.4 W output power Rankine design above requires 40% more hot air mass flow (0.14 g/s) than what is assumed exhausted by the MIT micro gas turbine (0.1 g/s). It is of interest to calculate what the maximum power output of a 2.3 cm by 2.3 cm Rankine machine for the hot air mass flow corresponding to the MIT micro gas turbine designs. The procedure for calculating the optimal performance of the Rankine machine with a fixed hot air mass flow rate (0.1 g/s) is very similar to the calculations discussed above. Table 2.3 summarizes some of assumptions used in these calculations. Table 2.4 summarizes the assumed dimensions for the LTHEX. It is apparent by comparing channel depth entry in Table 2.4 to that of Table 2.2a that the LTHEX in these calculations is half the size of the LTHEX discussed earlier. The low hot air mass flow rate results in low heat fluxes through the LTHEX. These low heat fluxes reduce the thermodynamic penalty of a reduced surface area in the LTHEX. The reduced channel depths also reduce the fabrication challenges in realizing such a design. The calculated net work output and thermal efficiency of the cycle as a function of the condenser discharge temperature, $T_7$, is shown in Figure 2.11.

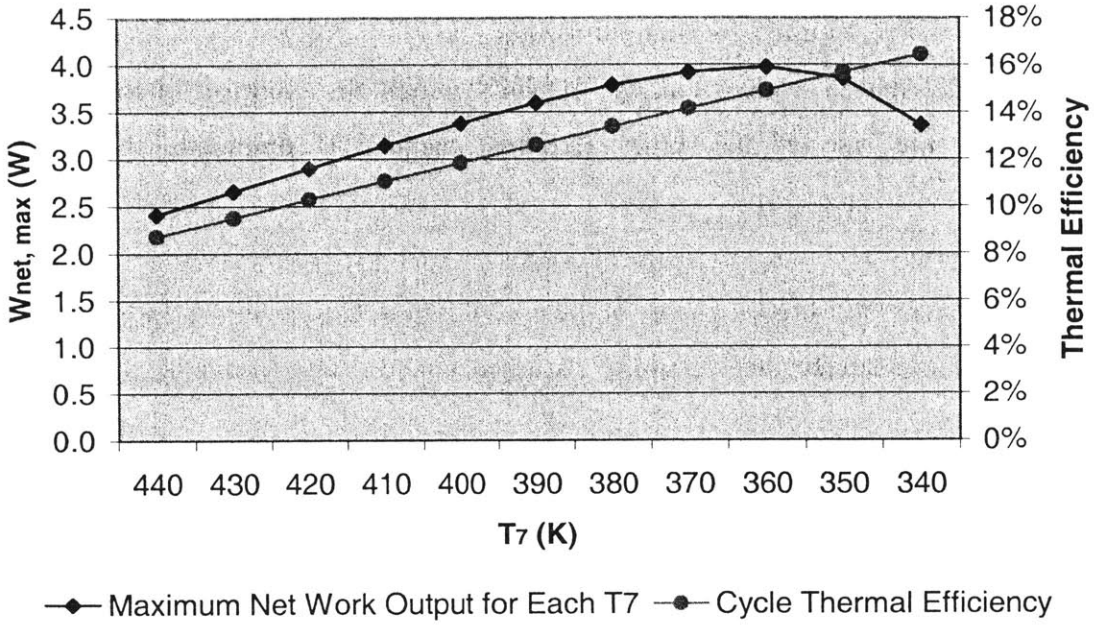


**Figure 2.11— Net work and $\eta_{thermal}$ vs. saturation temperature in the LTHEX Hot air mass flow rate equals to 0.1 g/s.**

| | | | |
|---|---|---|---|
| $P_{HTHEX}$ | 4 MPa | $\dot{m}_{H_2O}$ | 0.011 g/s |
| $T_{superheat}$ | 750 K | $T_7$ | 345~440 K |
| LTHEX footprint | ~2.3 cm × 2.3 cm | $\dot{m}_{hotair}$ | 0.1 g/s |

**Table 2.3—Selected cycle parameter assumptions for Figure 2.11**

| | | | |
|---|---|---|---|
| Channel depth | 1 mm | Number of air channels | 480 |
| Channel length | 5 mm | Number of stacks (for cooling air) | 2 |
| Channel width | 100 μm | Sets of channels per stack | 2 |
| Fin thickness | 100 μm | Footprint | ~5.3 $cm^2$ |

**Table 2. 4—LTHEX design for Figure 2.11**

One of the first observations on the performance of this machine is the reduction of the optimum power output of the machine from 22.4 W to 4.0 W. This is a result of the reduced energy available in the hot air stream and the reduced size of the LTHEX. The efficiency of the cycle at the maximum work output is substantially better than that for the large mass flow case discussed earlier (15 % vs. 10 %) primarily because the optimum condenser operating temperature is lower than the previous case (360 K vs. 420 K).

The disparity of the Rankine engine power output here in comparison to the previous unrestricted mass flow case makes it clear that running a 2.3 cm by 2.3 cm Rankine engine on the exhaust stream of a single gas turbine engine (of the current MIT design) underutilizes the Rankine engine. The Rankine engine is better utilized using the waste heat from a larger gas turbine or from an array of small gas turbines.

The pressure ratios across the power turbines in a Rankine machine are usually quite high. The cycles considered above are no exception. The turbine pressure ratios associated with the unrestricted hot air mass flow model above (whose results are shown in Figure 2.10) have turbine pressure ratios between 5.5 and 64.3. The turbine pressure ratios of the restricted hot air mass flow rate model (whose results are shown in Figure 2.11) have turbine pressure ratios between 5.5 and 147.1. Currently, micro turbines have been designed and built for pressure ratios of 2-3. It is likely that the first Rankine machines built will have a single-stage power turbine that will impose a low pressure ratio. Consequently, it is of interest to see what the effect on performance is if the pressure ratio across the power turbine is restricted to a low value.

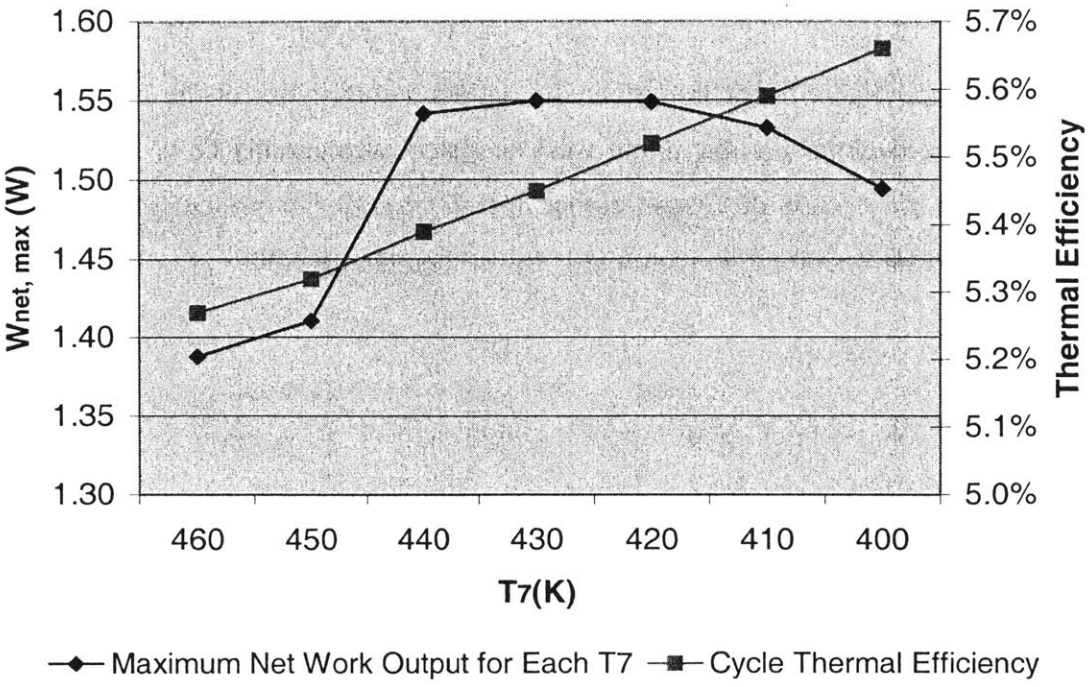


**Figure 2.12—Net work and $\eta_{thermal}$ vs. saturation temperature in the LTHEX Hot air mass flow equals to 0.1 g/s, and the turbine pressure ratio equals to 2.**

Figure 2.12 are the results of the a study of the expected power output when the pressure ratio across the power turbine has to a value of 2 and the hot air mass flow rate is held to a (the rather small) flow rate of 0.1 g/s. These calculations mimic the previous set of calculations, the dimensions of the LTHEX are the same as those cited in Table 2.4 and the turbine inlet temperature is held at 750 K. It is apparent by comparing Figure 2.12 to Figure 2.11 that restricting the pressure ratio in the power turbine significantly reduces the overall cycle performance. The optimum net power output and the thermal efficiency of the low pressure ratio cycle is about one half to one third of that shown in Figure 2.11 (1.55 W vs. 4 W and 5.5% vs. 15 %, respectively).

The reduction in the efficiency is a direct result of the low pressure ratio across the turbine. The turbine exhaust temperature for the low pressure ratio turbine is higher than that for a high pressure ratio turbine. These higher temperature gases have more

available energy that is not harvested by the turbine but rather is rejected to the condenser.

Substantial improvement of the performance of the restricted hot air mass flow (0.1 g/s) restricted pressure ratio ($\pi_{turbine}$ = 2) can be made if the temperature of the steam into the turbine inlet is allow to be higher than 750 K. Figure 2.13 are plots of the net work for the cycle as a function of the condenser exit temperature for several turbine inlet temperatures. The raising of the turbine inlet temperature from 750 K to 980 K, a 30% increase in temperature, results in an increase in the net work output from 1.55 W to 4.06 W, a 162 % increase in power output.

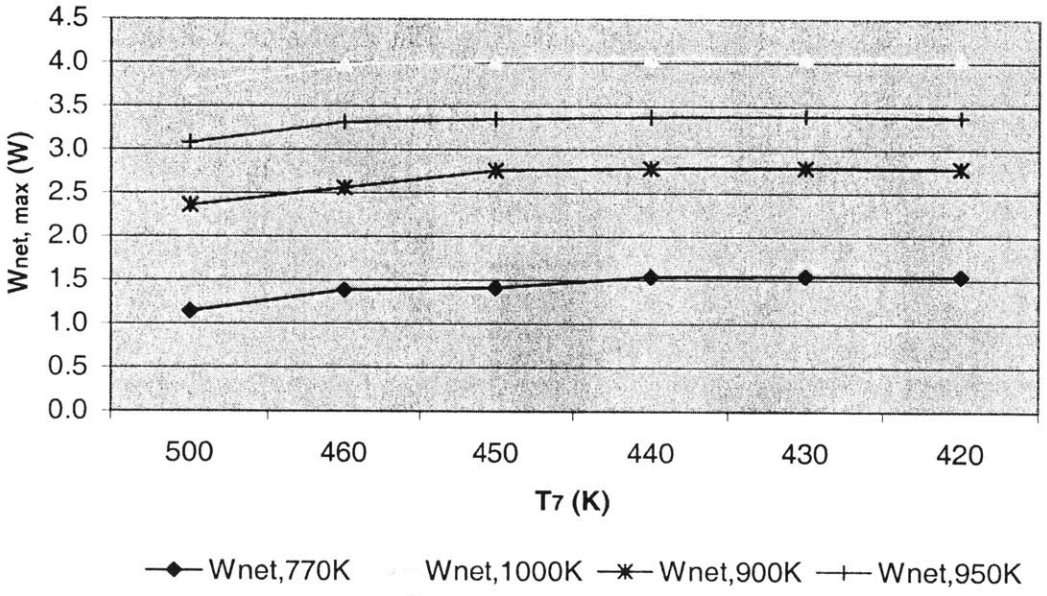


**Figure 2.13—Net work output as a function of the LTHEX saturation temperature The temperature of the micro gas turbine engine exhaust gas or hot air from a micro combustor is assumed 770 K, 900 K, 950 K and 1000 K (corresponding to steam power turbine inlet temperatures of 750 K, 880 K, 930 K and 980 K). The mass flow rate of the hot air is 0.1 g/s, and the turbine pressure ratio equals to 2.**

Other than increasing the turbine inlet temperature, better heat exchanger designs can also improve the net power output of the machine. In the chapter that follows, a new low temperature heat exchanger design will be introduced, in which the air channels are many holes in the direction of the thickness of the silicon wafers (a "hole-type" heat exchanger). This design effectively arranged more short channels in the heat exchanger with a similar footprint. A mirror calculation process of Figure 2.10 was done, only replacing the fin-type heat exchanger by the hole-type heat exchanger. For a steam cycle with the hole-type heat exchanger, the net work output is projected to be 37.4 W (compared to the 22.4-W cycle of the same cycle parameters with a fin-type LTHEX). If the restriction of the hot air mass flow rate and LTHEX size is relaxed, even more power output can be expected. Figure 2.14 shows a cycle with unrestricted steam mass flow rate and with a LTHEX footprint of 6 $cm^2$. The maximum power output reaches 41.4 W at $T_7$ equals to 420 K. The dimensions of this hole-type heat exchanger are listed in Table 2.5. The detailed design of the hole-type heat exchanger will be discussed in Chapter 3.

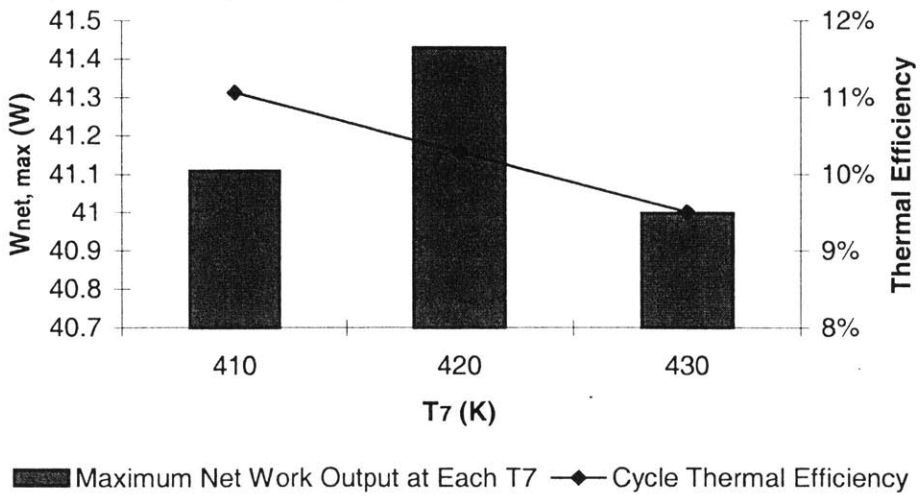


**Figure 2.14—Net work output and cycle thermal efficiency of a Rankine cycle with a hole-type LTHEX design**

**LTHEX footprint is about 6 $cm^2$. Turbine pressure ratio and steam mass flow rate are unrestricted. Turbomachinery efficiency equals to 50%.**

| | | | |
|---|---|---|---|
| Hole Diameter | 0.2 mm | Wafer Thickness | 1.5 mm |
| Number or Rows | 57 per stack | Number of Stacks | 3 |
| Holes per Row | 75 per stack | Footprint | 6 $cm^2$ |
| Distance b/t holes | 0.1 mm | | |

**Table 2.5—Hole-type LTHEX dimensions (air side) for Figure 2.14**

### 2.1.5 Summary, Restrictions and Problems of the Designs

By studying the above cycles performances, there are some useful conclusions made:

1. Power output of the cycle is expected (1~41 W);
2. Device footprint can be as small as 2.3 cm by 2.3 cm;
3. LTHEX is the limiting component of device size;
4. Flows in heat exchangers are always laminar;
5. The mass flow of cooling air needed for the cycle can be expected an almost linear correlation with $\dot{m}_{H_2O}$ ($\frac{\dot{m}_{H_2O}}{\dot{m}_{coolingair}} \approx \frac{1}{10}$) given fixed LTHEX dimension. And net power output is highly dependent on the pressure drop and the mass flow rate of the cooling air in the LTHEX, which are determined by LTHEX dimensions;
6. For a fixed $\dot{m}_{hotair}$, there's always a best LTHEX discharge temperature ($T_7$) for the optimum $\dot{W}_{net}$ and for a fixed $T_7$, there's always a best $\dot{m}_{H_2O}$ for an optimum $\dot{W}_{net}$;
7. Blower becomes the dominant power consumer of turbine;
8. Increasing $T_{hot\ air}$ can improve $\dot{W}_{net}$;
9. Thermal efficiency increases when $T_7$ decreases;
10. For fixed LTHEX dimensions and $T_{hotair}$, the maximum $\dot{W}_{net}$ results from tradeoff between cycle thermal efficiency and blower power consumption by varying $T_7$.

11. The 20 K temperature defect between the hot air temperature and superheated vapor temperature can be varied depending on the requirement to the high temperature heat exchanger.

There are still some restrictions and problems in the cycle stated above:

1. As per the current fabrication technology, it is difficult to bond together several wafers of thickness more than 1mm each. In the first design shown in Figure 2.10 and Figure 2.11, this fabrication issue was not taken into account (fin height=2 mm). For a fin-type heat exchanger, reducing the height of the channels while keeping the same amount of $\dot{W}_{net}$ will increase the size of the device. For example, to decrease the fin height by 50%, the width will have to be increased by >50% for same $\dot{W}_{net}$;
2. If the turbine inlet pressure is increased with other parameters remain the same, the power output can be increased. But there are component stress limits and turbine pressure ratio restrictions (maximum $\pi_{turbine}$ = 3 per stage currently). In addition, the working fluid might go supercritical which was avoided in this design;
3. Thermal efficiency is lower than the macro power plants because of turbomachinery and dimensional restrictions;
4. Blower is a much bigger consumer of the turbine power output compared to the feedpump;
5. Mass flow rates of $H_2O$ is very small. The existing micro turbines cannot match such low $\dot{m}_{H_2O}$'s.
6. Heat transfer between hot and cold components and components to the ambient was not taken into account in the preliminary calculations.
7. In state 7, the working fluid is assumed as saturated water. If taking the pressure drop of the working fluid into consideration, the working fluid may not be in 100% liquid phase. To solve the problem, sub-cooling might be needed, which will result in more blower power consumption.

## 2.2 Micro Rankine Cycles Under State-Of-the-Art Technology

### 2.2.1 Stand-alone Rankine cycle

Many of the restrictions imposed on the design of the Rankine cycle above were imposed by the fairly artificial constraints of a bottoming cycle to the current MIT gas turbine engine designs. These constraints included a rather low gas turbine exhaust gas temperature of 770 K and a low hot air mass flow rate of 0.1 g/s. Here we examine the potential of "first generation" stand-alone Rankine machine where the mass flow and temperature limits that earlier were imposed to match the gas turbine are relaxed. In the calculations that follow, the Rankine machine superheat temperature, mass flow rates, and size are not restricted to match the micro gas turbine engine. The steam turbine pressure ratio will initially be held to a value of 2. This will be followed by a calculation where the turbine pressure ratio is relaxed to a value of 4. The forced airflow through the HTHEX is driven by the combustor and the calculations below assume that there are no penalties to the Rankine cycle for driving that flow through that heat exchanger.

The analysis proceeds in a vein similar to the calculations described above. The low temperature heat exchanger dimensions assumed for the calculation are summarized in Table 2.6. The maximum allowable superheat temperature allowed in the calculation is 1000 K. (The silicon turbine will begin to soften and suffer creep at a lower temperature than the inlet gas temperature). The pressure ratio across the turbine is assumed to be 2.

| | | | |
|---|---|---|---|
| Channel depth | 1 mm | Number of air channels | 240 |
| Channel length | 5 mm | Number of stacks (for cooling air) | 2 |
| Channel width | 100 μm | Sets of channels per stack | 2 |
| Fin thickness | 100 μm | Footprint | ~2.5 $cm^2$ |

**Table 2.6—LTHEX design for Figure 2.15**

The net work output for this Rankine device is plotted in Figure 2.15 as a function of the condenser saturation temperature for turbine inlet temperatures of 900 K, 950 K and 1000 K. The mass flow rates and thermal efficiencies corresponding to the plotted points in Figure 2.15 are listed in Table 2.7. The designed LTHEX footprint for these calculations is only half of the ones used in the bottoming cycles (2.5 $cm^2$ vs. 5 $cm^2$). If a same-sized LTHEX were used here, about 100% of power output improvement could be expected by increasing the steam mass flow rate of the cycle. Thus, a comparison of the net power output of this cycle to the constrained cycle results shown in Figure 2.11 suggests an increase in the achievable "first-generation" device from 4 W to 16 W. (Here, "first-generation" refers to a device that uses a rather conservative turbine design with a pressure ratio of 2.)

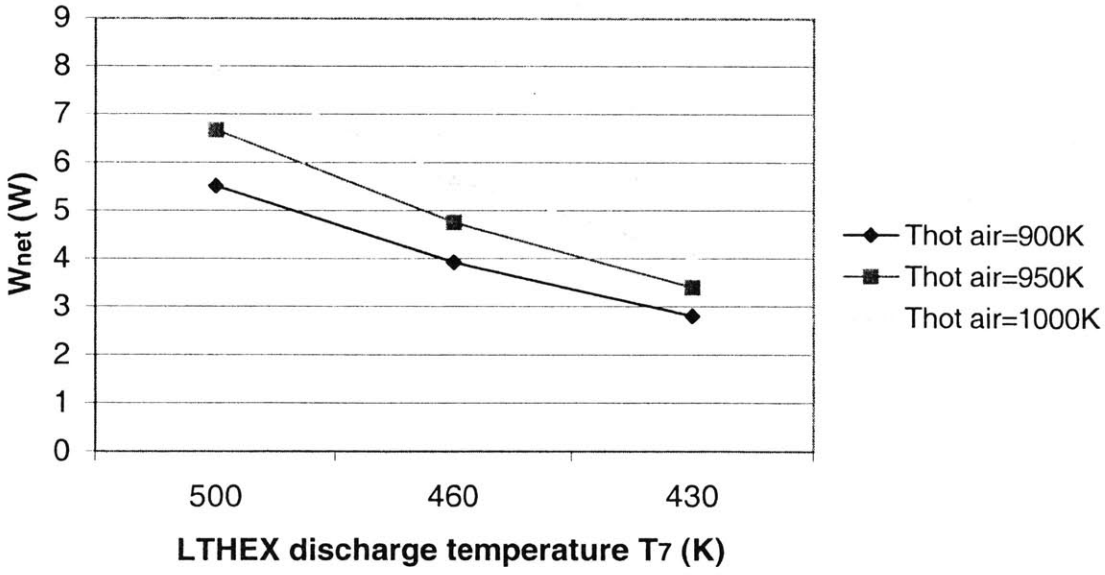


**Figure 2.15—Single cycle: the LTHEX saturation temperature vs. net work output $T_{hot\ air}$ is assumed 900 K, 950 K and 1000 K respectively (The corresponding turbine inlet temperature $T_{superheat}$ is then 880 K, 930 K and 980 K respectively). The turbine pressure ratio equals to 2.**

$T_{hot\ air}$=900 K

| $T_7$ | $\dot{m}_{vapor}$ | $\dot{m}_{coolingair}$ | $\dot{m}_{hotair}$ | $\dot{W}_{net}$ | $\eta_{thermal}$ |
|---|---|---|---|---|---|
| (K) | (g/s) | (g/s) | (g/s) | (W) | (%) |
| 500 | 0.058 | 0.73 | 0.40 | 5.52 | 6.6 |
| 460 | 0.039 | 0.66 | 0.26 | 3.93 | 6.9 |
| 430 | 0.025 | 0.54 | 0.16 | 2.81 | 7.1 |

$T_{hot\ air}$=950 K

| $T_7$ | $\dot{m}_{vapor}$ | $\dot{m}_{coolingair}$ | $\dot{m}_{hotair}$ | $\dot{W}_{net}$ | $\eta_{thermal}$ |
|---|---|---|---|---|---|
| (K) | (g/s) | (g/s) | (g/s) | (W) | (%) |
| 500 | 0.061 | 0.80 | 0.38 | 6.68 | 7.3 |
| 460 | 0.039 | 0.68 | 0.24 | 4.76 | 7.6 |
| 430 | 0.027 | 0.60 | 0.604 | 3.41 | 7.8 |

$T_{hot\ air}$=1000 K

| $T_7$ | $\dot{m}_{vapor}$ | $\dot{m}_{coolingair}$ | $\dot{m}_{hotair}$ | $\dot{W}_{net}$ | $\eta_{thermal}$ |
|---|---|---|---|---|---|
| (K) | (g/s) | (g/s) | (g/s) | (W) | (%) |
| 500 | 0.064 | 0.88 | 0.37 | 7.95 | 7.9 |
| 460 | 0.04 | 0.72 | 0.23 | 5.67 | 8.2 |
| 430 | 0.027 | 0.62 | 0.16 | 4.06 | 8.5 |

**Table 2.7—Mass flow rates, net work output and thermal efficiency of the single cycle at different hot air supply**

A substantial improvement can be made if the turbine pressure ratio is increased to a value of 4 and expanding the LTHEX channel depth from 1 mm to 2 mm. Figure 2.16 shows the predicted net power output and thermal efficiency of the single steam cycle based on the above change. The LTHEX discharge temperatures are assumed from 440 K to 480 K.

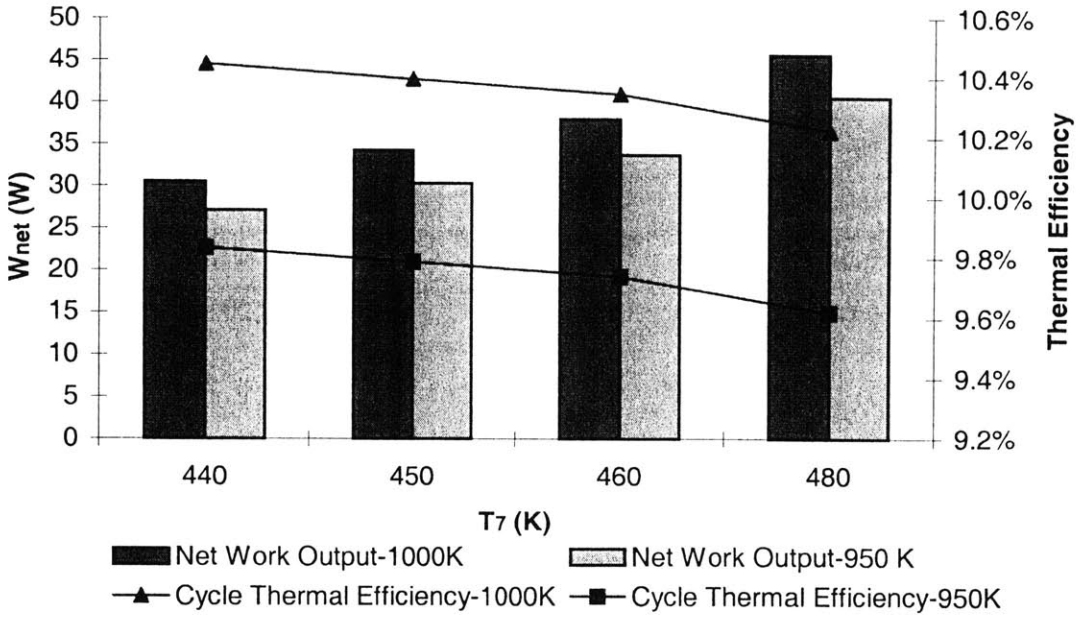


**Figure 2.16—Net work output and thermal efficiency of a single cycle as a function of LTHEX discharge temperature**

**$T_{hot\ air}$ is assumed 950 K and 1000 K respectively (The turbine inlet temperature $T_{superheat}$ then equals to 930 K and 980 K respectively). The turbine pressure ratio equals to 4 and the LTHEX air channel depth equals to 2 mm and number of channels equals to 480 (the rest dimensions are shown in Table 2.6).**

Figure 2.16 shows that the net power output for this design is about 30.5 W to 45.6 W. The highest power output (45.6 W) is at $T_{superheat}$ = 1000 K and $T_7$ = 480 K. The net work output increases monotonically with increasing condenser outlet temperature, $T_7$. This is because for an assumed $T_7$, a corresponding LTHEX discharge (saturation) pressure is found, and since the turbine pressure ratio is fixed, $P_{superheat}$ and thus the pressure drop across the turbine increases with the increase of $T_7$. Therefore, turbine power is increased for a fixed $T_{superheat}$ and steam mass flow rate. At the same time, with a higher $T_7$, more heat can be transferred in the LTHEX (under the same external conditions) and the mass flow rate of the steam can be increased. The increased steam mass flow rate combined with the increase pressure drop across the turbine results in a higher net work output.

Ideally, the net work output of the cycle can be increased above the values shown in Figure 2.16 by further increasing $T_7$. There is, however, a practical upper limit to the pressures that can be sustained in the silicon structure. The turbine inlet pressure when $T_7$ is chosen to be 480 K is about 7 MPa which we have (somewhat arbitrarily) chosen here as a limiting pressure for the cycle.

### 2.2.2 Other Working Fluid Choices for Combined Cycle

We have assumed that micro turbines could be built to handle the small steam mass flow rates required for the bottoming cycle applications discussed earlier. The mass flow rates in the steam are approximately ten times smaller than the mass flow rates associated with the hot air flow. This small mass flow rate combined with the relatively high density of high-pressure steam results in small volumetric flows through the power turbine. These volumetric flows are outside the range of designs that have been examined as part of the MIT micro engine project. For example, in one of the bottoming Rankine machine designs ($T_7$ = 440K) in Figure 2.10, the mass flow rate of the steam is about 0.2 g/s. However, the mass flow rate for an MIT 4-mm turbine design with similar pressures, temperatures and pressure ratio is about 6 g/s.

There are several approaches to accommodate the small volumetric flow of the working fluid. The first is to reduce the size of the turbine, which will be limited by current manufacturing capabilities. Another is to increase the size of the heat exchanger (to increase the working mass flow rate), which will increase the footprint of the device.

The volumetric flow rate through the turbine can be increased by choosing a new working fluid. Several working fluids, listed in Table 2.8, were considered for analysis [10]. The criteria for choosing a new working fluid include:

1. A lower latent heat (L.H.) than water, the large latent heat of water results in a small mass flow a given heat transfer rate in the HTHEX.

2. A reasonable critical pressure: $P_{critical} \sim 4\ MPa$. This is to avoid excessive pressures in the device.
3. The liquid phase must exist at 10 °C with a vapor pressure above one atmosphere, which will avoid sub-atmospheric operation in the cycle. This can be interpreted as requiring the 1 atm boiling temperature to be below 283 K.
4. Preferably a vapor density lower than that of water vapor to increase the turbine inlet volumetric flow rate for the same mass flow.
5. No chemical reactions with silicon.
6. Chemically stable.
7. Available thermophysical property tables.

| Molecular formula | $T_{melt}$ (K) | $T_{boiling}^{*}$ (K) | $T_{critical}$ (K) | $P_{critical}$ (MPa) | Comments |
|---|---|---|---|---|---|
| $H_2O$ | 273.15 | 373.15 | 647.14 | 22.06 | L.H. high |
| $C_6H_6$ | 278.68 | 353.24 | 562.16 | 4.898 | Poisonous |
| $H_3N$ (Ammonia) | 195.41 | 239.72 | 405.50 | 11.35 | $T_b$ too low |
| $H_4N_2$ (Hydrazine) | 274.5 | 386.70 | 653 | 14.70 | Data n/a |
| $CH_3NO_2$ | 244.60 | 374.35 | 588 | 5.87 | Data n/a |
| $C_5H_8O$ | 221.80 | 403.90 | 624.50 | 4.60 | Data n/a |

**Table 2.8— Selected Physical Constants of Substances**

**$^{*}T_{boiling}$ is measured at ambient pressure (1 atm).**

Benzene ($C_6H_6$) was considered to be the best of the fluids considered as an alternative to water. Hydrazine's higher critical temperature might make it more attractive than benzene as a working fluid. However, benzene has a more complete set of published thermophysical properties [10]. We have not concerned ourselves with other issues such as toxicity (benzene is a carcinogen) or flammability of the working fluid.

The benzene mass flow rates will typically be about 5-7 times larger than the steam mass flow rate for the same heat transfer in the HTHEX. (The latent heat of water is about seven times that of benzene at T= 420 K).

The mass flow rates for the benzene out of the HTHEX must be matched to the power turbine. The question remains whether the resulting flow from the HTHEX can be matched by a reasonably sized turbine (from a fabrication point of view). To this end, the mass flow results of a steam turbine design study were scaled to benzene by assuming the volumetric flows for benzene through the turbine were the same as that for steam under similar conditions. (The assumed dimensions of the turbine are outlined in Table 2.9 and the steam turbine design study is discussed in more detail in Chapter 5.) The results of these mass scalings are shown in Table 2.10 for several turbine pressure ratios, turbine inlet pressures and temperatures ($\pi_{turbine}$, $P_{superheat}$ and $T_{superheat}$). The compressibility factor, Z≡PV/RT, is also included in the table. The benzene compressibility factors for the conditions studied are all larger than 0.8, suggesting that the ideal gas turbine analysis used to predict the mass flow rates through the turbine is appropriate. (An ideal gas has a compressibility factor of 1.) It is apparent from Table 2.10 that the benzene mass flow rate through a turbine of this size is about 1-2 g/s.

| Metrics | Baseline Design |
|---|---|
| Rotor inlet radius | 3 mm |
| Rotor exit radius | 2 mm |
| Revolutions per minute (RPM) | $1.2 \times 10^6$ |
| Stage pressure ratio | 1.5 to 3.5 |
| Stage efficiency | 50% |

**Table 2.9—The turbine assumed in the benzene cycle calculation based on the MIT micro gas turbine**

| Pressure Ratio | | $\pi_{turbine} = 1.5$ | | $\pi_{turbine} = 2$ | | | $\pi_{turbine} = 3$ | | $\pi_{turbine} = 3.5$ | | |
|---|---|---|---|---|---|---|---|---|---|---|---|
| $P_{superheat}$ \ $T_{superheat}$ | | 550K/ 700Kfor 3MPa | 600K | 550K/ 700Kfor 3MPa | 600K | 650K | 550K/ 700Kfor 3MPa | 600K | 550K/ 700Kfor 3MPa | 600K | 650K |
| 1MPa | $\dot{m}_{benzene}$ | 0.98 | 0.96 | 1.14 | 1.10 | --- | 1.75 | 1.70 | 1.88 | 1.83 | --- |
| | Z | 0.93 | 0.95 | 0.93 | 0.95 | --- | 0.93 | 0.95 | 0.93 | 0.95 | --- |
| 2MPa | $\dot{m}_{benzene}$ | 1.03 | 0.97 | 1.20 | 1.12 | --- | 1.84 | 1.72 | 1.98 | 1.85 | --- |
| | Z | 0.84 | 0.88 | 0.84 | 0.88 | --- | 0.84 | 0.88 | 0.84 | 0.88 | --- |
| 3MPa | $\dot{m}_{benzene}$ | 0.89 | 1.01 | 1.02 | 1.17 | 1.09 | 1.57 | 1.79 | 1.70 | 1.93 | 1.80 |
| | Z | 0.90 | 0.81 | 0.90 | 0.81 | 0.86 | 0.90 | 0.81 | 0.90 | 0.81 | 0.86 |

**Table 2.10—Estimation of mass flow needed (g/s) & compressibility (Z) under different pressure and temperatures**

**$\gamma$ was assumed to be equal to 1.1.**

Models for a Rankine cycle using this turbine (Table 2.9) and heat exchangers with dimensions described in Table 2.11 and 2.12 were constructed. The number of LTHEX air channels was varied in order to examine the sensitivity of the net work output vs. the size of the low temperature heat exchanger. Several sets of operating conditions were analyzed using the methods described earlier. The hot air mass flow rates were adjusted to match the assumed benzene mass flow rates through the HTHEX. The results of these calculations are shown in Table 2.13. Within a footprint of 24 $cm^2$ (~ 5 cm by 5 cm), a benzene power machine with a turbine pressure ratio equals to 2 could generate 22.5 W work, when the turbine inlet pressure and temperature is 3 MPa and 650 K.

| | | | |
|---|---|---|---|
| Channel height (a) | 1.5 mm | Number of channels (n) | 800 - 1200 |
| Channel width (b) | 0.1 mm | Number of stacks (air) | 2 |
| Channel length (L) | 4 mm | Total width | 3.8 cm |
| Wall thickness (d) | 0.1 mm | Total length | 4 – 6 cm |

**Table 2.11—Dimensions of the LTHEX in benzene-powered cycle**

| | | | |
|---|---|---|---|
| Channel height (a) | 1.5 mm | Wall thickness (d) | 0.1 mm |
| Channel width (b) | 0.1 mm | Number of channels (n) | varies |
| Channel length (L) | 3 mm | Number of stacks (air) | 2 |

**Table 2.12—Dimensions of the HTHEX in benzene-powered cycle**

| | **Low temperature heat exchanger footprint** | Cycle net work output ($\dot{W}_{net}$) | |
|---|---|---|---|
| | | $\pi_{turbine}$ **=2** | $\pi_{turbine}$ **=3 or 3.5** |
| $T_{superheat}$ = 600 K | 4 cm × 4 cm, n* = 800 | 11.3 W | -- |
| | 5 cm × 4 cm, n = 1000 | 14.7 W | 6.9 W ($\pi_{turbine}$ =3) |
| | 6 cm × 4 cm, n = 1200 | 16.7 W | 20.7 W ($\pi_{turbine}$ =3)<br>12.8 W ($\pi_{turbine}$ =3.5) |
| $T_{superheat}$ = 650 K | 4 cm × 4 cm, n = 800 | 15.4 W | -- |
| | 5 cm × 4 cm, n = 1000 | 19.9 W | -- |
| | 6 cm × 4 cm, n = 1200 | 22.5 W | 12.0 W ($\pi_{turbine}$ =3.5) |
| Note: *n is the number of air channels in LTHEX and $P_{superheat}$ = 3 MPa for all cases. | | | |

**Table 2.13—Comparison of performance under different pressure ratio, $P_4$ and $T_4$**

It can be seen from Table 2.13 and Figure 2.17 that larger LTHEX's result in larger net work output of the cycle. For the case in Figure 2.17, 50% increase of the LTHEX size results in about 50% gain of power.

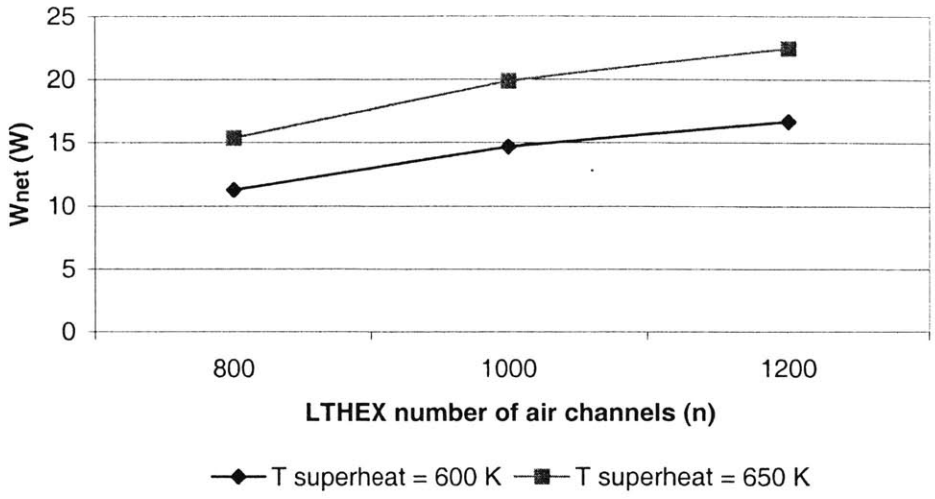


**Figure 2.17—Benzene power cycle net work output as a function of LTHEX size This figure corresponds to the net work output column at $\pi_{turbine}$ =2 in Table 2.12.**

It may seem that increasing the turbine pressure ratio will increase the net power out of the cycle. This is not the case where the turbine inlet pressure and temperature are 3 MPa and 600 K where for the number of LTHEX air channels n = 1000, the design with $\pi_{turbine}$ = 2 is larger than the design with $\pi_{turbine}$ =3 (see the second row of Table 2.13). The reason for this is that too large a pressure ratio in the turbine depresses the condenser's operating temperature towards the ambient temperature. With a fixed-size heat exchanger, the blower power must be disproportionately increased to compensate. The result is that the net work of the cycle decreases as the turbine pressure ratio is increased further.

Increasing the turbine inlet temperature generally improves the Rankine cycle efficiency. The column for $\pi_{turbine}$ =2 and Table 2.13 shows that higher turbine inlet temperature (650 K vs. 600 K) results in higher net work output (11.3 W vs. 15.4 W, 14.7 vs. 19.9 W and 16.7 vs. 22.5 W for the three LTHEX sizes).

At this point, one set of operating parameters was chosen from the array presented in Table 2.13 to allow further refinement of the heat exchanger design. The operating

parameters chosen were a turbine pressure ratio of 2, a turbine inlet temperature of 650 K, a turbine inlet temperature of 3 MPa and a benzene mass flow rate of 1.1 g/s. These parameters do not yield the best net work but rather their choice is a compromise between cycle performance and practical considerations. (Large pressure ratios may be hard to achieve in a first generation device.) The performance of the cycle above mentioned could be further improved by investigating different fin-type heat exchanger designs. In this work, the width of the cooling air channels ("*b*") was simply varied with the footprint and other LTHEX dimensions fixed (the wall thickness, *d*, was assumed equal to *b*, and thus changes in order to ensure the structural stability of the LTHEX). Figure 2.18 shows the impact on the net work output of the change of *b*.

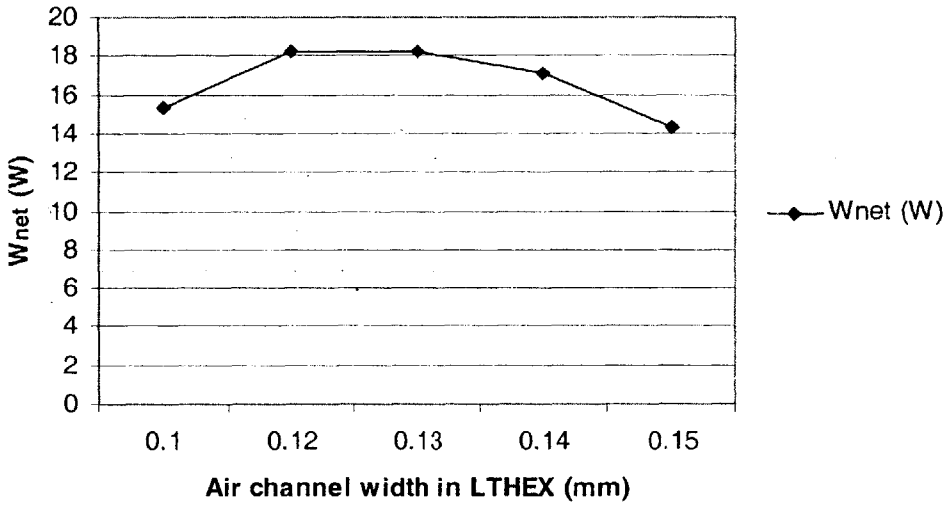


**Figure 2.18—Maximum net work output obtained by varying channel width in the LTHEX with a fixed footprint**

**LTHEX footprint equals to 4 cm by 4 cm. Turbine inlet pressure and temperature equal to 3 MPa and 650 K. Turbine pressure ratio is 2 and turbomachinery efficiency equals to 50%.**

Figure 2.18 shows that for a fixed footprint and particular assumptions of cycle parameters (such as the turbine inlet temperature and pressure, pressure drop across the turbine, etc.), there are two optimized points for $\dot{W}_{net}$ at $b = 0.12$ mm and 0.13 mm.

One drawback of this benzene cycle is its poor thermal efficiency (5%). Nevertheless, the Rankine power machine using benzene as the working fluid could generate net power of about 15 W to 20 W, and more importantly, it may be a more practical approach to physically realize the Rankine-based micro power machines.

# Chapter 3 Heat Exchanger Analysis

Heat exchanger performance is critical to achieving high efficiency in micro-scale Rankine cycles. In this chapter, counter-flow and cross-flow heat exchanger concepts are introduced. This is followed by a discussion of the design, structure and optimization of the fin-type heat exchangers. A second type of micro-scale heat exchanger design—the "hole-type" heat exchanger is also introduced and discussed.

In the macro scale, the physical size of the heat exchangers for a Rankine cycle is generally not a limitation. (An electric utility steam generator can be many stories high.) In the case of a micro-Rankine cycle, the size of the device is limited by silicon wafer size (typically 4 or 6 inches in diameter) and the wafer bonding fabrication limits. To achieve high power density in these devices, forced flow (rather than natural convection) heat exchangers must be used.

It has been shown in Chapter 2 that achieving high performance in the low temperature heat exchanger (LTHEX) is particularly important to achieving a high performance Rankine cycle system. Since the heat transfer rate and pressure drop in the LTHEX passages improve with the heat exchanger size, the LTHEX is likely to be the component with the largest footprint in the micro-scale Rankine-based engine. Thus, the LTHEX design is the focus of this chapter where the tradeoff between heat exchanger size and pressure drop through the LTHEX (blower power consumption) is considered.

## 3.1 Heat Exchanger Introduction

There are two types of heat exchangers in the micro Rankine cycle. The high temperature heat exchanger takes high temperature gas (the hot air from a micro gas turbine or a combustor) and uses that gas to boil and superheat the Rankine cycle engine's working fluid. The second heat exchanger uses ambient air to cool down and condense the working fluid in the Rankine cycle engine.

The first step in the heat exchanger design is to choose the type of heat exchanger. Figure 3.1 shows the fluid temperature variations within the exchanger for single stream, parallel flow, counter-flow and cross-flow configurations. The subscripts H and C denote the hot stream and the cold stream respectively. In the single-stream configuration, shown in Figure 3.1a, the temperature of only one of the two streams changes in the heat exchanger. The phase change region of the combined cycle LTHEX can be considered to be single-stream. In the single-stream heat exchanger, the temperature difference for the heat transfer ($T_H$-$T_C$) decreases in the flow direction.

In the parallel flow configuration, in Figure 3.1b, the two fluids flow in the same direction and, similar to the single-stream heat exchanger, the temperature difference for heat transfer decreases in the flow direction. In such a configuration, the outlet temperature of cold stream must be lower than the hot stream.

In the counter-flow configuration the fluid also flows in two parallel channels but in opposite directions. The temperature difference between the flows may decrease or increase along the length of the heat exchanger depending on the heat capacity flow rates in the fluid streams. As shown in Figure 3.1 the cold fluid outlet temperature can exceed the outlet temperature of the hot fluid. This trait allows the counter-flow heat exchanger to achieve a higher effectiveness than all other designs and it is preferred in practice. For this reason, the heat exchanger configuration chosen for the HTHEX and the LTHEX in the micro bottoming cycle is the counter-flow configuration.

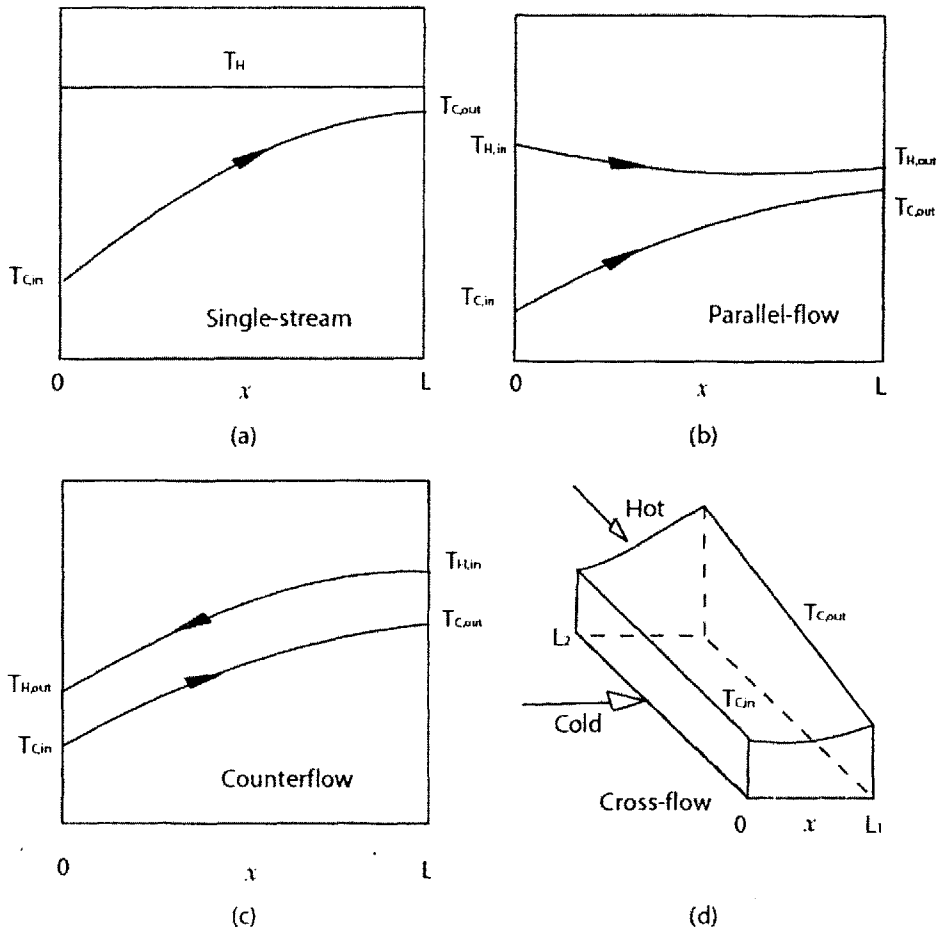


**Figure 3.1—Characteristic fluid temperature variations for various heat exchanger configurations**

Finally, the cross-flow configuration, shown in Figure 3.1d, the two streams flow at right angles to each other. It has a more complex two-dimensional temperature variation pattern that is shown in Figure 3.1d [7].

Although the counter-flow heat exchanger configuration has the highest effectiveness, in practice, other factors should also be considered. Sometimes effectiveness has to be traded off against other requirements which are equally or even more critical to the overall design. In systems where the size of the heat exchanger is a constraint, the fluids must be pumped through the heat exchanger. In the micro-Rankine machines discussed here the air must be forced (or pumped) through the heat exchanger passages. The parasitic pump power required to flow the air through the heat exchangers is taken

directly from the power turbine and is proportional to the product of the air volumetric flow rate and the pressure drop across the heat exchanger (see Equation 2.4). The optimum heat exchanger design is achieved by trading the parasitic pumping losses required against the heat transfer losses in that heat exchanger.

A cross-flow design was adopted for the heat rejection heat exchanger (HRHEX) and the cold heat exchanger (CHEX) in the micro heat pump, which will be discussed in detail in Section 3.3 and in Chapter 4. Since the heat pump design requires large forced air flows through two low temperature heat exchangers (versus one heat exchanger in the case of bottoming cycle Rankine machine), the pumping losses for that air flow are an important design parameter. As a result, a new cross-flow heat exchanger design is proposed here that has a much lower pressure drop along the air channels.

There have been air-to-air fin-type micro heat exchangers that were designed and demonstrated for the micro gas turbine engine project, see Figure 3.2 [4]. These heat exchangers were designed as the recuperators of the micro gas turbine engine. They were built by etching parallel channels into a silicon wafer and capping these channels with a silicon cover plate. Alternating channels in this array carry the hot and cold gases. There may be some mixing between these flows due to imperfections in the bonding between the cover plate and the top of the etched channel walls. These bond leaks can be tolerated in a gas turbine recuperator application because both hot and cold flows are air. In the heat exchangers of the Rankine engine, the alternating passages carry air and $H_2O$. Leakage of $H_2O$ into the air channels or air leakage into the water channels cannot be tolerated. The amount of water in the Rankine engine is very limited and any water loss results in an engine failure; leakage of air into the Rankine engine can result in a "vapor lock" in the heat exchangers or in the feedpump, again resulting in engine failure. For these reasons, the first heat exchanger design considered here, what will be referred to as the fin-type heat exchanger, will have the airflow and the water flow in channels set in separate wafers. This approach minimizes of the length of leak-tight water-to-air bonds that must be made in the heat exchanger.

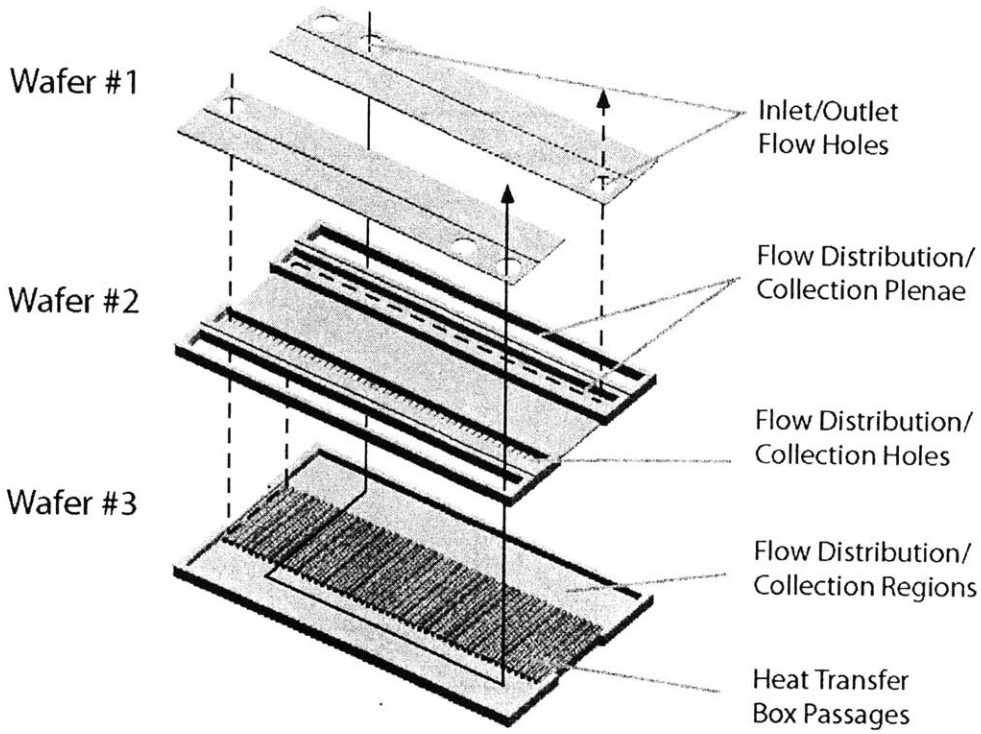


**Figure 3.2—A demonstrated air-to-air fin-type heat exchanger design**

## *3.2 Fin-Type Heat Exchanger Design and Optimization*

In this study, a stack element of a micro fin-type heat exchanger consists of a base plate with an integral set of fins, as shown in Figure 3.3. (Figure 3.3 is a cutaway view of two stacking elements and a capping plate of a typical fin-type heat exchanger.) The fins stand parallel to each other, and form fluid passages (or channels) with the base of the upper stack base. The channels in the very top stack are sealed by bonding a cap on top of the open passages. The cross-section of the channels is rectangular. The fins and the base are usually fabricated from etching into a layer of the silicon wafer.

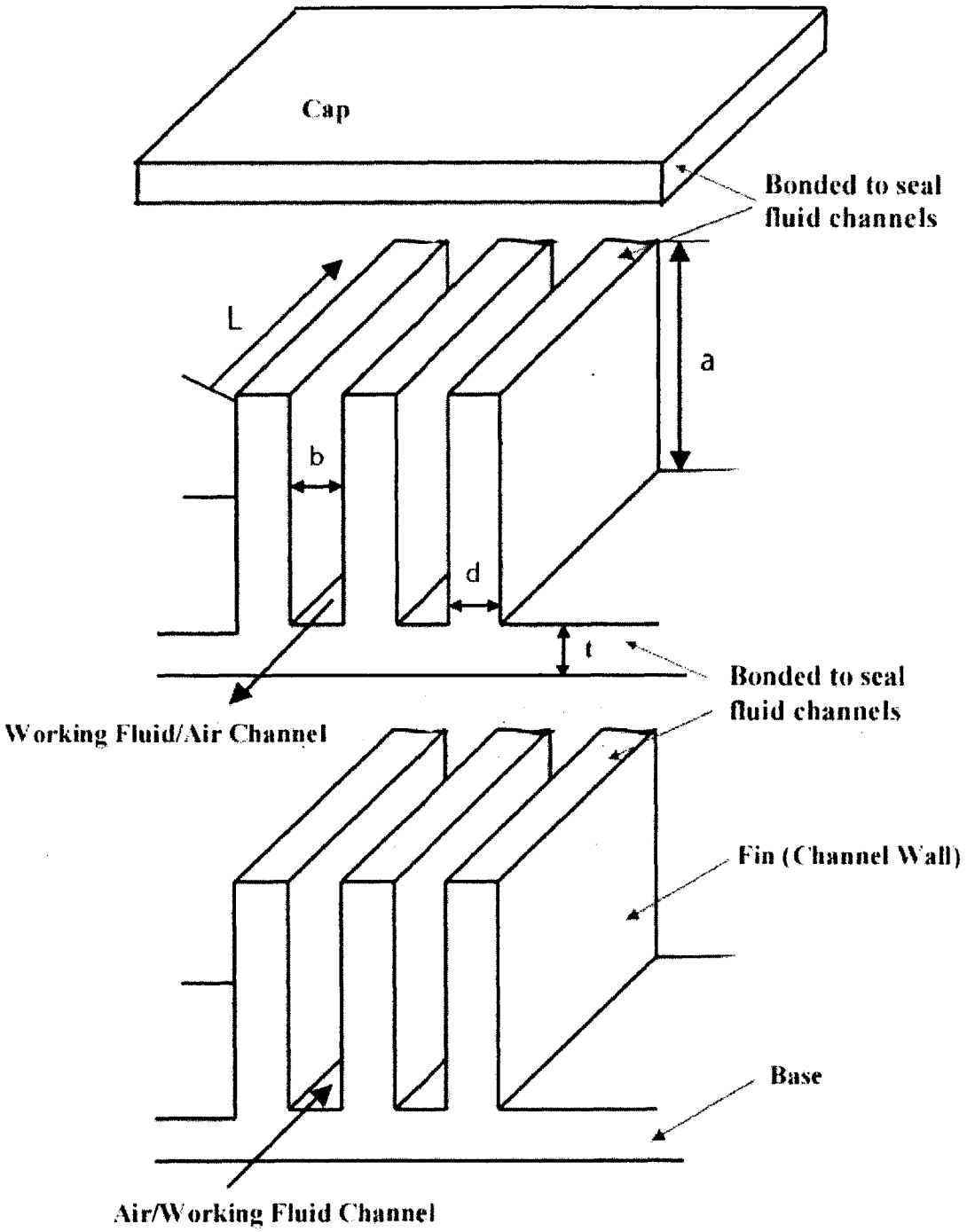


**Figure 3.3—Cutaway sketch of a fin-type heat exchanger**

**Two stacks with a sealing cap. Single channel geometry: channel width (b), fin/wall thickness (d), channel depth (a), channel length (L) and base thickness (t); number of channels: n, number of stacks: N**

The fin-type configuration was initially chosen for this work because the fabrication of fin-type geometries had been previously demonstrated [4]. A generic fin-type heat exchanger is shown in Figure 3.4. There are eight sets of parameters that must be determined to establish the design of a specific heat exchanger. The first is the air inlet and outlet conditions, namely pressure, temperature and the mass flow. The second set is the working fluid inlet and outlet conditions. The remaining sets of parameters are: the heat exchanger channel width, b; the heat exchanger channel depth, a; the heat exchanger channel length, L; the number of total channels, n; the heat exchanger fin thickness, d; and N, the number of silicon stacks. These parameters define the heat exchanger geometry and ultimately determine the cycle performance.

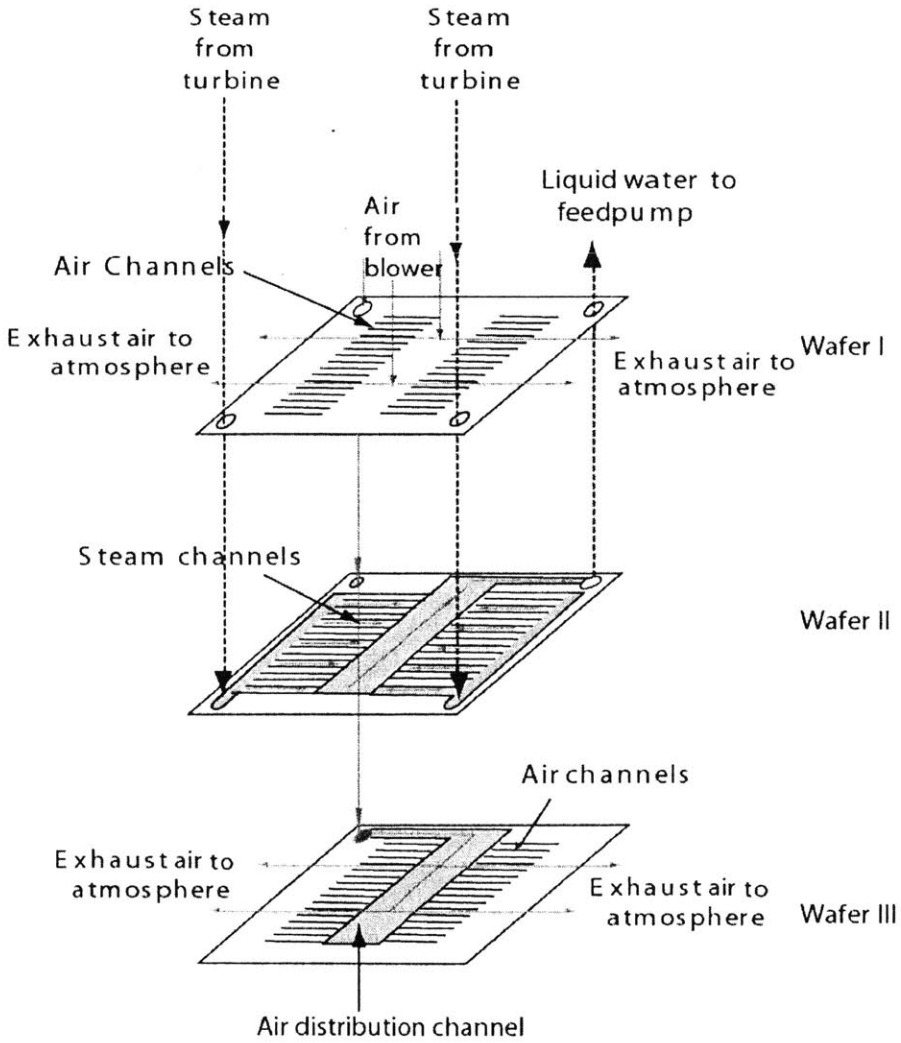


**Figure 3.4—Generic fin-type heat exchanger design**

The heat transfer in the LTHEX will be primarily determined by the effective thermal conductance on the airside of the heat exchanger. The heat of the condensing steam in the LTHEX must travel through three successive thermal resistances. The first thermal resistance is due to the liquid layer between the condensing vapor and the silicon wall of the channel. The heat then travels through the thermal resistance of the silicon walls between the air and the steam. Finally, the heat must travel through the thermal resistance of the boundary layer between the silicon wall and the air.

An estimation of the relative contributions to the heat conduction for each of the process can be made by considering a typical local LTHEX geometry shown in Fig 3.5. A simple thermal circuit equivalent is shown in Figure 3.6a and Figure 3.6b. $R_{air}$ is the thermal resistance between the air in the flow channel and the contacting surface of the silicon walls. It is equal to the reciprocal of the heat transfer coefficient ($h_{air}$) times the heat exchanger surface area exposed to the flowing air. $R_{H2O}$ is the total thermal resistance between the water in its flow channel and the contacting surface of the silicon walls. The thermal resistance through the silicon is modeled using a direct resistance, $R_{Si,2}$, and two thermal resistances through the fins, $R_{Si,1}$, and $R_{Si,3}$. These latter two resistances can be further broken down into component resistances. In the case of $R_{Si,1}$ , the components are: $R_{Si,11}$, the resistance contribution of the water-side fin; $R_{Si,12}$, the thermal resistance of the silicon between the base of the water side fin to the air-side fin; $R_{Si,13}$, the resistance contribution of the air-side fin. Using this model, it can be shown that the total thermal resistance between the flows is dominated by $R_{air}$. To show that this is the case, we use values typical to the heat exchanger for cycle Design III discussed in Chapter 2 (see Table 2.5). Since the flow is laminar, for fixed channel geometries and cooling air conditions, the heat transfer coefficient for flowing air is fixed regardless of the cycle thermal parameters. In the heat exchanger design in Table 2.5, the heat transfer coefficient of air was 1244 W/m$^2$-K with an airside surface area of 11mm$^2$ for a single channel. In this case, $R_{air}$'s value is $1/hA$= 73.1 (K/W).

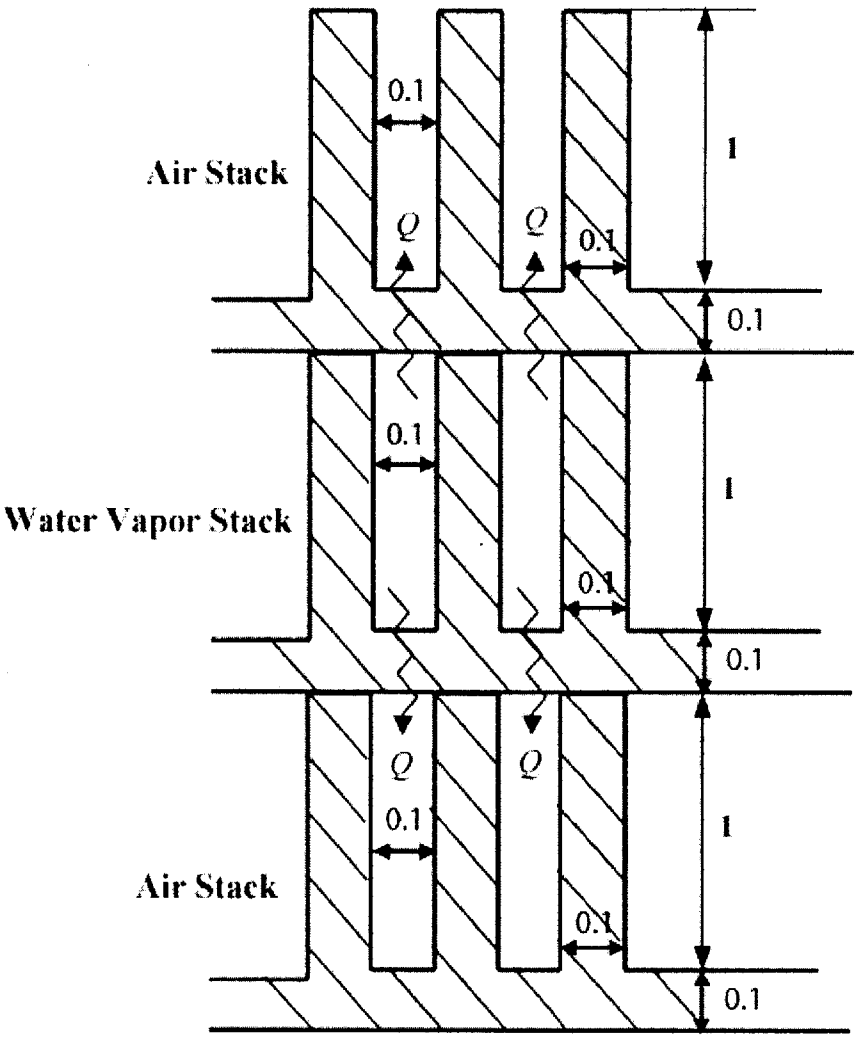


**Figure 3.5—Cross-sectional geometry of a typical LTHEX**

**Channel width = 0.1 mm, channel depth = 1 mm, fin thickness = 0.1 mm, base thickness = 0.1 mm, channel length = 5 mm.**

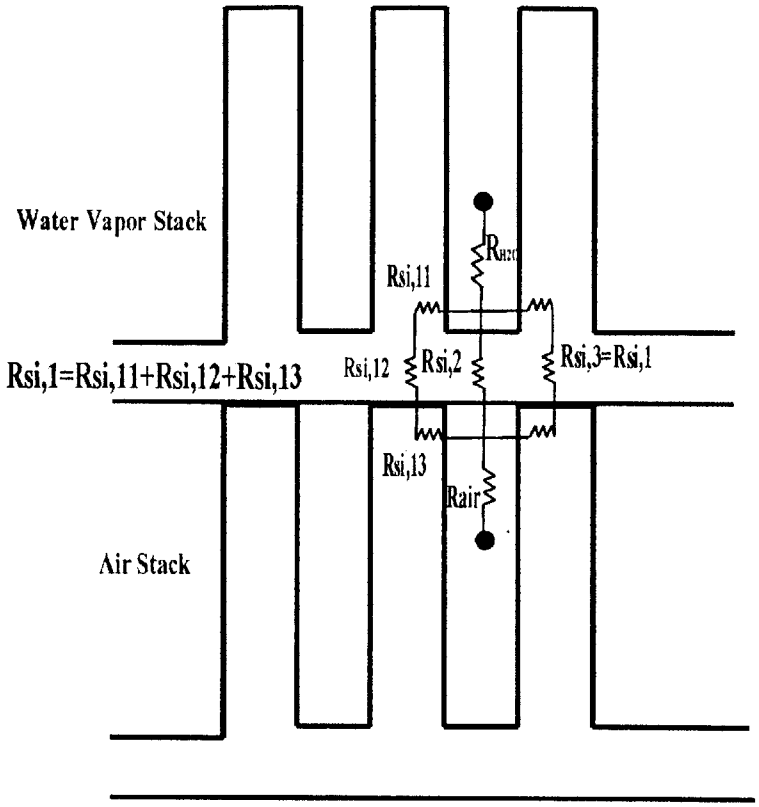


(a)

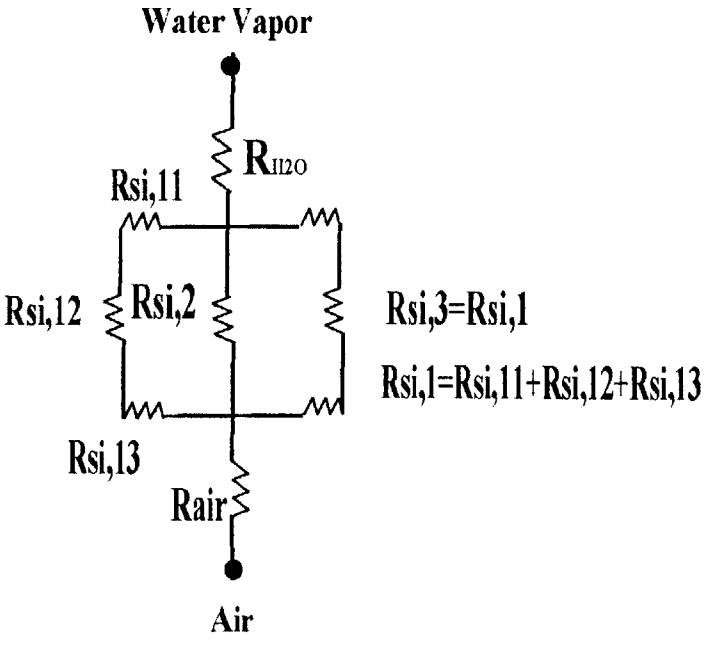


(b)

**Figure 3.6—Thermal resistance circuit equivalent of the LTHEX**

The thermal resistance of the silicon wall can be estimated using the "conduction equation" for a solid:

$$R_{Si} = \frac{L}{kA} \tag{3.1}$$

where L is the silicon wall thickness; k is the thermal conductivity of the solid and A is the heat transfer area. The thermal conductivity of silicon varies from a value of 148 W/m-K at 300 K to a value of 61.9 W/m-K at 600 K [11]. For the LTHEX a value of 100 W/m-K is appropriate, at a temperature of 400 K. In the configuration depicted in Figure 3.4, the cooling air has two sets (or stacks) of channels, on both sides of the water vapor stack. The reciprocal of the total resistance of silicon is the sum of the reciprocals of the component resistances or $\frac{1}{R_{Si,total}} = \frac{1}{R_{Si,1}} + \frac{1}{R_{Si,2}} + \frac{1}{R_{Si,3}} = \frac{2}{R_{Si,11} + R_{Si,12} + R_{Si,13}} + \frac{1}{R_{Si,2}}$.

Table 3.1 shows the geometric values used for calculating the silicon thermal resistances.

The value of $R_{Si,\ total}$ is then equals to 1.7 (K/W). $R_{steam}$ is equal to the reciprocal of the heat transfer coefficient ($h_{steam}$) times the heat exchanger surface area exposed to the steam. The heat transfer coefficient for condensing steam has a typical value of 28200 W/m$^2$-K. The surface area of the heat exchanger in contact with the steam is 5.5 mm$^2$ (to the air stack downwards). $R_{steam}$'s value is then: 1/hA = 6.4 (K/W). The total resistance is the sum of these resistances ($R_{tot} = R_{air} + R_{silicon} + R_{steam} = 73.1 + 1.7 + 6.4 = 81.2$(K/W)).

| | $R_1$ (=$R_3$) | | | $R_2$ |
|---|---|---|---|---|
| | $R_{11}$ | $R_{12}$ | $R_{13}$ | |
| L (mm) | 0.05 | 0.6 | 0.05 | 0.1 |
| A (mm$^2$) | 2.5 | 0.25 | 5 | 0.5 |
| k (W/mm-K) | 0.1 | 0.1 | 0.1 | 0.1 |
| L/kA (K/W) | 0.2 | 24 | 0.1 | 2 |
| Subtotal | $R_1$=$R_3$=24.3 K/W | | | $R_2$=2 K/W |
| Total | $R_{Si,\ total}=(1/R_1+1/R_2+1/R_3)^{-1}$=1.7 K/W | | | |

**Table 3.1—Thermal resistances of silicon walls**

The largest contribution to the thermal resistance is the resistance between the silicon wall and the air. Neglecting the contributions of the steam and the solid silicon results in a 10% error for the total thermal resistance between the two flows. Hence it is reasonable to ignore the contributions of the solid wall and condensation resistances to the total thermal resistance in the LTHEX. For this reason, all analysis in this work will assume that the thermal resistances attributed to the silicon and the condensing vapor are negligible.

The intent of this work is to optimize heat exchanger designs for the micro Rankine power systems. That is, necessarily, a compromise between the size of and the performance of the overall device. In the case of the bottoming cycle, the low temperature heat exchanger dominates the size of the device. Whereas, in the case of the waste heat driven refrigerator, the heat exchanger that rejects heat to the environment (HRHEX) dominates the size of the device (see Section 4.5). The performance of the heat exchanger is related to a product of the overall heat transfer coefficient, U, and the effective surface area of the heat exchanger, A. Equation (3.2) shows the expression of UA:

$$UA = \frac{A_{surface} \times k_{air} \times Nu}{(D_h)_{channel}} \tag{3.2}$$

The larger the UA product, the more heat is transferred for the same temperature difference of the two fluids in the heat exchanger. Seen from the equation, the UA product can be increased by either increasing the surface area (or size) of the heat exchanger (A) or increasing the heat transfer coefficient between the fluids and the heat exchanger surfaces (U). The latter increase can be achieved, for example, by increasing the fluid velocity over the heat exchange surface or decreasing the size of the channels in the heat exchanger. Unfortunately, increasing the surface area of the heat exchanger may lead to an unacceptably large device. Similarly, increasing the fluid velocity (or decreasing channel size) generally leads to unacceptably large pumping losses.

The performance of the heat exchanger is characterized by the overall effectiveness of the heat exchanger, ε, defined as the ratio of the actual heat transfer rate to the heat transfer rate of an ideal heat exchanger. This effectiveness of the low temperature heat exchanger is calculated under the assumption that, the walls of the air-channels are isothermal. This assumption can be justified by realizing that this heat exchanger involves a phase change of the working fluid (water). There is no sub-cooling in the low temperature heat exchanger, and the phase change process is dominant along the working fluid channels. The relative areas for the phase change region (where the walls are essentially isothermal) to that of the de-superheating region (where the walls change temperature) can be estimated in the following way.

The typical LTHEX design in Chapter 2 (Figure 2.10) has a water vapor inlet temperature of $T_5$ = 590 K, outlet temperature of $T_7$ = 420 K (saturated liquid), and a cooling air temperature of $T_{air,in}$ = 300 K. The mass flow rate of cooling air is 3.5 g/s, and mass flow rate of water is 0.15 g/s. Therefore, the total heat transfer can be derived: $\dot{Q}_{1-phase} = (\dot{m}C_p \Delta T_{1-phase})_{H_2O} = 53(W)$, $\dot{Q}_{2-phase} = \dot{m}_{H_2O} \times h_{fg} = 318(W)$, where $h_{fg}$ is the latent heat of water, and thus $\dot{Q}_{total} = \dot{Q}_{1-phase} + \dot{Q}_{2-phase} = 371(W)$. The heat capacity of water is evaluated at P=0.44MPa, and T=505K. Then $T_{air,out}$ can be obtained from the equation $\dot{Q} = (\dot{m}c_p \Delta T)_{air} = 371(W)$ : $T_{air,out}$ =405K. Where heat capacity of air is evaluated at T=400K and atmospheric pressure. Use LMTD (Log Mean Temperature Difference) method to estimate the UA needed for one-phase region: $(UA)_{1-phase} = \dot{Q}_{1-phase} / T_{lm} = 0.62(W/K)$. Since the water vapor side channel configuration is the same as the airside (see Figure 3.5a), except for that the channel number is half of the air channel number ($n_{vapor}$ = 450), the area needed for one-phase vapor is: $A_{1-phase} = (UA)_{1-phase} / h = 5 \times 10^{-4}(m^2)$. This is about one-sixth of the typical total surface area of $3 \times 10^{-3}(m^2)$. Thus most of the area of the heat exchanger is devoted to the phase-change process where the walls are isothermal.

There is an additional effect that tends to make the walls of the heat exchanger isothermal. The high thermal conductivity of silicon makes the longitudinal conduction in the walls of the heat exchanger non-negligible. This effect tends to mitigate the temperature variation in the one-phase region of the heat exchanger. Therefore, it is reasonable to assume the working fluid channel arrays as a heat sink where the temperature is constant.

Since the airside resistance is dominant in these heat exchangers and the walls of the heat exchangers are essentially isothermal, the heat exchanger effectiveness reduces to the form:

$$\varepsilon = 1 - e^{(-NTU)} \tag{3.3}$$

where NTU is the number of heat transfer units [7]:

$$NTU = UA/\dot{m}c_p \tag{3.4}$$

Much research on the optimization of heat exchangers on macro and micro scale has been done [12, 13, 14, 15]. Generally speaking, in the heat exchanger design, there are several interactive factors:

First, the heat exchanger must be able to transfer the heat flux required. The heat transfer rate can be calculated from the following:

$$\dot{Q}_{HEX} = \varepsilon \times \dot{Q}_{\max} = \varepsilon \times (T_{H_2O,in} - T_{air,in})(\dot{m}C_p)_{air} \tag{3.5}$$

Secondly, in micro-scale steam engines, the value of UA product is restricted by a limited heat exchanger footprint size. For example, given others fixed, the more the air channels, the more heat transfer area it has, and thus the more effective the heat exchanger (Equation 3.3 and 3.4).

Thirdly, the total cross-sectional area of the air passages in the heat exchanger (i.e. channel dimensions and number of channels) determines the amount of ambient air needed and pressure drop through low temperature heat exchanger channels. Seen from

equation (2.4), $\dot{W}_{blower}$ is determined by pressure drop and air mass flow. As the blower is powered by the steam turbine, and $\dot{W}_{turbine}$ is fixed by the designed cycle parameters, so the bigger the heat exchanger air passages, the lower the $\dot{W}_{blower}$, and thus the more net power output from the turbine. This can be seen as a tradeoff between heat exchanger/cycle performance and heat exchanger/cycle dimensions.

The optimized heat exchanger design then is one that provides high heat transfer rates with low pressure drop (requiring only a low power blower to blow air through it) with a small footprint. The analysis that follows shows the tradeoff between geometric design of the heat exchanger and the performance of the heat exchanger in the micro-scale Rankine cycles, including pressure drop, heat transfer rate, as well as its impact on the blower power consumption and overall cycle efficiency after it is embedded in the micro bottoming cycle. The ambient (cooling) air properties are all evaluated under $P_{ambient}$ = 1 atm and $T_{ambient}$ = 300 K and the walls are assumed isothermal. All flows are laminar and the heat exchanger dimensions indicated are those of the air channels of the heat exchanger.

The calculations indicate that deep channels in the heat exchanger give better flow performance (less pressure drop) and allow a smaller footprint than those having shallow channels. Figure 3.7 represents the correlation of the LTHEX channel depth vs. the blower power consumption. The heat exchanger inlet/outlet conditions, and the heat transfer rate are all based on the typical bottoming cycle designs. Specifically, the heat transfer rate of the heat exchanger is fixed ($\dot{Q}_{LTHEX}$ =350 W) with $T_{hot,in}$= $T_7$ = 420 K, and the mass flow rate of the cooling air always equals to 3.5 g/s. Channel aspect ratios (AR = *a/b*) are varied from a value of eight to two and the number of channels is increased accordingly to attain the required heat transfer rate. The channel width is fixed (0.1 mm), and the channel length is kept fixed to 3 mm and there are four sets of channels distributed on two silicon wafers. As can be seen from Figure 3.7 the work required to drive the blower decreases with increasing channel aspect ratio for a fixed heat transfer rate (again, $\dot{Q}_{LTHEX}$ = 350 W). This is because of the smaller pressure drop in deep

channels with $\dot{m}_{air}$ =*constant*. Note that the hydraulic diameter ($D_h$=$4A_c/P$) increases with the increase of the aspect ratio, and the Nusselt number as well as the product of friction factor ($f$) times Reynolds number are only functions of AR in the fully developed laminar flow, and $f$ does not change monotonically since both $fRe$ and $Re$ increase with AR. Non-linearly and non-monotonically changing though the friction factor, the dominant increase of hydraulic diameter $D_h$ overcomes this small perturbation. Thus $\Delta P$, the combination of these variables monotonically increases with the decrease of AR, which explains the growing $\dot{W}_{blower}$. Also note that the biggest AR is associated with the smallest footprint, because the deep channels give heat transfer area in the direction of their height rather than expanding the width or length of the heat exchanger. Table 3.2 lists the data for Figure 3.7.

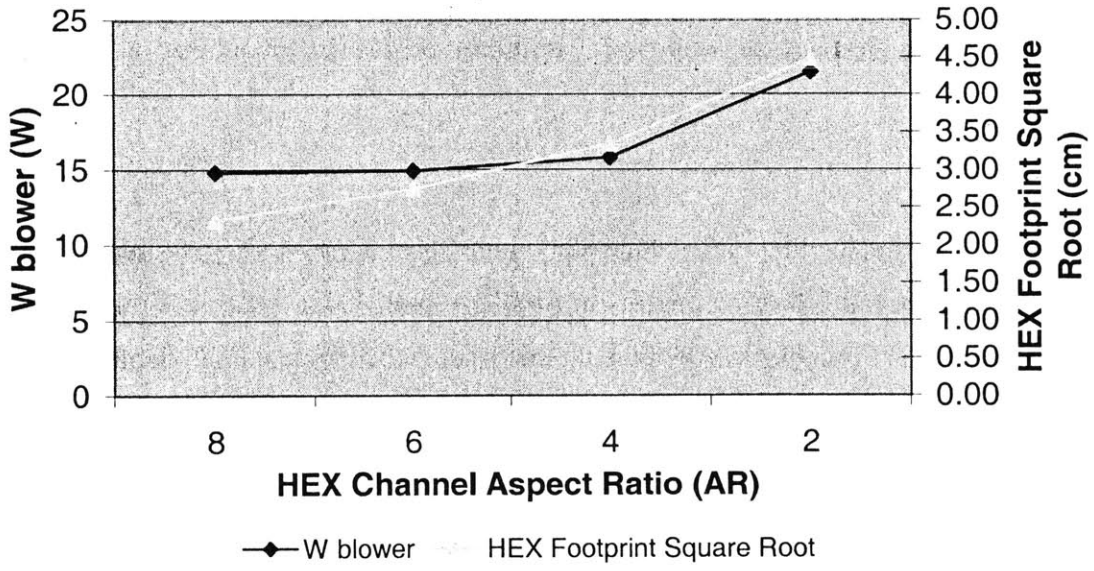


**Figure 3.7—Blower power consumption and LTHEX size as a function of channel aspect ratio**

**Assumptions:** $\dot{Q}_{LTHEX}$ **= 350 W,** $\dot{m}_{air}$ **= 3.5 g/s** $T_{hot,\ in}$**=** $T_7$**= 420 K,** $\eta_{blower}$ **= 50%, (channels distributed on 2 stacks, 2 sets of channels per wafer, and b=0.1mm)**

| Channel Length (cm) | Total Width of LTHEX (cm) (on 2 stacks, 2sets per stack) | $\sqrt{A_{footprint,LTHEX}}$ (cm) | $\dot{W}_{blower}$ (W) | Channel Aspect Ratio |
|---|---|---|---|---|
| 0.3 | 6.03 | 2.33 | 14.83 | 8 |
| 0.3 | 8.35 | 2.74 | 14.94 | 6 |
| 0.3 | 12.4 | 3.34 | 15.81 | 4 |
| 0.3 | 22.3 | 4.48 | 21.51 | 2 |

**Table 3.2—LTHEX data for Figure 3.7**

In the bottoming cycle, the cycle output work ($\dot{W}_{net}$) will therefore increase with the channel aspect ratio given other parameters are fixed. Experiments showing deep-channel heat exchangers' advantages on performance were done and presented by researchers such as Harpole [12], Samalam [13] and Harms [15].

It is well known that the heat transfer rate increases with the increase of UA. And it is obvious in Equation (3.3) and (3.4) that higher UA results in higher effectiveness. But there are restrictions to UA so that it cannot be infinitely increased: 1) Bigger UA has to be realized by the compensation of larger heat exchanger size. 2) Calculation shows that the heat flow rate per footprint area $\dot{q}_f$ of the heat exchanger decreases with the increase of UA. $\dot{q}_f$ is defined as the heat exchanger heat transfer rate divided by the footprint area of the heat exchanger defined in Equation (3.6):

$$\dot{q}_f = \frac{\dot{Q}_{HEX}}{A_{footprint}} \tag{3.6}$$

Figure 3.8 shows the correlation of UA and $\dot{Q}_{LTHEX}$ and $\dot{q}_f$ of the LTHEX performances. Similarly, $T_{hot,in} = T_7 = 420\ K$, and the mass flow rate of the cooling air equals to 3.5 g/s. And the geometry of a single channel is assumed fixed as described in the caption of Figure 3.8). The change of UA is realized by varying the number of channels only. As mentioned above, UA is an indicator of the quality of heat exchangers. Apparently, as all of the other parameters are fixed except for the number of channels, therefore, the larger

the UA, the higher the effectiveness of the LTHEX is expected (Equation 3.3 and 3.4). With fixed $\dot{Q}_{max}$, higher UA gives higher heat transfer rate (Equation 3.5).

The drop of $\dot{q}$ indicates that the heat transfer rate per unit footprint area gets smaller although the heat exchanger is able to transfer more heat per unit time. This is because the footprint expands at a rate faster than total heat transfer rate increase. Table 3.3 shows the data corresponding to Figure 3.8. "q" is the heat transfer rate per unit area of the heat exchanger footprint.

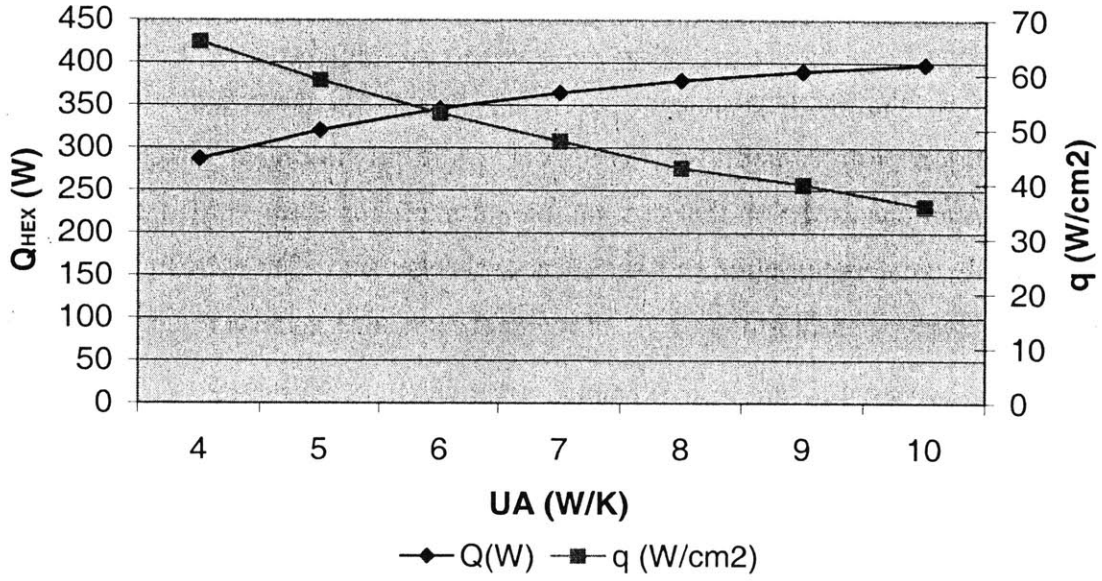


**Figure 3.8—Correlation of LTHEX UA and performance**

**Assumptions: Fixed $\dot{m}_{air}$ = 3.5 g/s $T_{hot,\,in}$= 420 K and channel geometry: b = 0.1 mm, a = 1 mm, d = 0.1 mm, and L = 3 mm.**

| $\dot{Q}_{HEX}$ (W) | $q$ (W/cm$^2$) | UA (W/K) |
|---|---|---|
| 287 | 132 | 4 |
| 320.6 | 118 | 5 |
| 345.9 | 106 | 6 |
| 364.9 | 96 | 7 |
| 379.2 | 86 | 8 |
| 390 | 80 | 9 |
| 398.2 | 72 | 10 |

**Table 3.3—Data for Figure 3.8**

When designing a LTHEX, more cooling air mass flow rate makes it easier to satisfy the heat transfer rate desired. While for a fixed heat exchanger geometric design, this can lead to high blower power consumption by two ways: first, the increase of $\dot{m}_{air}$ results in a higher pressure drop. Second, $\dot{m}_{air}$ itself is associated with the value of $\dot{W}_{blower}$, seen from Equation (2.5) and (2.14). From the calculation results, in the bottoming cycle LTHEX pressure drop is under 3.5 kPa, and does not exceed 5 kPa in order to keep a tolerable $\dot{W}_{blower}$ (cycle output $\dot{W}_{net} > 0$). Therefore, it is of interest to examine the impact of cooling air mass flow rate on the cycle performance.

Figure 3.9 shows the variation of $\dot{W}_{net}$, $\eta_{thermal}$, and $\Delta P$ in the LTHEX with $\dot{m}_{coolingair}$ for the Rankine bottoming machine. Under fixed water mass flow rate, the mass flow rate of the cooling air in the LTHEX varies from 1.7 g/s to 4.6 g/s. Accordingly, the water saturation temperature at the exit of the condenser, $T_7$, varies from 440 K to 360 K. Then the cycle power output $\dot{W}_{net}$ was optimized at each $T_7$, by following the calculation process described in Chapter 2. The dimensions of the low temperature heat exchanger are: b = d = 0.1 mm, a = 2 mm, L = 5 mm, and n = 480. Table 3.4 shows the data corresponding to Figure 3.9.

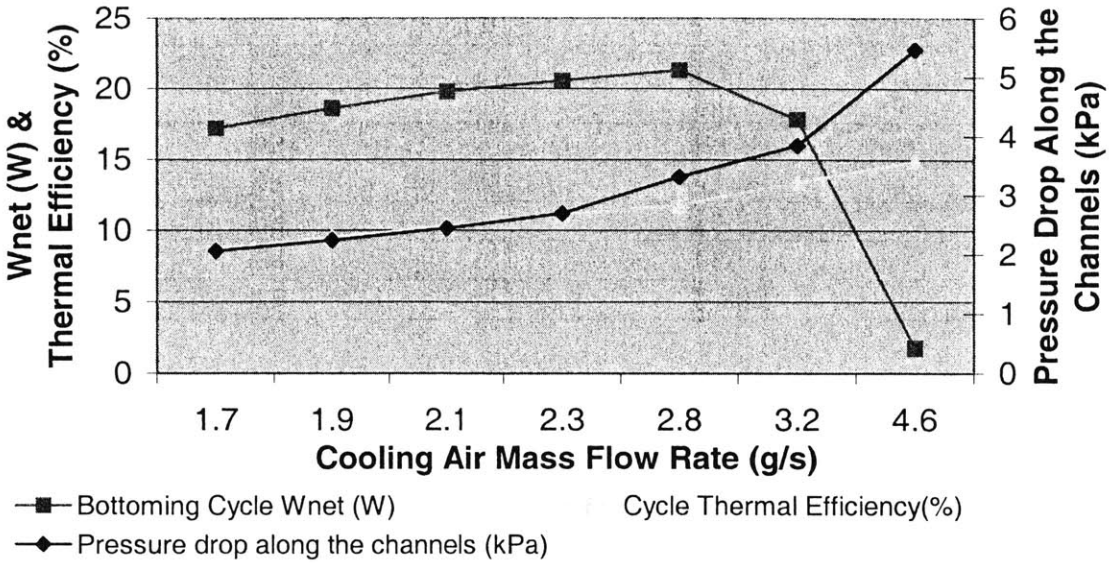


**Figure 3.9—Rankine bottoming power machine & LTHEX performance as a function of $\dot{m}_{coolingair}$.**

**Assumptions: Cycle: fixed $\dot{m}_{hotair}$ =1 g/s, $T_4$=770K, $T_7$=440~360 K, $\eta_{turbomachinery}$=50%.**

**Channel geometry: b = d = 0.1 mm, a = 2 mm, L = 5 mm, and n = 480.**

| $T_7$ (K) | $\eta_{thermal}$ (%) | $\dot{W}_{net}$ (W) | $\dot{m}_{coolingair}$ (g/s) | $\Delta P$ (kPa) |
|---|---|---|---|---|
| 440 | 8.73 | 17.24 | 1.7 | 2.06 |
| 430 | 9.5 | 18.64 | 1.9 | 2.24 |
| 420 | 10.3 | 19.8 | 2.1 | 2.44 |
| 410 | 11.1 | 20.59 | 2.3 | 2.69 |
| 400 | 11.8 | 21.31 | 2.8 | 3.31 |
| 380 | 13.4 | 17.86 | 3.2 | 3.84 |
| 360 | 14.9 | 1.79 | 4.6 | 5.46 |

**Table 3.4—Data for Figure 3.7**

Seen from Figure 3.9, the addition of cooling air mass flow rate results in higher thermal efficiency, since the condition of the hot side of the bottoming cycle doesn't change when the cold side temperature decreases (from 440 K to 360 K). The pumping losses due to pressure drop in the heat exchanger eventually starts to increase faster than thermal efficiency at some point ($\dot{m}_{coolingair}$ = 2.8 g/s, or $T_7$ = 420 K), which makes the additional eventually negates and dominates the gains from increasing cycle efficiency. This leads to a maximum in $\dot{W}_{net}$, in Figure 3.9. Therefore, the mass flow rate of the cooling air should be carefully chosen to balance these effects.

For a restricted footprint, deep-channel heat exchangers have better performances than those with shallower channels, and tradeoffs must be made between dimensions and performance. From practical aspects, there are other issues to be considered in the design work, such as fabrication and manufacturability. For example, the limitation of fabrication techniques should also be considered when high aspect ratio channels are desired. Under the current silicon etching ability, the maximum channel aspect ratio is about 20:1. Therefore the channel aspect ratio should not be designed bigger. There is also a limitation on the silicon wafer bonding. The MIT micro engine group has successfully bonded six-wafer stacks with an average thickness of 1 mm. Bonding of more wafers is possible, but currently bonding more than nine wafers of this type is still practically impossible. Besides the wafer number, bonding ability is also associated with the wafer thickness. Simply speaking, the thicker the wafers, the harder it is to be bond together because of the stiffness. The stiffness is proportional to (wafer diameter)×(wafer thickness)$^3$. For example, the upper limit of bonding two 4-inch wafers is about 1mm, so for a 6-inch wafer, the maximum thickness allowed is 1.14mm. However, it is easier to bond rather thinner wafer (~0.5 mm) to a fairly thick wafer (~2 mm).

Another design option for the channel type heat exchanger geometry is shown in Figure 3.10 where the working fluid channels and the cooling air channels are etched from opposite sides of one silicon wafer. In this design, the working fluids are supplied from different sides of the wafer. Since adjacent channels on one side of the wafer contain the same working fluid, channel-to-channel leaks due to imperfect cap-to-wall bonds do not

result in a net loss of the working fluid. Another advantage of this design is that the air and working fluid channels are in more intimate thermal contact since both passages are etched into the same wafer. In the design discussed above, the air channels are placed on one wafer and the working fluid channels on another wafer.

There are negative aspects to this design. Since the air volumetric flow rate is much bigger (about ten thousand times) than that of the water in the bottoming cycle, at least two stacks of air channels are needed in order to keep a small footprint. Making the water vapor channels on the same level of the air channels inevitably increases the dimension of the total width of the passages. Therefore, at least two stacks of these passages will be needed, which makes the fluid distribution more complicated. In addition, adoption of this design may need additional fluid distribution layers, resulting in more complex design to fabricate.

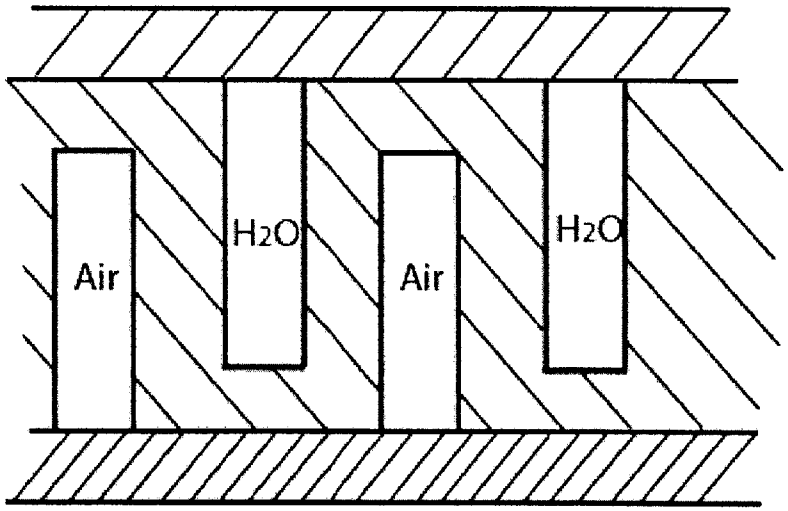


**Figure 3.10—An alternative counter-flow heat exchanger design (cross-section)**

## *3.3 Hole-Type Heat Exchanger Design*

Typically, the blower in the bottoming cycle discussed in Chapter 2 consumes more than 40% of the turbine power output. This can be improved by increasing the cross sectional area of the heat exchanger channels. This would require an increase in the footprint of the fin-type heat exchanger, given the fabrication restrictions (fin thickness, channel depth, etc.). In this section a new concept micro heat exchanger, a "hole-type" heat exchanger, is introduced and analyzed. The new design reduces the blower power consumption by an order of magnitude by reducing the pressure drop for the same heat transfer rate and with the same footprint as the fin-type heat exchanger.

### 3.3.1 Hole-type Heat Exchanger Introduction

Figure 3.11 is a schematic drawing of the hole-type heat exchanger structure. This heat exchanger is a cross-flow type. Air streams flow vertically through etched holes in the silicon plate (The diameter of these holes is between 200 and 300 microns). The air comes from the blower and is released to the ambient after passing through those holes. Rectangular channels for the working fluid are etched between these arrays of holes. To get the best heat transfer effect, rows of the air holes and working fluid passages should be alternated on the wafer surface (one-to-one ideally).

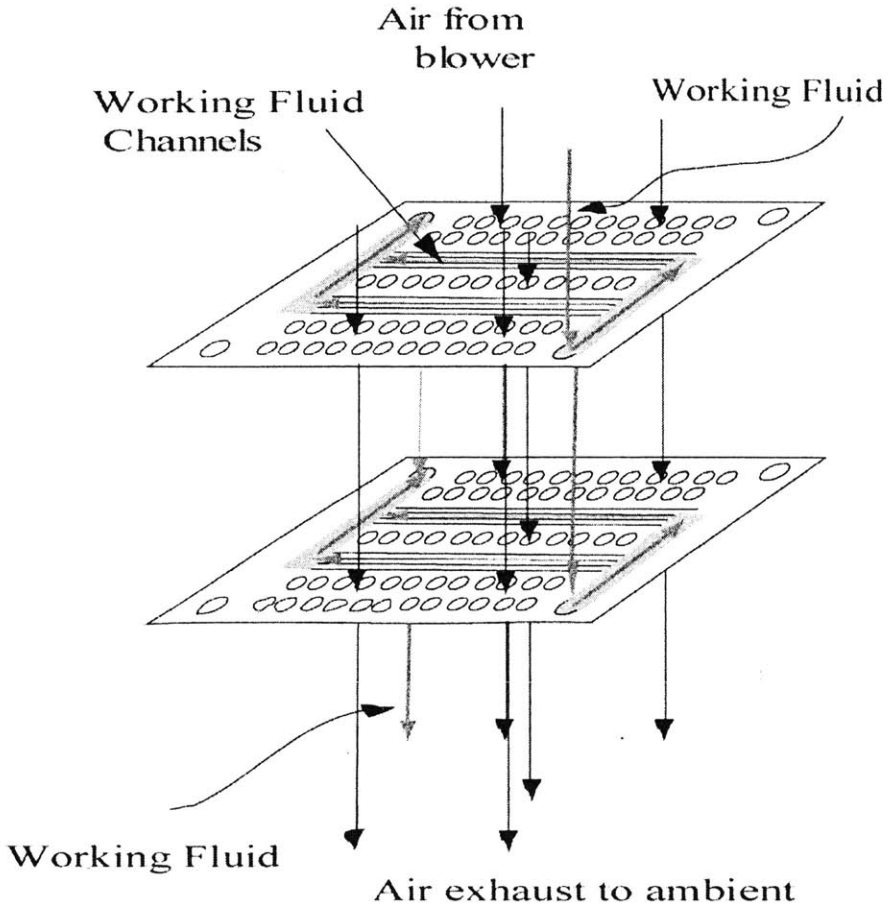


**Figure 3.11—A schematic hole-type heat exchanger structure**

Figure 3.12 is a cutaway view of the hole-type heat exchanger (one stack only). In this figure, the horizontal working fluid channel passes between the vertical air holes. It can be seen that the air holes are etched through the whole thickness of the silicon wafer, and a heat exchanger could have several bonded stacks with the holes aligned. Thus the length of the holes is equal to thickness of the wafer times the number of the stacks.

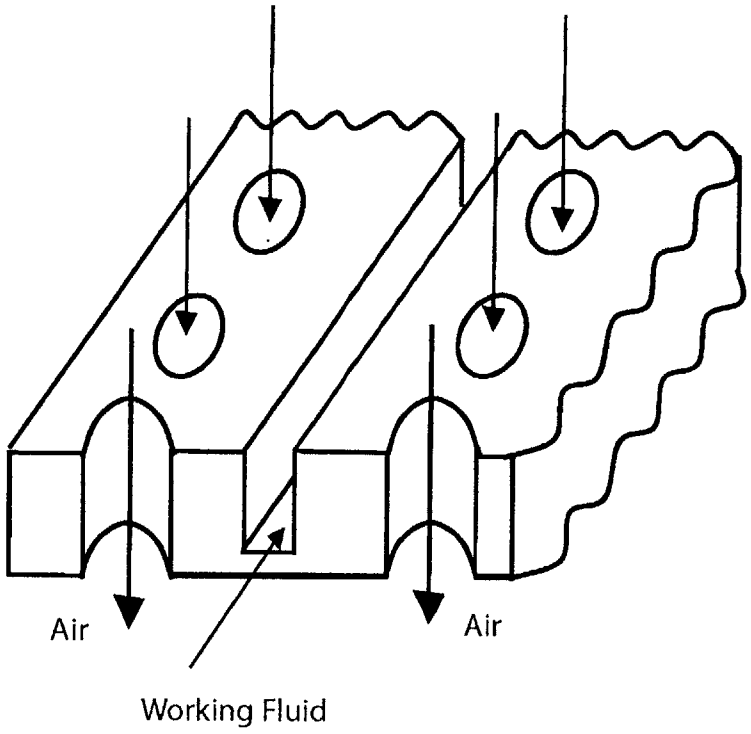


**Figure 3.12—Hole-type heat exchanger cutaway**

The primary advantage of the hole-type heat exchanger over the fin-type heat exchanger is the low airside pressure drop under similar heat transfer rates and heat exchanger sizes. For example, if the hole-type design were adopted in the bottoming cycle, the airside pressure drop would be in the order of $10^2$ Pa compared to $10^3$ Pa for a fin-type design. The low pressure drop of the hole-type heat exchanger comes from the use of many short air passages that can easily be formed by etching directly through the short dimension of the wafer (its thickness). In the fin-type design, the channels run in the long direction of the wafer. Short channel designs in the long direction of the wafer result in a significant waste of wafer "real estate" for fluid distribution channels. The net effect is that the hole-type heat exchanger performance is superior to that of the fin-type.

Another advantage of the hole-type design over the fin-type is that the all the etched layers of the hole-type are identical, requiring only one mask to fabricate it, whereas the fin-type will probably require at least two masks to fabricate it.

The fabrication of hole-type design heat exchangers is easier than fin-type heat exchangers because the "drilling" of small holes in the wafer is less complicated than etching deep channels. The hole-type heat exchanger design also makes the flow paths of both working fluid and air less complicated. The alignment of holes in different layers is easily done. Wafers are routinely aligned to a precision of 1 micron, which is far smaller than the diameter of the air holes (order of 100 microns).

### 3.3.2 Comparison of the Fin-type and Hole-type Heat Exchanger Performances

Results of calculations for two comparable heat exchanger designs, one of the fin-type and the other of the hole-type, are shown in Figure 3.13. This figure contains plots of the heat transfer rates and pressure drops versus air mass flow rate for the two heat exchanger designs with the same footprint. From these plots, the heat transfer rates of these heat exchangers are nearly identical; however, the pressure drop of the hole-type heat exchanger is about twenty times lower than the fin-type design.

The assumptions and specifics of the heat exchanger geometries used in the calculations for Figure 3.13 are shown in Table 3.5. The calculations were done by considering the airside only, regardless of the working fluid. Concluding from the chart, the hole-type design has much lower pressure drop than the fin-type design heat exchangers, and theoretically, decreasing the pressure drop in the LTHEX by a factor of ten would result in a significant increase of the $\dot{W}_{net}$. As stated before, hole-type heat exchangers make more efficient use of the silicon wafer area, shown in this case, that the hole-type design gives more cross-sectional area (490 $mm^2$ vs. 72 $mm^2$), which explains the tremendous pressure drop improvement.

There are also some drawbacks and challenges for the hole-type heat exchanger. For example, this cross-flow design increases the risk of leakage between the working fluid and air passages, because the length of the critical seals made by the wafer bonds are longer in the hole-type design than in the fin-type design heat exchanger.

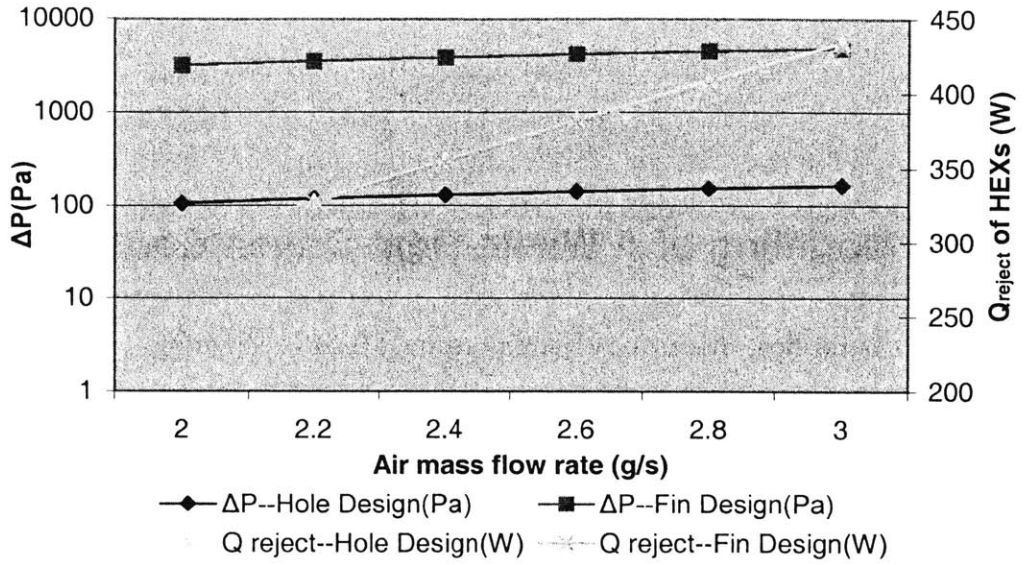


**Figure 3.13—Performance comparison of fin-type design and hole-type design The two heat exchanger designs have the same footprint (5.75 $cm^2$) and dimensions are shown in Table 3.5.**

| | | | |
|---|---|---|---|
| $\dot{m}_{air}$ | 2-3 g/s | $P_{ambient}$ | 1 atm |
| $T_{ambient}$ | 300 K | $T_{working\ fluid,\ in}$ | 450 K |
| Footprint | 5.75 $cm^2$ | Total number of silicon stacks | 3 |
| **Hole type:** | | | |
| Hole diameter | 0.13 mm | Distance between hole centers | 0.1 mm |
| Rows of holes per stack | 123 | Wafer thickness | 1 mm |
| Number of holes per row | 75 | Length of holes | 1 mm × 3 stacks |
| **Fin type:** | | | |
| Channel width | 0.08 mm | Wall thickness | 0.08 mm |
| Channel depth | 1 mm | Sets of channels per stack | 4 |
| Channel length | 3.04 mm | Number of air channels | 450 × 2 stacks |
| Note: There is a third stack in the fin-type heat exchanger for the working fluid. | | | |

**Table 3.5—Assumptions and specifics of the LTHEX geometries for Figure 3.13**

# Chapter 4 Modeling of A Waste-Heat-Driven Cooler

It is possible to build heat-driven heat pumps using MEMS technology. Such a heat pump could take advantage of the waste heat of the micro gas turbine to provide cooling. Possible applications of such a device would include cooling biological suits and condensing drinking water from the surrounding air.

In this chapter, the prospect of a waste-heat-driven cooler (or "heat pump" or "waste heat cooler" hereafter) is discussed. The cycle overview of the combined Rankine cycle/vapor compression cycle system is introduced. A straw man design of a practical device is discussed followed by a discussion of the method of analysis and assumptions of that analysis. A heat-driven heat pump necessarily interacts with three thermal reservoirs: the high temperature heat source, the cooled low temperature reservoir, and the ambient thermal reservoir to which all waste heat is rejected. Five different designs, each operating with a different refrigerant discharge temperature from the ambient heat exchanger, were developed and analyzed using an ambient temperature of 300 K. The design with the best performance under these conditions was chosen for further analysis. There were several limitations imposed on these designs, for example, the footprint of the cooler was required to be smaller than a 7cm by 7cm, and each heat exchanger in the cooler was limited to a maximum of four wafers. The best performer of these designs was further analyzed under varied conditions of humidity and ambient temperature. This analysis also considers the effect of an improved turbomachinery performance. The chapter concludes with a summary of the results of the analysis.

## 4.1 Cycle Overview

The cycle analyzed here consists of a Rankine cycle driving a vapor compression cycle, as shown in Figure 4.1. Here the Rankine engine absorbs heat from the hot gases passing through its high temperature heat exchanger and discharges heat to the ambient air. The work generated by the Rankine engine is used to drive a vapor compression refrigerator that absorbs heat from the air driven through its low temperature heat exchanger and rejects heat to the ambient. Water in the air driven through the cold heart exchanger will condense as the air is cooled and can be collected.

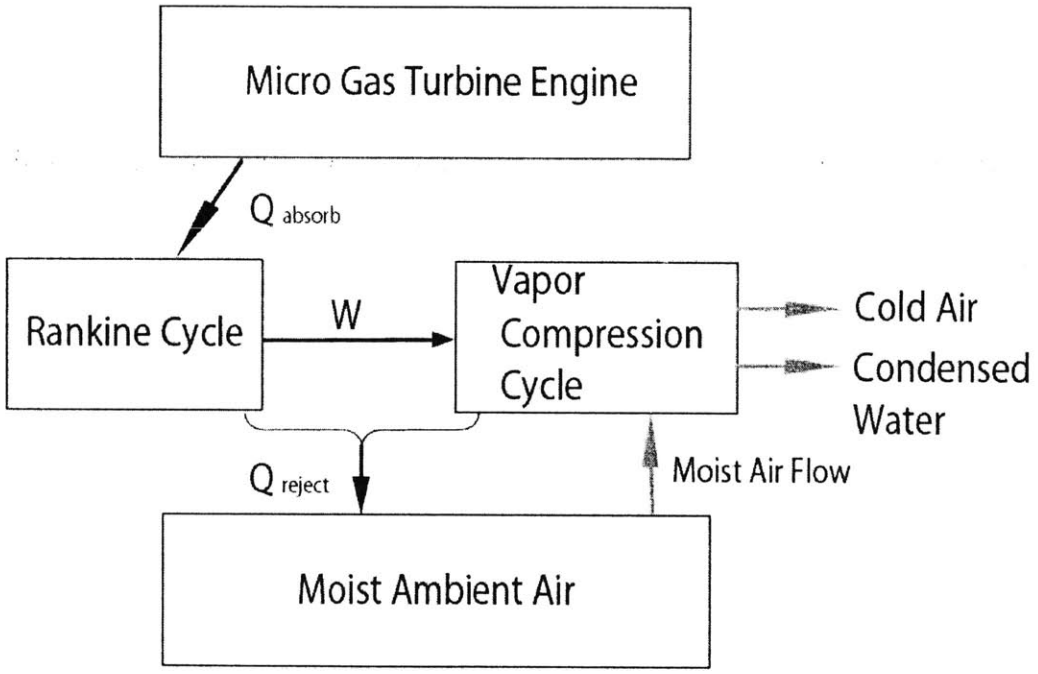


**Figure 4.1— Block diagram of a micro waste heat cooler**

A simple vapor compression cycle and its T-s diagram are shown in Figure 4.2 and Figure 4.3. In this cycle vapor is compressed (state a-b), condensed to saturated liquid (state b-c), and expanded (state c-d). From state d to state a, the low-pressure two-phase fluid is vaporized and starts the compression process again. The condensation and the vaporization processes are realized in two heat exchangers, the condenser that rejects heat with the ambient air and the evaporator that absorbs heat from the cold air stream.

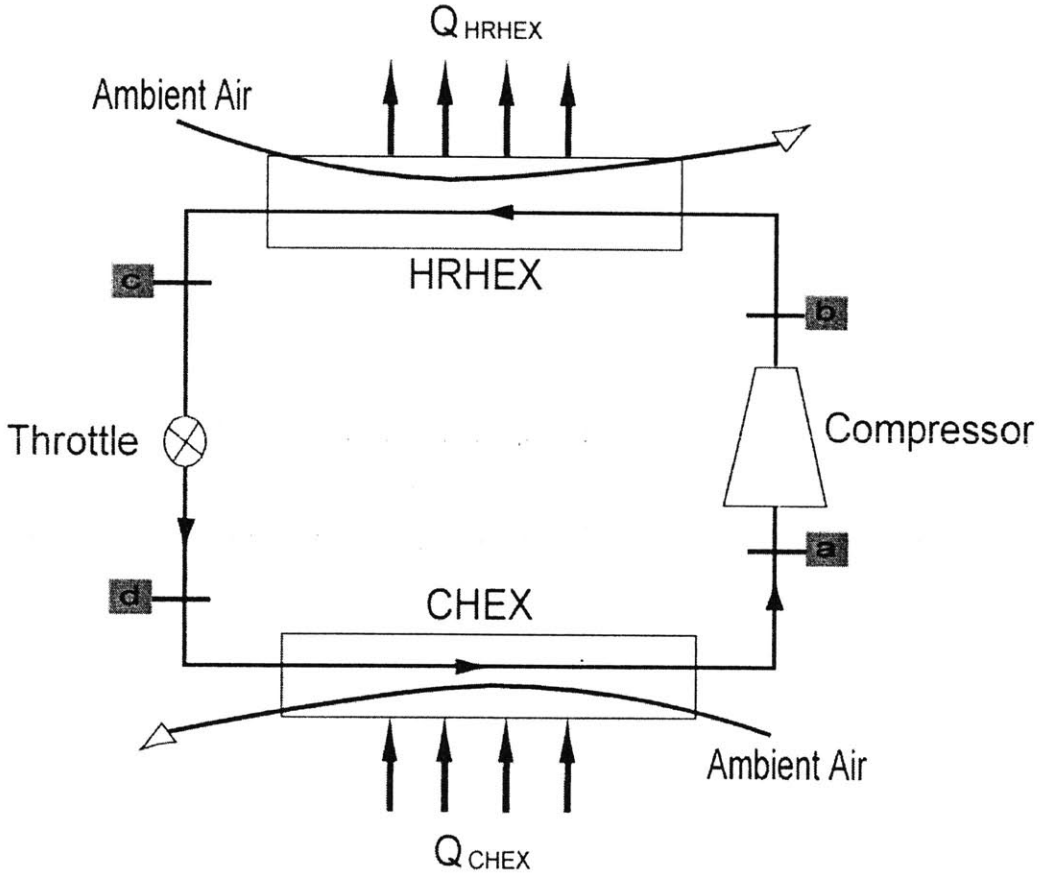


**Figure 4.2—Block diagram of a vapor compression cycle**

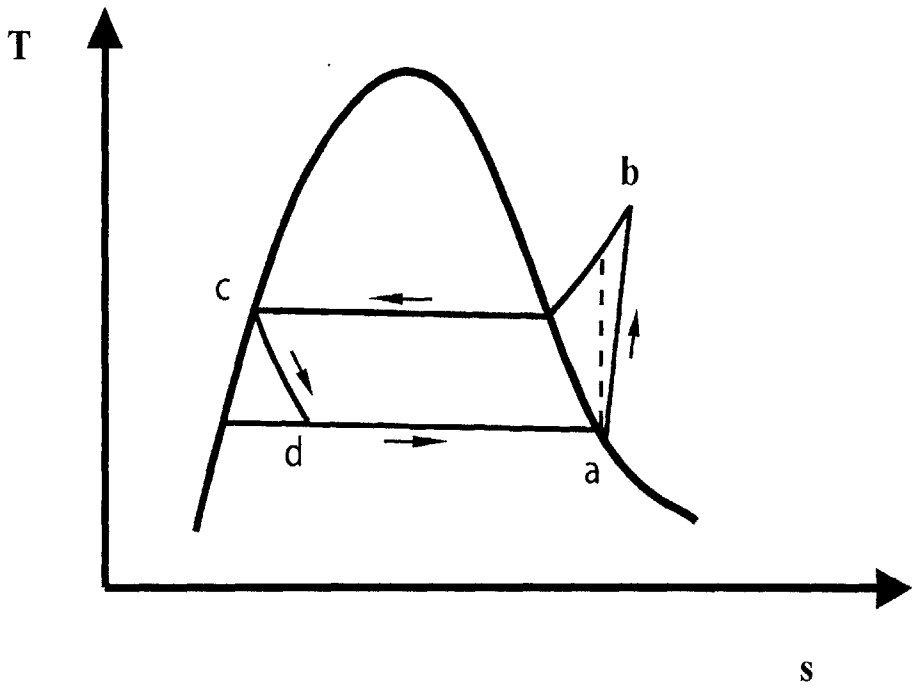


**Figure 4.3— Vapor compression cycle T-s diagram**

In a conceptually simple heat pump design, the Rankine engine output shaft is directly connected to the vapor compression cycles compressor drive shaft. The working fluid in the Rankine cycle is separate from the working fluid of the vapor compression machine. In a more practical (less complex) design the working fluid of the Rankine and vapor compression machines can be the same allowing the cycles to share their ambient temperature heat exchanger. Figure 4.4 is the T-s diagram of the combined refrigeration cycle and Figure 4.5 is its block diagram.

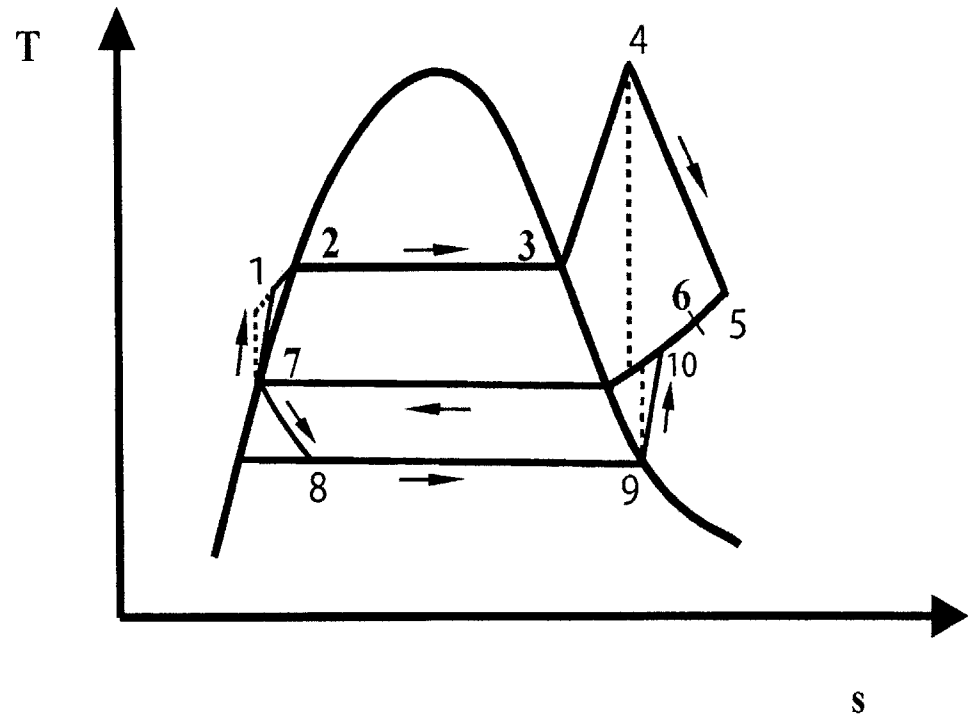


**Figure 4.4— Combined heat pump cycle T-s diagram**

The fluid that flows around the upper loop of Figure 4.5 executes the Rankine cycle. More specifically, it is the fluid that flows through the high temperature heat exchanger (HTHEX) into the turbine through the heat rejection heat exchanger (HRHEX) and then through the feedpump back to the high temperature heat exchanger (states 1-4-5-6-7-1) that executes the Rankine cycle. Similarly, the vapor compression cycle is executed by the fluid that flows around the lower loop of Figure 4.5. The working fluid going out of the HRHEX enters the throttle to lower its pressure, and goes through the cold exchanger (CHEX) into the compressor. The high-pressure working fluid then goes back to the HRHEX. The "vapor compression" fluid particle goes through states 6-7-8-9-10-6.

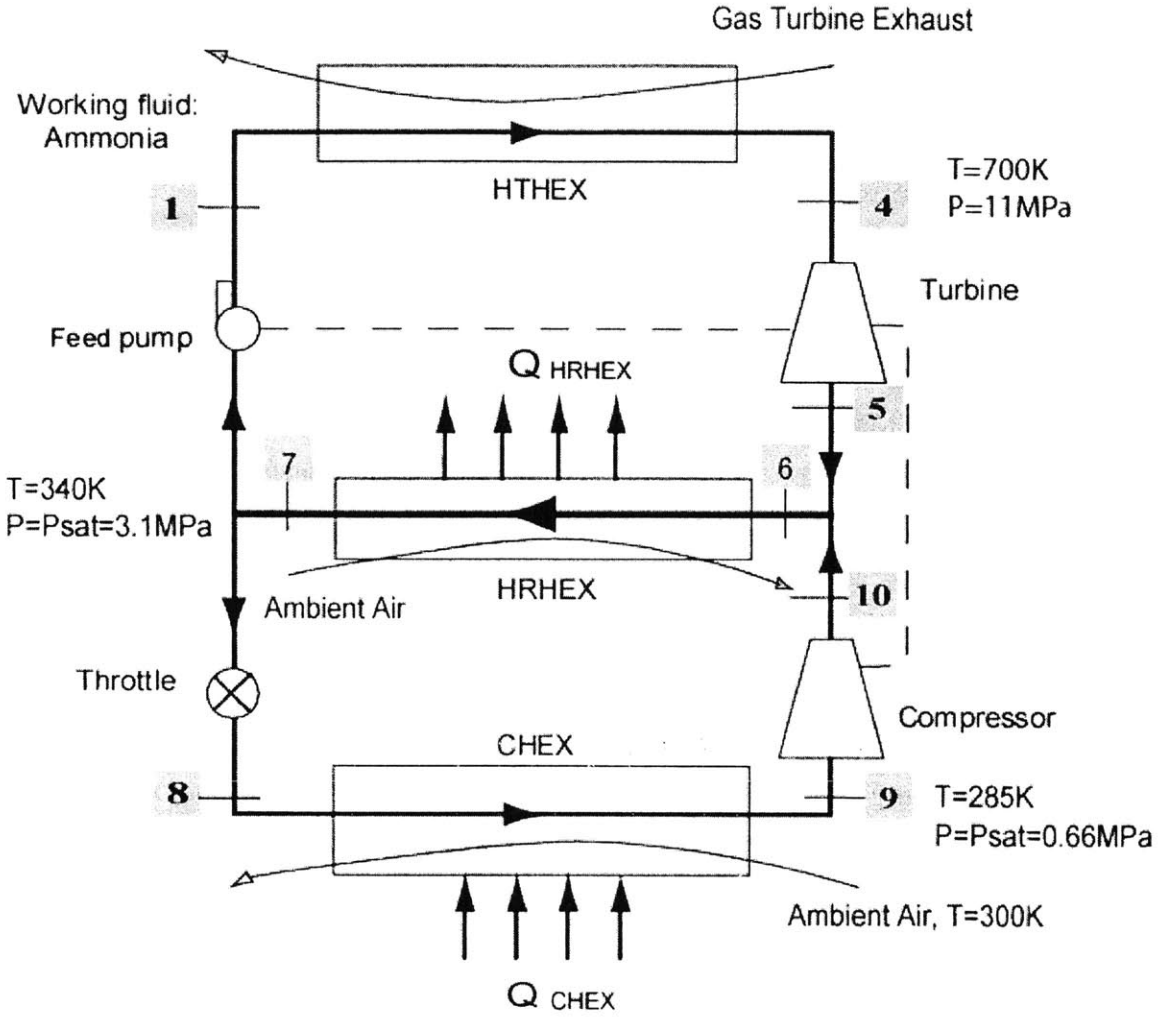


**Figure 4.5— Schematic Graph of A Waste Heat Cooler**

The compressed vapor in the vapor compression cycle meets and mixes with the vapor stream coming out of the turbine from the Rankine cycle at the entrance of the HRHEX (state 6). The HRHEX cools and condenses this mixed vapor to a saturated liquid state (state 7). (This process is the same as the LTHEX in Chapter 2's bottoming Rankine power cycle.) Most of the saturated liquid then flows into the feedpump, with the remainder flowing through the throttle to the cold heat exchanger. The flow directions are as shown in Figure 4.4 and Figure 4.5.

Forced convection is needed to keep the overall size of the heat exchangers reasonable. As a result, a blower is necessary to blow the ambient air through the HRHEX and the CHEX. Therefore, the waste-heat driven heat pump consists of eight parts: a HTHEX, a feedpump, a turbine, a blower, a compressor, a throttle, a HRHEX and a CHEX. The feedpump, blower and compressor are all powered by the turbine.

In this work, the working fluid is assumed to be ammonia. Ammonia is widely known to be an excellent refrigerant for temperatures around 300 K. The working pressures are also reasonable. For example, the vapor pressure of ammonia is 0.66 MPa at 280 K and 3.08 MPa at 340 K. In addition, ammonia is stable to the high temperatures assumed in this work. In the calculations that follow, a typical pressure is 655 kPa in the CHEX, 3 MPa in the HRHEX and 11MPa in the HTHEX.

## *4.2 System Layout and Design*

One possible "straw man" design of the combined gas turbine and heat-driven heat pump is shown in Figure 4.6. The whole device is composed of 4 modules: a micro gas turbine engine and the HTHEX module, turbomachinery module, HRHEX module, CHEX and water collection reservoir module.

In the micro gas turbine engine and HTHEX module, ambient air is ingested by the gas turbine engine, compressed, mixed with fuel and combusted, and expanded through the turbine. This air then passes through the HTHEX channels into the atmosphere as shown. The turbomachinery module contains all of the heat pump's turbomachinery: a turbine, a pump, a compressor and a blower. The blower drives ambient air through the HRHEX and CHEX air channels as shown by the paths in Figure 4.6.

The HRHEX and CHEX modules are also shown in Figure 4.6. The cross-flow hole-type heat exchanger design is assumed for the HRHEX and the CHEX to minimize the blower power consumption (see section 3.2). The water vapor contained in the ambient air is condensed in the CHEX, which is then collected in the water collection reservoir.

Connecting tubes between these modules allow fluid flow between the modules as well as thermal isolation. As already discussed in Chapter 2, current fabrication practice limits wafer stacks to about five wafers. This tube-connected module approach allows several five-wafer modules to be connected into an operating machine.

Figure 4.7 illustrates details of the flow paths in the waste heat cooler. Note that there are two additional silicon layers under the blower and the HRHEX respectively for the purpose of air distribution into the hole-type heat exchangers. The water collection reservoir is not shown in this figure.

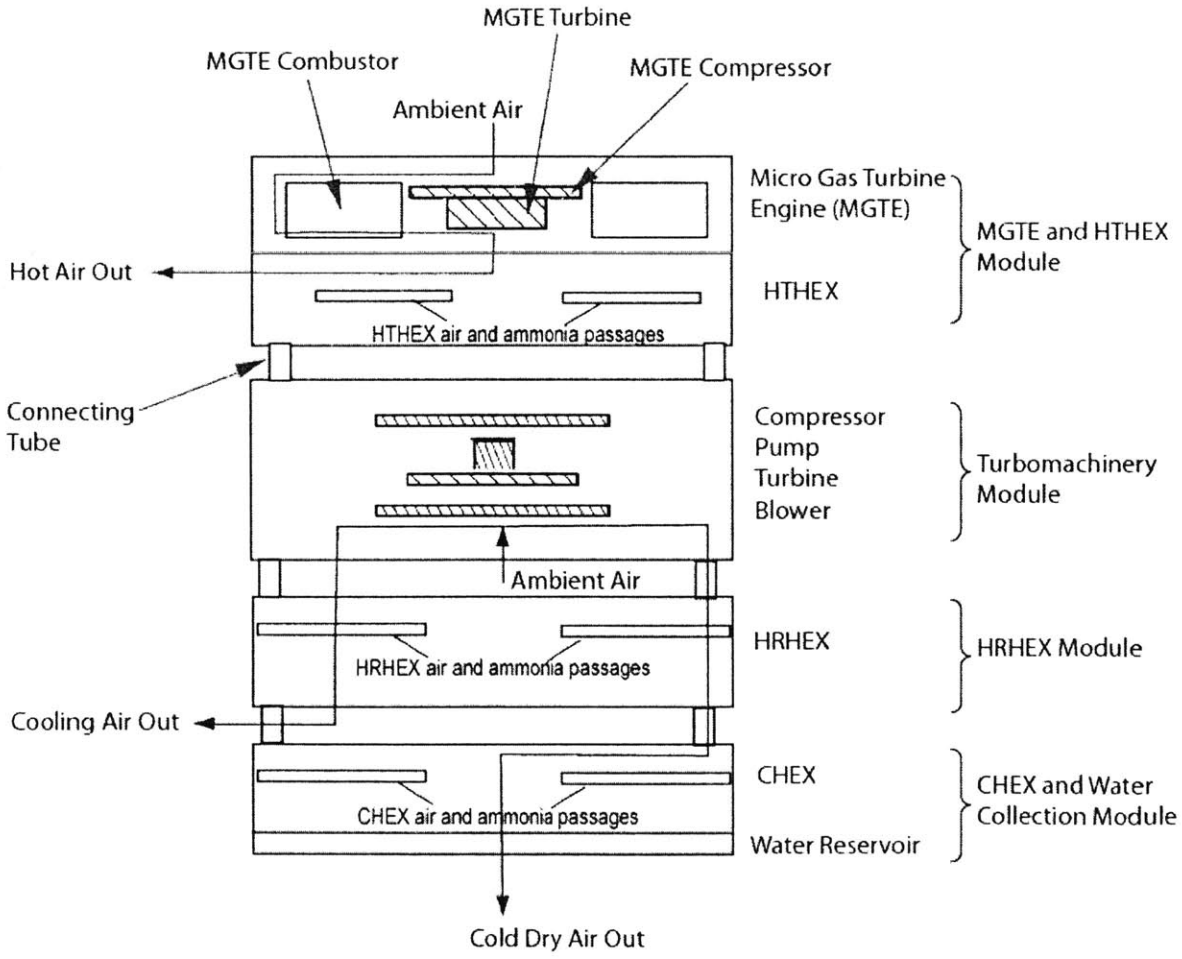


**Figure 4.6—Modular design for the combined waste heat cooler**

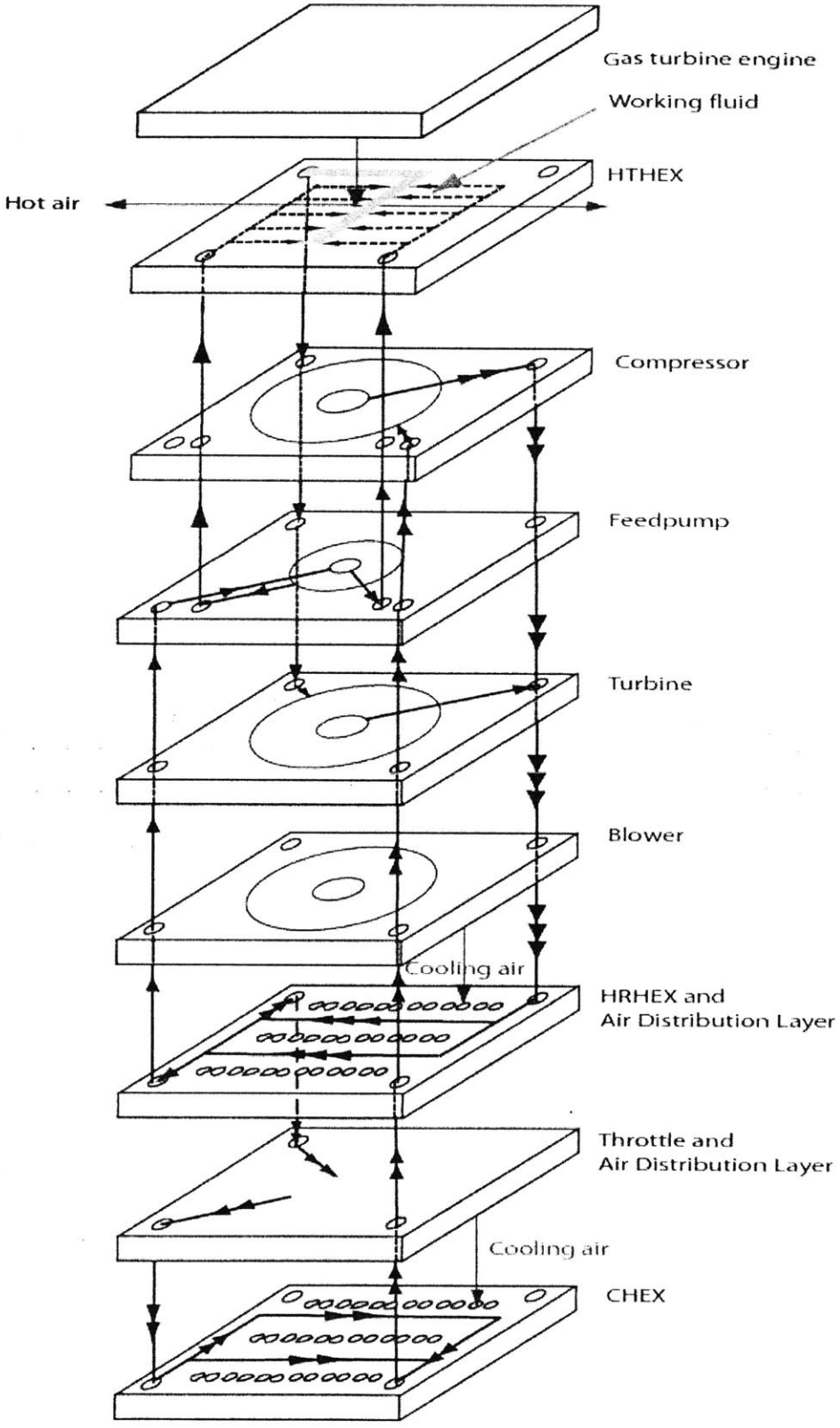


**Figure 4.7—Flow paths of the combined waste heat cooler**

## 4.3 Basic Assumptions and Modeling

The operating conditions assumed for this analysis of the waste heat cooler are summarized in Table 4.1. The analysis also assumes that the heat exchanger walls are isothermal in the HRHEX and the CHEX. The flows are counter-flow in the HTHEX and cross-flow in the HRHEX and CHEX. The interfaces between turbine, blower, compressor and pump were assumed adiabatic. And the ammonia coming out of the HRHEX is assumed saturated liquid. All the thermal properties of ammonia are obtained from the *NIST* "thermodynamic properties of chemicals" database [16]. Minor losses in the heat exchangers are neglected.

In view of the overall cycle, the energy balance is shown in the following equations:

$$\begin{cases} \dot{Q}_{HTHEX} = \dot{Q}_{HRHEX\ upper\ loop} + \dot{W}_{turbine} + \dot{W}_{pump} \\ \dot{Q}_{CHEX} + \dot{W}_{turbine} = \dot{Q}_{HRHEX\ lower\ loop} + \dot{W}_{blower} + \dot{W}_{compressor} \\ \dot{W}_{turbine} = \dot{W}_{blower} + \dot{W}_{compressor} \end{cases}$$

$$\rightarrow \underbrace{\dot{Q}_{HTHEX} + \dot{Q}_{CHEX}}_{} = \underbrace{\dot{Q}_{HRHEX} + \dot{W}_{turbine} + \dot{W}_{pump}}_{}$$

(Heat absorbed into the cycle) = (Heat rejected + Power generated from the cycle)

| | Parameters | Values |
|---|---|---|
| Ambient Conditions | $P_{ambient}$ | $1.013\times10^5$ Pa |
| | $T_{ambient}$ | 290 K~310 K, typically 300 K |
| | Humidity | 0~100% |
| Gas Turbine Exhaust Gas Conditions | $P_{hot\ air}$ | $\leq$ 5000 Pa + $P_{ambient}$ |
| | $T_{hot\ air}$ | 760 K |
| | $T_{superheat}\ (T_4)$ | 700 K |
| | $\dot{m}_{hot\ air}$ | 1 g/s |
| Heat Exchanger | Footprint | < 7 cm × 7 cm |

**Table 4.1—Assumptions in the waste heat cooler calculation**

where $\dot{Q}_{HTHEX}$ is the rate of heat absorbed by the HTHEX from the hot air stream, $\dot{Q}_{HRHEX\ upper\ loop}$ (or $\dot{Q}_{HRHEX\text{-}upper}$) and $\dot{Q}_{HRHEX\ lower\ loop}$ (or $\dot{Q}_{HRHEX\text{-}lower}$) are the rates of heat rejected from the HRHEX corresponding to the working fluid in the upper and lower loop in Figure 4.4, $\dot{Q}_{CHEX}$ is the rate of heat absorbed by the CHEX. $\dot{W}_{turbine}$ is the power output of the turbine, $\dot{W}_{pump}$ $\dot{W}_{blower}$ and $\dot{W}_{compressor}$ are the powers absorbed by the pump, blower and compressor. Zero net work output from the cycle was assumed.

The performance of the whole cycle can be evaluated by the cycle outputs. The *total cooling power* $\dot{Q}_{cooling}$ of the refrigeration cycle is equal to the value of $\dot{Q}_{CHEX}$:

$$\dot{Q}_{cooling} = \dot{Q}_{CHEX} \tag{4.1}$$

$\dot{Q}_{cooling}$ consists of two parts: the work used to condense water and the power used to lower the ambient air temperature, which is defined as *effective cooling power:*

$\dot{Q}_{effective\ cooling} \equiv \dot{Q}_{CHEX} - [\dot{m}_{water}(h_{vapor,in} - h_{liquid,out})]$, where $\dot{m}_{water}$ is the mass flow rate of water condensation, $h_{vapor,in}$ is the enthalpy of the water vapor at the inlet of the CHEX, and $h_{liquid,out}$ is the enthalpy of the condensed liquid water at the exit of the CHEX.

Both effective cooling power and water production can be expected from the initial design. Water production rate varies depending on the ambient conditions. The water vapor in the air will condense when the air temperature reaches its dew point temperature. The relative humidity, $\Phi$, is the ratio of the actual vapor pressure of the water present in the air to the saturated vapor pressure of water at the temperature of that air or

$$P_{vapor} = \Phi \times (P_{vapor})_{saturation} \tag{4.2}$$

Further more, the water production/condensation rate can be obtained from the following relations [17]:

$$\dot{m}_{water} = \dot{m}_{driedair}(\omega_{in} - \omega_{out}) \tag{4.3}$$

where

$$\omega_{in} = 0.622 \times \frac{(P_v)_{in}}{(P_{air})_{in}} \tag{4.4}$$

$$\omega_{out} = 0.622 \times \frac{(P_v)_{out}}{(P_{air})_{out}} \tag{4.5}$$

$$\dot{m}_{driedair} = \frac{\dot{Q}_{CHEX}}{(h_{air})_{out} - (h_{air})_{in} + \omega_{out} \times (h_g)_{out} - \omega_{in} \times (h_g)_{in} + (h_f)_{out}(\omega_{in} - \omega_{out})} \tag{4.6}$$

where $\dot{m}_{driedair}$ is the mass flow rate of the ambient air without the water vapor that is going to be condensed. Subscripts "in" and "out" indicate the inlet and outlet of the CHEX; $P_v$ and $P_{air}$ are the pressures of the water vapor and air, and $h_g$, $h_f$ and $h_{air}$ are the enthalpies of the water vapor, liquid water and air at the inlet and outlet of the CHEX.

Besides power output and/or water production rate, the performance of the cycle can also be presented by thermal efficiencies. The thermal efficiency of the bottoming sub-cycle is

$$\eta_{thermal} = \frac{\dot{Q}_{HTHEX} - \dot{Q}_{HRHEX-upper}}{\dot{Q}_{HTHEX}} \tag{4.7}$$

For the refrigeration part, the maximum value of the coefficient of performance is designated as shown in Equation (4.8) [11]. It is an indicator of the thermal efficiency of the refrigeration cycles.

$$\beta_{\max} = \frac{T_c}{T_h - T_c} \tag{4.8}$$

In the calculations that follow, the thermal efficiency of the Rankine bottoming sub-cycle in this chapter is typically around 10% and the coefficient of performance of the vapor compression sub-cycle has a typical value of 5 for this micro waste heat cooler.

The calculations for the combined heat pump cycle, covered in detail in Appendix 1, are similar to the Rankine cycle calculations outlined in Chapter 2.

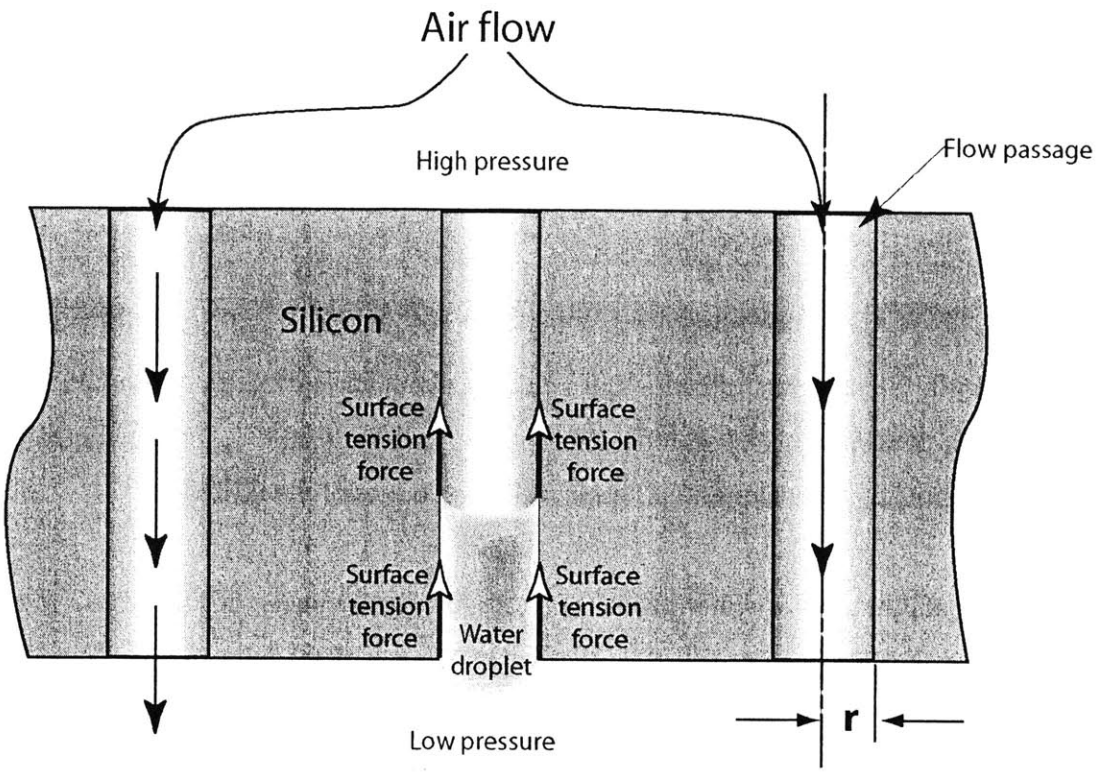


**Figure 4.8—Water condensation with surface tension in the CHEX**

One of the design issues present in the heat driven heat pump but not present in the Rankine cycle machines discussed earlier is the condensation of water in the flow channels of the cold heat exchanger (CHEX). In the hole-type heat exchanger, the water is supposed to flow out of the air passages and into a water collection reservoir. But since the diameter of the air passages are small, the water may stay in these passages due to capillary forces and thus block the flow of air. Figure 4.8 is a cross-sectional drawing of three of the CHEX air passages with a water droplet blocking the central air passage. The surface tension forces of interest act on the water droplet at the solid-liquid-air interface in the direction shown in the figure. There are several possible positions that the water droplet could occupy in the heat exchanger. The configuration shown in Figure 4.8 is the one that requires the highest pressure differential across the passage to blow the water droplet out of the passage. (This configuration is the worst-case scenario.)

The air is cooled as it flows in the downward direction. The air upstream of the passages is at higher pressure than that downstream. Water condensation starts when the air temperature reaches the dew point temperature. The radius of the hole is "$r$" and the surface tension is denoted as $\sigma$. The free surfaces of the water droplet are assumed to have the same radius as that of the air passages (The contact angle is assumed to be zero). If the water droplet is not moving there is no airflow through the blocked passage and the pressure in the passage is the same as the pressure upstream of the passages, $P_{high}$. The pressure on the downstream side of the passages, $P_{low}$, is ambient pressure. Mechanical equilibrium requires that the forces on the droplet sum to zero and assuming gravity acts in the downward direction in Figure 4.8,

$$4\pi r\sigma = (P_{high} - P_{low})\pi r^2 + m_{water\ droplet}\, g \tag{4.9}$$

where $m_{water\ droplet}$ is the mass of the water droplet. Since the gravity force is much smaller than the surface tension and pressure forces ( $\frac{\pi r^2 P}{m_{waterdroplet}\, g} \approx 10^5$ ), it can be neglected. Equation 4.9 becomes

$$P_{high} - P_{low} = \frac{4\sigma}{r} \tag{4.10}$$

for mechanical equilibrium. The term $P_{high}$ - $P_{low}$ is equal to the total mass flow rate through the CHEX multiplied by the impedance of all the flow passages in parallel with the blocked passage. If the pressure drop across these other passages is larger than the maximum effective back pressure that surface tension can muster in the blocked passage ($4\sigma/r$), the pressure difference across the blocked channel will be sufficient to push the water droplet out of that channel. Blockage of the CHEX channels should not be an issue if $P_{high} - P_{low} > \frac{4\sigma}{r}$.

## 4.4 Cycle Analysis

The performance of the waste-heat-driven heat pump strongly depends on the saturation temperature of the working fluid flowing through the HRHEX. In the work described below an optimum saturation temperature for the fluid in the HRHEX is determined given several constraints on the system. These constraints include a restriction on the footprint of the HRHEX (< 7 cm × 7 cm), an ambient temperature and relative humidity of 300 K and 90% respectively, and that there is no net work output from the cycle (the total power consumed by the negative-work components equal the power output of the turbine). Based on this optimum saturation temperature, the design of the waste-heat-driven heat pump was then fixed (primarily the heat exchanger areas were determined).

Following this, a model is described that was used to predict the performance for the (above) optimized design for several different ambient conditions to check the design's sensitivity to the environmental conditions. Finally, the effect of increased turbomachinery efficiency on the optimized design is examined.

The waste-heat-driven heat pump design is shown in Figure 4.9. The hot air entering the HTHEX is assumed to have a mass flow rate of 1 g/s and a temperature of 780 K. The HTHEX air passage design is limited by a maximum pressure drop across the HTHEX of 5000 Pa, which can be easily accommodated by increasing the number of passages in the HTHEX. (The air passages in the HTHEX are assumed to have fixed dimension.) The increasing of the number of passages in the HTHEX for the pressure drop requirement does not significantly add to the overall size of the device since the HRHEX, not the HTHEX, dominates the overall size of the device.

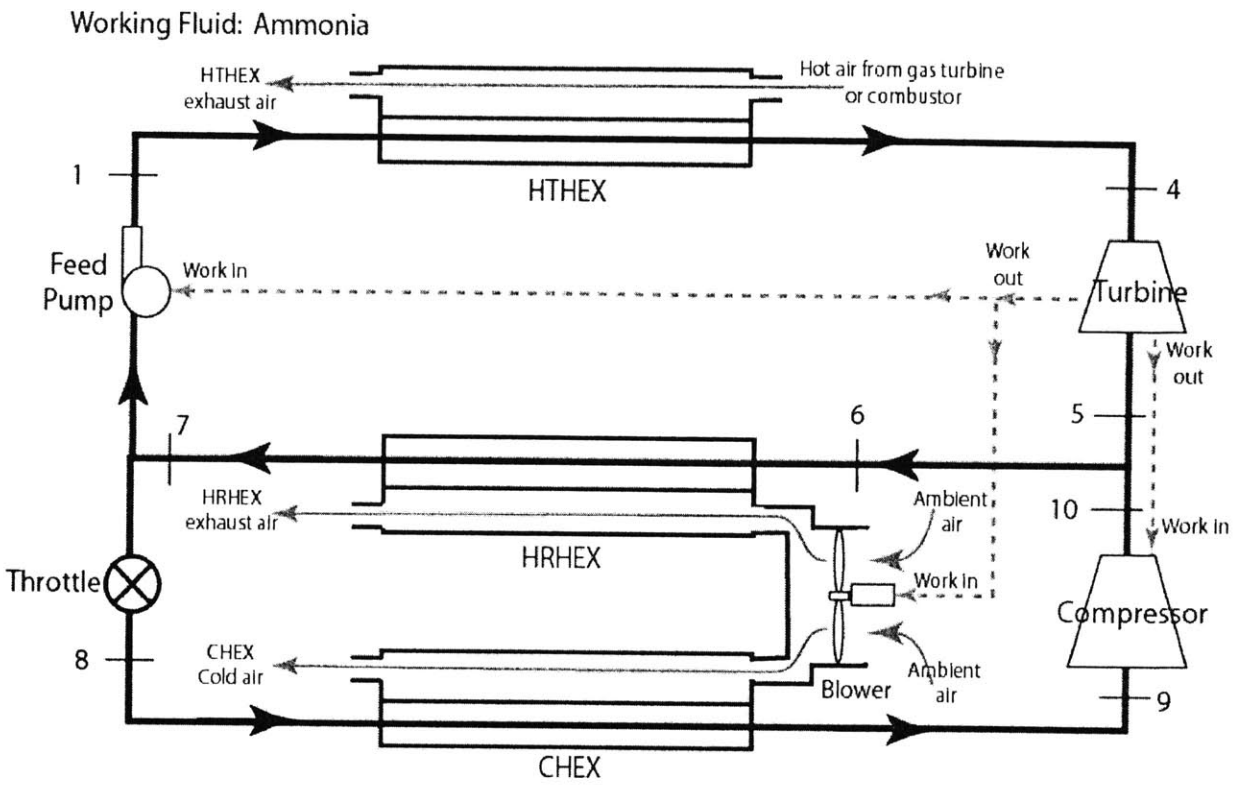


**Figure 4.9—A diagram of the waste heat cooler**

**The dashed lines indicate the work transfer from the turbine to the feedpump, compressor and blower. A single blower is used to provide air to the HRHEX and the CHEX.**

The discharge temperature of the ammonia in the hot heat exchanger (or the turbine inlet temperature, $T_4$) is assumed to be 700 K. (This was an upper limit set by the *NIST* equation of state used in the model.) The ammonia discharged from the CHEX is assumed to be saturated vapor at a temperature of 285 K ($T_9$). This temperature is 15 °C below ambient conditions, a reasonable temperature drop for "air-conditioning" applications. These two temperatures were held fixed throughout all subsequent calculations.

A value for the temperature of the ammonia at the discharge of the HRHEX ($T_7$) was then selected from an array of potential values between 330 and 350 K. The temperature of

the cold air discharge from the HTHEX is assumed to be 370 K. This choice is reasonable in that it sets the temperature defect in the HTHEX between 20 and 40 K; and consequently, the size of the HTHEX remains reasonable. With the choice of the temperature $T_7$, the specific design of the HTHEX can be made.

The mass flow rate of the ammonia through the HTHEX is determined by matching the total enthalpy change of the two fluids in the heat exchanger (first law). With this mass flow rate, the work output of the turbine ($\eta_{turbine}$=0.5) and the work input to the feedpump ($\eta_{pump}$=0.5) can be calculated. The difference of these works determines the work available to drive the compressor and the blower.

A reasonable ammonia mass flow rate through the CHEX is now assumed and the work necessary to drive the compressor is calculated. The work left to drive the blower can now be determined. Since the state of the ammonia entering the CHEX is known (the enthalpy of state 8 is the same as state 7 and the pressure in state 8 is the saturation pressure at temperature $T_9$) and the state of the ammonia leaving the CHEX is known (saturated vapor at $T_9$), the heat transfer rate in the CHEX can be calculated. The dimensions of the air channels in the CHEX are assumed fixed (for these dimensions see tables that follow) and their number is varied, within the limitation of the 7 cm × 7 cm footprint for the overall device. For a given number of passages the pressure drop and air mass flow rate for the required heat transfer rate is calculated.

The HRHEX can now be designed. Since the ammonia mass flow rate and the ammonia inlet and outlet states are known, the heat transfer rate in the HRHEX can be calculated. The pressure drops across both the heat exchangers are the same (see the assumed configuration in Figure 4.8). As in the case of the CHEX, the dimensions of the air channels in the HRHEX are assumed fixed (once again, these dimensions are in tables that follow) and their number is varied, within the limitation of the 7 cm × 7 cm footprint. The given heat transfer rate for the HRHEX essentially determines the number of air passages (area) necessary in the heat exchanger. The pressure drop across the heat exchanger essentially determines the number of passages that are in parallel and the

number of passages in series. The HRHEX configuration was varied to match both the required heat transfer and pressure drop. With this configuration, a mass flow rate through the HRHEX can be determined.

The blower work input is now calculated using the sum of the air mass flow rates through the HRHEX and the CHEX, the pressure drop through these heat exchangers, and the assumed turbomachinery efficiency of 50%. This work derived from the heat exchanger performance is then compared to the work discussed earlier that is available from the turbine. If these works do not match, the assumed mass flow rate of the ammonia in the CHEX is changed to a new value and the design of the heat exchangers is re-implemented. The calculation is repeated until these heat-exchanger-based and turbine-based blower works are equal. Once the solution has converged the cooling power and the water condensation rate of the cycle is calculated.

A new temperature of the ammonia discharged from the HRHEX ($T_7$) is now chosen from the array of values between 330 and 350K and the calculations are repeated to determine the new cycle's cooling power and the water condensation rate. The results of several of these calculations are shown in Figure 4.10.

To summarize, Figure 4.10 shows the total cooling power, the water condensation rate, the heat-transfer power density of the HRHEX and the length of the footprint edge of the HRHEX (the shape of the footprint is assumed square) for five different designs of heat-driven heat pumps. These designs correspond to operating values for $T_7$ of 330, 335, 340, 345 and 350 K. In all five designs, the ambient atmospheric conditions were assumed to be 300 K, 1 atm, and a relative humidity of 90%. The temperature and pressure of the ammonia discharged by the HTHEX (state 4 in Figure 4.9) is kept constant in all cases (700 K, 11 MPa). The hot air entering the HTHEX is assumed to have a temperature of 760 K and a pressure of 5 kPa greater than ambient. The discharge conditions of the CHEX are also fixed, namely the ammonia is saturated vapor at 285 K that the saturation temperature in CHEX always equals to 285 K. In all of these calculations the turbomachinery efficiency was assumed to be 50%.

From Figure 4.10 it can be found that the cooling power ranges from about 20 W to 30 W, and water production about 18-27 ml/hr, with a footprint that ranges from 5 cm by 5 cm to 6.3 cm by 6.3 cm. Within this range total ammonia mass flow rate through the HRHEX varies from 0.231 to 0.235 g/s, and the pressure ratio across the turbine and the compressor ranges over values between 2 and 6. The cooling power output and water production rate decrease with the increase of $T_7$. The thermal efficiency of both the upper (power producing) cycle and the lower (cooling) cycle decrease with increasing HRHEX discharge temperature, $T_7$. Unfortunately, lower values of $T_7$ necessarily require the HRHEX to be larger, as can be seen in Figure 4.10 (wafer edge length). In addition, lower $T_7$ also results in the need for more ambient air to cool the HRHEX which increases the blower power required.

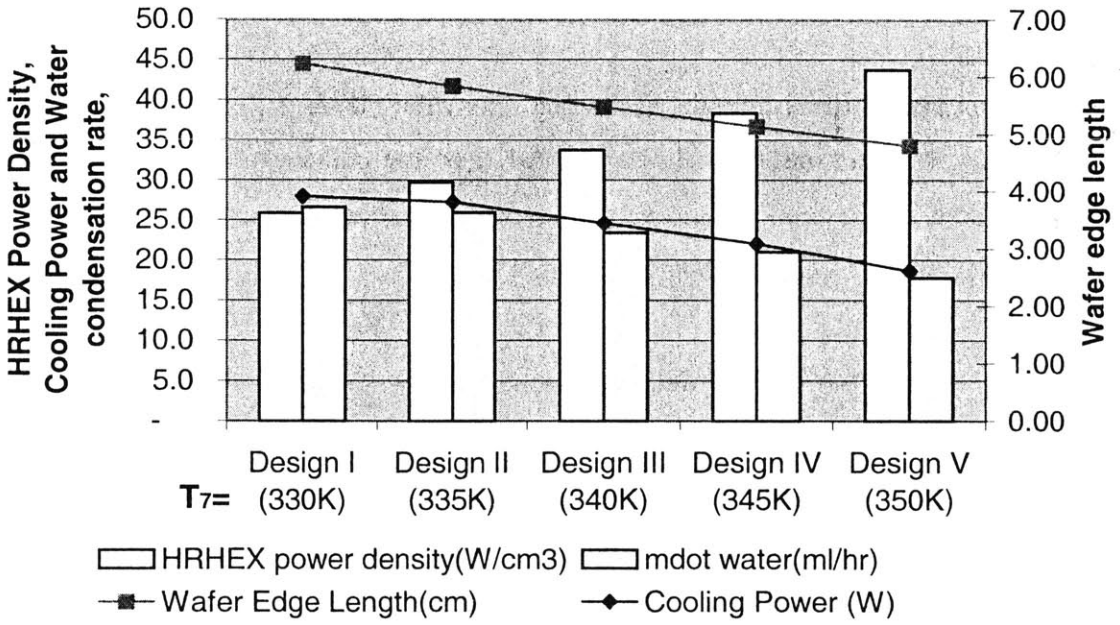


**Figure 4.10—Performance and size of the waste heat cooler as a function of the ammonia temperature discharged by the HRHEX.**

**The turbine inlet temperature is 700 K and the compressor inlet temperature is 285 K. Ambient conditions are assumed to be 300 K, 1 atm, and a relative humidity of 90 %. The turbomachinery efficiency equals to 50%.**

As a compromise between dimension and performance, "Design III" in Figure 4.10 was chosen as the preliminary design of this waste heat cooler. Table 4.2 and Table 4.3 list the details of assumptions, performance and heat exchanger dimensions of Design III.

Assumptions:

| **Basic Assumptions** | | **Working Fluid and Other Assumptions** | | | |
|---|---|---|---|---|---|
| $\eta_{turbomachinery}$ | 50% | $T_{HTHEX}$ | $T_{sat}$ =**700 K** | $P_{HTHEX}$ | 11 MPa |
| $\Phi_{ambient}$ | 90% | $T_{HRHEX}$ | $T_{sat}$ =**340 K** | $P_{HRHEX}$ | $P_{sat.\ @\ T_{HRHEX}}$ |
| $T_{ambient}$ | 300 K | $T_{CHEX}$ | $T_{sat}$ =285 K | $P_{CHEX}$ | $P_{sat.\ @\ T_{CHEX}}$ |
| $P_{ambient}$ | 1 atm | $\dot{m}_{upperammonia}$ | 0.026 g/s | $\pi_{compressor}$ | 4.70 |
| $T_{hot\ air}$ | 760 K | $\dot{m}_{lowerammonia}$ | 0.21 g/s | $\pi_{turbine}$ $(=\pi_{pump})$ | 3.57 |
| $\dot{m}_{hotair}$ | 1 g/s | $\dot{m}_{totalammonia}$ | 0.23 g/s | $\pi_{blower}$ | 1.01 |

Performance:

| | | | | | |
|---|---|---|---|---|---|
| $\dot{Q}_{cooling}$ | 24.6 W | $\dot{m}_{water}$ | 23 ml/hr | $\dot{W}_{turbine}$ | 38.9 W |
| $\dot{Q}_{effective\ cooling}$ | 8.6 W | $\dot{m}_{driedair}$ | 1.22 g/s | $\dot{W}_{compressor}$ | 12.2 W |
| $\eta_{thermal}$ | 8.2% | $\dot{m}_{totalair}$ | 1.23 g/s | $\dot{W}_{blower}$ | 20.4 W |
| $\beta_{max}$ | 5.2 | $(T_{air/water})_{cooled}$ | 290.2 K | $\dot{W}_{pump}$ | 6.2 W |

**Table 4.2—Selected assumptions and performance of the preliminary design of the waste heat pump (Design III)**

1. HTHEX (air side)

| | | | | | |
|---|---|---|---|---|---|
| Channel width | 0.15 mm | Channel length | 4.6 mm | # of Stacks | 2 |
| Channel height | 0.75 mm | Total length | 1.25 cm | $\Delta P_{hot\ air}$ | 4.28 kPa |
| # of channels | 500 | Total width | 3.13 cm | $\dot{m}_{hotair}$ | 1 g/s |
| Fin thickness | 0.1 mm | Total height | 2.1 mm | UA | 6.11 W/K |
| Base thickness | 0.2 mm | Sets of channels per stack | 2 | $\varepsilon$ | 0.997 |
| Note: The ammonia side design is the same as the airside in the HTHEX. Graphic design is shown in Figure 3.4. | | | | | |

2. HRHEX (air side)

| | | | | | |
|---|---|---|---|---|---|
| Hole diameter | 0.2 mm | Total height | 4 mm | $\dot{m}_{coolingair}$ | 10.81 g/s |
| Number or rows | 130 | Total length | ~6.2 cm | $\Delta P$ | 1.02 kPa |
| Holes per row | 162 | Total width | 4.8 cm | $\dot{W}_{blower}$ | 18.9 W |
| Distance b/t holes | 0.1 mm | Number of stacks | 4 | UA | 29 W/K |
| Wafer thickness | 0.1 mm | | | | |
| Note: The ammonia side dimensions: b=d=0.1 mm, a=0.9 mm, t=0.1 mm, L=64.4 mm, n=130. (a, b, d, t, L, and n were defined in Figure 2.7). The channels alternate one-by-one with the rows of holes. Graphic design is shown in Figure 3.11 (with four stacks) | | | | | |

3. CHEX (air side)

| | | | | | |
|---|---|---|---|---|---|
| Hole Diameter | 0.57 mm | Total length | ~5.4 cm | $\dot{m}_{coolingair}$ | 0.85 g/s |
| Number or Rows | 70 | Total height | 2 mm | $\Delta P$ | 1.02 kPa |
| Holes per Row | 70 | Total width | 5.4 cm | $\dot{W}_{blower}$ | 1.49 W |
| Distance b/t holes | 0.2 mm | Number of stacks | 4 | UA | 6.20 W/K |
| Wafer Thickness | 0.1 mm | | | | |
| Note: The ammonia side dimensions: b=d=0.1 mm, a=0.9 mm, t=0.1 mm, L=54 mm, n=70. (a, b, d, t, L, and n were defined in Figure 2.7). The channels alternate one-by-one with the rows of holes. Graphic design is shown in Figure 3.11 (with four stacks) | | | | | |

**Table 4.3—Heat exchanger designs of the preliminary design of the waste heat cooler (Design III)**

In general, the waste heat cooler will not be operated under design conditions (300 K and 90% relative humidity). The performance of a specific cooler will depend on the ambient conditions. The performance of the Design III cooler was calculated for ambient temperatures ranging from 290 to 310 K and ambient relative humidity from 0 to 100%.

In these calculations the heat exchanger geometries are fixed (Design III) otherwise the calculation procedure is similar to that discussed above. The turbine inlet temperature ($T_4$) and the compressor suction temperature ($T_9$) are fixed at values of 700 K and 285 K, respectively. The turbine inlet pressure ($P_4$) is held constant at 11 MPa. The vapor at the suction side of the compressor is assumed saturated. The turbomachinery efficiency is assumed to remain at a value of 50% for all operating conditions. The HTHEX air mass flow rate (1 g/s) and air inlet and discharge temperatures (760 K and 370 K, respectively) are assumed fixed.

The calculation procedure to determine the performance of the Design III device as a function of ambient temperature is summarized below. Since the HTHEX air mass flow rate and air temperatures are fixed, the ammonia mass flow rate through the HTHEX is also fixed. Following a procedure similar to that outlined above, the work associated with the turbine and the pump can then be calculated. The difference of these works gives the power available to drive the compressor and the blower. Following this, a value for the ammonia mass flow rate through the CHEX is assumed and the required work for the compressor is calculated, from which the work left for driving the blower is determined. From the inlet and outlet conditions of the CHEX, the heat transfer rate can be determined and the effectiveness can be obtained from the geometry and the inlet condition (assumed temperature) of the air. (As an aside: the air flow through this heat exchanger is always laminar.) The mass flow rate of the ambient air necessary for the CHEX is then calculated and blower power needed for this heat exchanger is determined. Similarly, with the assumption of equal pressure drop in the air side and fixed geometry of HRHEX, the blower power for that heat exchanger can also be calculated. These two blower powers are summed and can be compared to the blower power available from the rest of the turbomachinery. The ammonia mass flow rate through the CHEX is varied

until the heat-exchanger-based and turbine-based blower works are equal. The performance of the waste heat cooler under this specific ambient condition can then be calculated. This procedure was followed for ambient temperatures of 290, 295, 300, 305 and 310 K and the resulting cooling powers and water condensation rates are graphed in Figure 4.11.

The cooling power of the waste heat cooler varies from 15.1 to 25.5 W as shown in Figure 4.11. There is a maximum in the cooling power for an ambient temperature of 295 K. This is (thermodynamically) unexpected since lowering the ambient temperature will, in general, improve the performance of both the power producing and cooling cycles. This result is really an artifact of the assumptions made in these calculations. The saturation temperatures (of the two-phase fluid in the HTHEX, HRHEX and the CHEX) of the cycle are all held constant regardless of the ambient conditions. The mass flow rates (of both the air and the ammonia) through the HRHEX and the CHEX are varied to achieve a steady state solution. For example, since the saturation temperature of the ammonia in the CHEX is held fixed throughout these calculations, the reduction of the ambient air temperature will require larger air flows through the CHEX to maintain the energy balance between the ammonia and the air streams. This larger air flow influences the power required to drive the blower and hence the overall power required to drive the cycle.

In fact, most of the air mass flow from the blower is used to handle the heat rejection from the HRHEX (93% of the air from the blower goes through the HRHEX –and the other 7 % of blower air flows through the CHEX under design conditions, 300 K ambient). Lower ambient temperatures result in a reduction of air mass flow rate to the HRHEX, an increase of the air mass flow rate to the CHEX and a decrease in the power necessary to drive the blower. This decrease in the blower power allows the compressor to consume more turbine power and increase the ammonia mass flow rate in the lower loop (see Figure 4.9, the mass flow through state 9). Eventually, as the ambient temperature approaches ammonia saturation temperature in the CHEX, the air mass flow rate necessary to cool the ammonia in the CHEX becomes very large. The power

required to drive the blower begins to increase again, reducing the available compressor power and reducing the lower loop ammonia mass flow rate. At this point, the cooling power of the device peaks and then begins to drop as the ambient temperature is lowered.

In Figure 4.11, the water production decreases monotonically with the increase of ambient temperature, ranging from 9.5 ml/hr to 54.9 ml/hr. This is initially a surprising result since the water available in constant relative humidity air increases with temperature. Unfortunately, the discharge air temperature of the CHEX increases with an increase in the ambient temperature (by assumption, the temperature of the saturated ammonia in this heat exchanger is held at 285 K). This increase in the CHEX air discharge temperature reduces the water condensation rate.

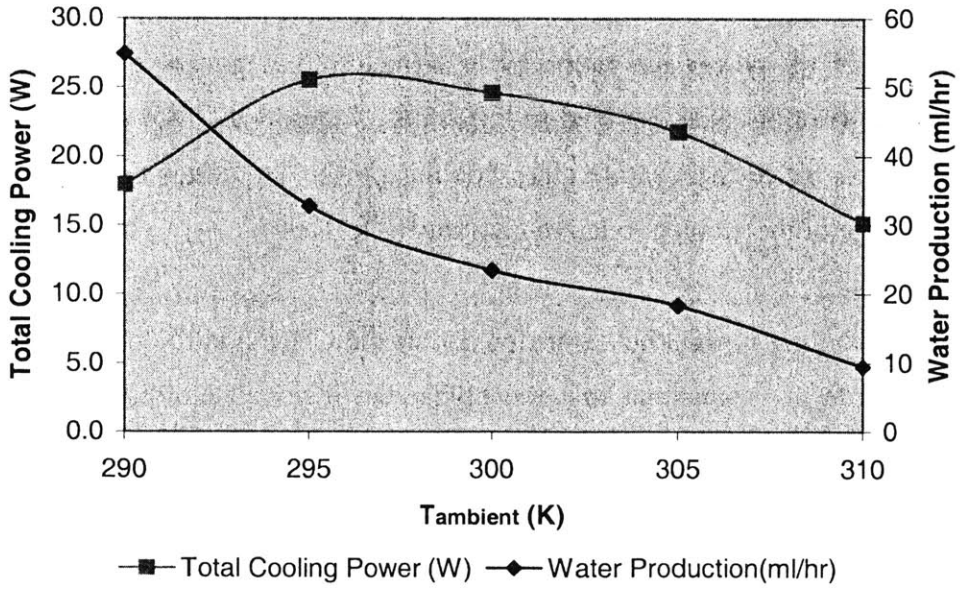


**Figure 4.11—Total cooling power & water production vs. $T_{ambient}$**

**Assumptions: Design III ($T_7$=340 K), Ambient pressure is 1 atm, and the ambient relative humidity is 90%. The HTHEX superheat temperature equals to 700 K, and the HTHEX pressure equals to 11 MPa. The saturation temperature in the CHEX equals to 285 K and turbomachinery efficiency equals to 50%.**

In a physical device the saturation temperatures will not be held constant with varying ambient conditions. These temperatures will depend on the ambient conditions, turbomachinery performance, the specifics of the system design (for example, possible ammonia storage or regulating volumes within the device) and the control algorithms used by the control circuitry. Since this work is a preliminary look at the performance of these Rankine-cycle-based devices and much of the above information is unavailable, i.e. off-design turbomachinery performance, there has no attempt here to devise more sophisticated models than the one outlined above.

The performance of the Design III device was also analyzed for differing relative humidity conditions at an ambient temperature of 300 K. Once again the temperatures of the saturated ammonia in the HTHEX, HRHEX and the CHEX are held constant in this analysis (700 K, 340 K and 285 K, respectively). The geometries of the heat exchangers are listed in Table 4.2, and turbomachinery efficiency is held at 50%. The mass flow rate of the ammonia in the power generation cycle is fixed to 0.21 g/s and the ammonia mass flow rate in the cooling cycle is fixed to 0.026 g/s. Figure 4.12 shows the variation of waste heat cooler performance (effective cooling power and water condensation rate) versus the change of the ambient relative humidity (0 to 100%).

Since the total cooling power (heat transfer rate of the CHEX) is fixed according to the assumptions made, it is apparent that the higher the relative humidity, the higher the water condensation rate, with a compensating lowering of the effective cooling power (power for air conditioning) as can be seen from Figure 4.12. Figure 4.12 also shows that when the ambient humidity is less than 40%, the production of water ceases because the due point temperature of the ambient air entering heat pump is lower than the coldest temperature in the CHEX. In this case all the cooling power (25 W) is directed to cooling the air passing through the CHEX.

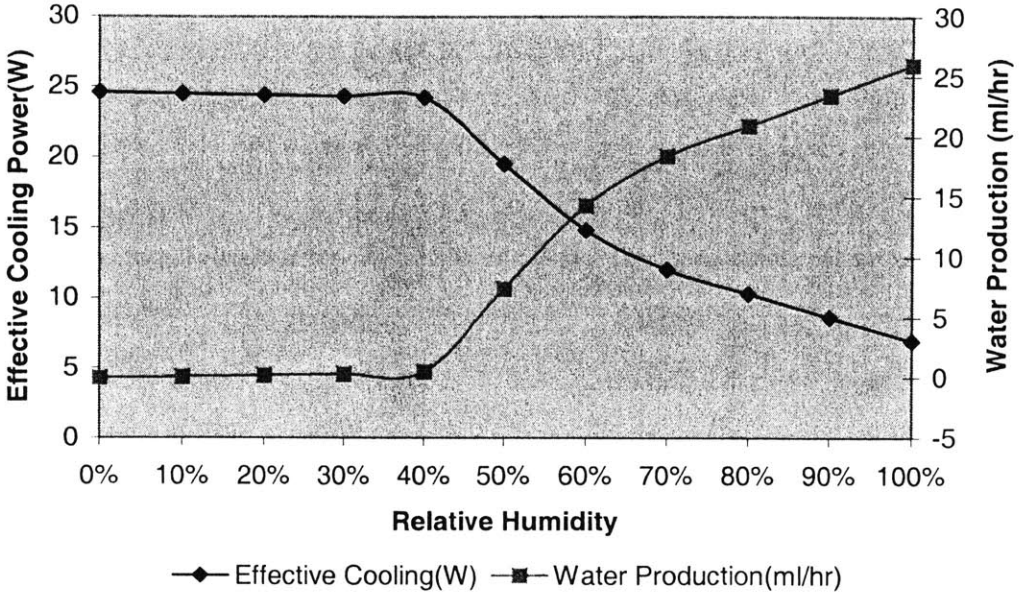


**Figure 4.12—Cooling power & water production vs. humidity**

**Assumptions: Design III ($T_7$=340 K), Ambient temperature equals to 300 K, and ambient pressure is 1 atm. The HTHEX superheat temperature equals to 700 K, and the HTHEX pressure equals to 11 MPa. The saturation temperature in the CHEX equals to 285 K and turbomachinery efficiency equals to 50%.**

The performance of the Rankine-based machine can be improved significantly by an increase in the efficiency of the turbomachinery, as seen in Figure 4.13. The cycle performances shown in Figure 4.13 are for a Design III cooler where all of the turbomachinery components have the same efficiency, varying from 0.4 to 1. Apart from differing turbomachinery efficiencies, the calculations used here proceed in the same way as described for that for the initial evaluation of Design III. The highest total cooling power shown in Figure 4.13 exceeds 170 W corresponding to a turbomachinery efficiency of 100%, about 7 times of the cooling power discussed earlier (corresponding to a turbomachinery efficiency of 50 %).

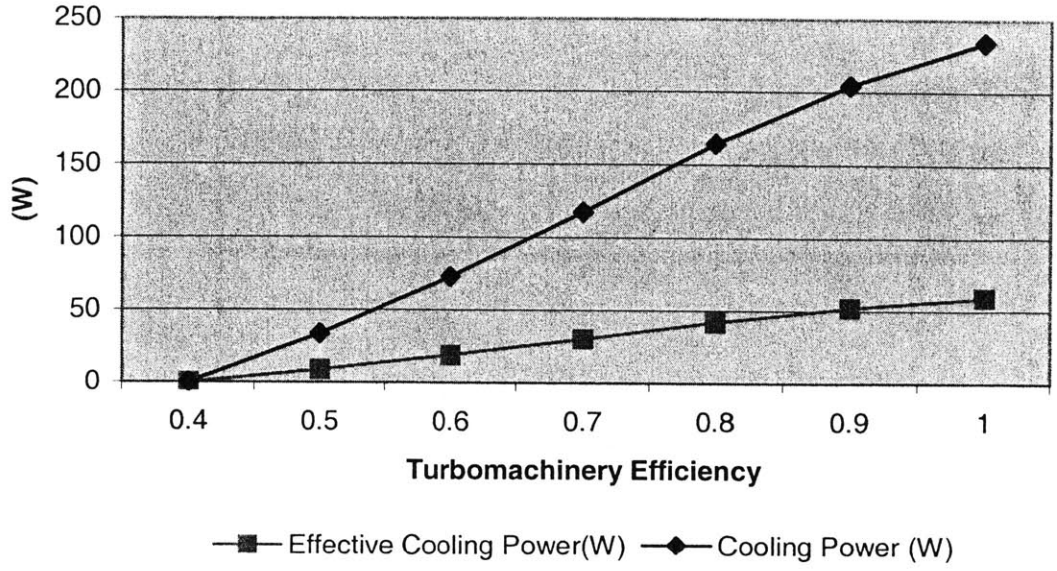


**Figure 4.13—Cooling Power vs. Turbomachinery Efficiency**

**Assumptions: Design III ($T_7$=340K), Ambient temperature equals to 300 K, ambient pressure is 1atm, and relative humidity equals to 90%. The HTHEX superheat temperature equals to 700 K, and the HTHEX pressure equals to 11 MPa. The saturation temperature in the CHEX equals to 285 K.**

## *4.5 Summary of the Waste Heat Cooler*

The micro waste heat cooler will be able to provide cooling power and produce water by using the exhaust heat from the micro gas turbine engine. The anticipated cooling powers can be as high as 25 watts assuming a 50% turbomachinery efficiency. The HRHEX dominates the dimensions of the whole device. For a waste heat cooler of about 25 W cooling power output (Design III), the footprint of the HRHEX is about 6 centimeters by 6 centimeters.

Water production of the waste heat cooler is very dependent on the ambient conditions. The water production rate may vary from 0 to about 60 ml/hr (60 g/hr) depending on the

ambient temperature and humidity (see Figures 4.11 and 4.12). This 60 g/hr water production rate is comparable to the fuel consumption rate of 180 g/hr of the waste heat source driving the cooler. (For a micro gas turbine engine, the fuel consumption rate is typically 5% of the air mass flow rate, thus for an engine of 1 g/s air mass flow, the fuel consumption is about 180 g/hr.) If water production is not needed in the micro heat pump application, the condensed water could be used to enhance the cooling and condensation processes in the HRHEX, and thus decrease the blower power consumption and/or decrease the size of the HRHEX.

The ammonia mass flow rate in the refrigeration cycle of the device is very small, typically 0.026 g/s versus 0.2 g/s in the power producing part of the cycle. This disparity in flow rates is primarily due to the rather low efficiencies of the turbomachinery in both the power producing and cooling cycles of the device.

There are three negative work components (the feedpump, the compressor and the blower) all driven by a turbine in the waste heat cooler. Although most of these components have been built as part of the MIT micro engine project, the waste heat cooler has the issue of how to transfer the turbine work to all the other components. The current micro gas turbine engine design is not applicable to the waste heat cooler, since there is only one compressor powered by the turbine. In addition, the connection between the blower and the turbine must be hermetic to avoid the leakage of the working fluid to the atmosphere. This might be achieved through the use of a magnetic coupling between the relevant turbo-machines and will be discussed in more detail in the next chapter.

The performance of the waste heat cooler can be increased many-fold through higher turbomachinery efficiency. (A seven-fold improvement can be realized by increasing the turbomachinery performance from fifty to one hundred percent. The MIT micro engine group has recently designed a new turbine, which has an anticipated theoretical efficiency of 70%. This will also be discussed further in Chapter 5.

All the calculations discussed in this work assume that all the turbo-machines are adiabatic, the heat exchangers are externally adiabatic and hence there is no conductive heat transfer between the components of the device. There will be some compromising of the performance of the waste heat cooler due to conduction between the components. The MIT micro engine group is working on the possible designs to reduce the thermal conduction between the micro turbine and the micro compressor, such as a spiral shaft design connecting the turbine and the compressor, introducing air gap between the turbomachinery components [2]. In addition, connecting tubes among the modules in the micro Rankine-cycle devices (shown in Figure 4.6) enables certain thermal insulation between the hot and cold components in the system.

# Chapter 5 Rotating Parts in the Micro Rankine-Based Devices

It is presumed that the turbomachinery used in the cycles described in this work are scaled versions of the turbomachinery used in the MIT micro gas turbine engines. There are additional challenges to the combined cycle turbomachinery design over that of the corresponding gas-turbine turbomachinery designs. In the combined cycles, the turbomachinery must spin at high speed in a working fluid that is at high pressure and/or high temperature. In addition, the turbomachinery may be more complex in the combined cycles because of possible phase change in the working fluid and additional rotating components. The current "extruded" shape approach in silicon micro-fabrication methods limits the turbomachinery performance to efficiencies of ~50%. New designs and new approaches to fabrication should increase the turbomachinery performance.

This chapter first presents an overview of the current state-of-the-art micro turbomachinery design and performance in the MIT micro engine project. Following this, the requirements and barriers of micro turbomachinery design, arrangement and fabrication in the micro Rankine-based devices are discussed, based on the single Rankine device "Max-Power Design" in Chapter 2 ($T_7$ = 420 K in Figure 2.10, with unlimited turbine pressure ratio and mass flow rate) and Waste-Heat-Driven Cooler "Design III" in Chapter 4. Possible solutions and future improvement are then discussed at the end of this chapter.

## 5.1 Choosing Rotating Parts in Combined Cycles

### 5.1.1 Overview of the Turbomachinery of MIT Micro Gas Turbine Engines

The planar fabrication approach (2-D etching) of the micro turbomachinery gives these rotating components constant blade height as well as the centrifugal-single-stage configuration. The parameters and performance of the micro turbomachinery designed by MIT micro engine research group are summarized in the following sections.

**1. Micro Turbine**

Figure 5.1 shows the 2-D and 3-D geometrical configurations of the baseline turbine (with different numbers of blades) [2].

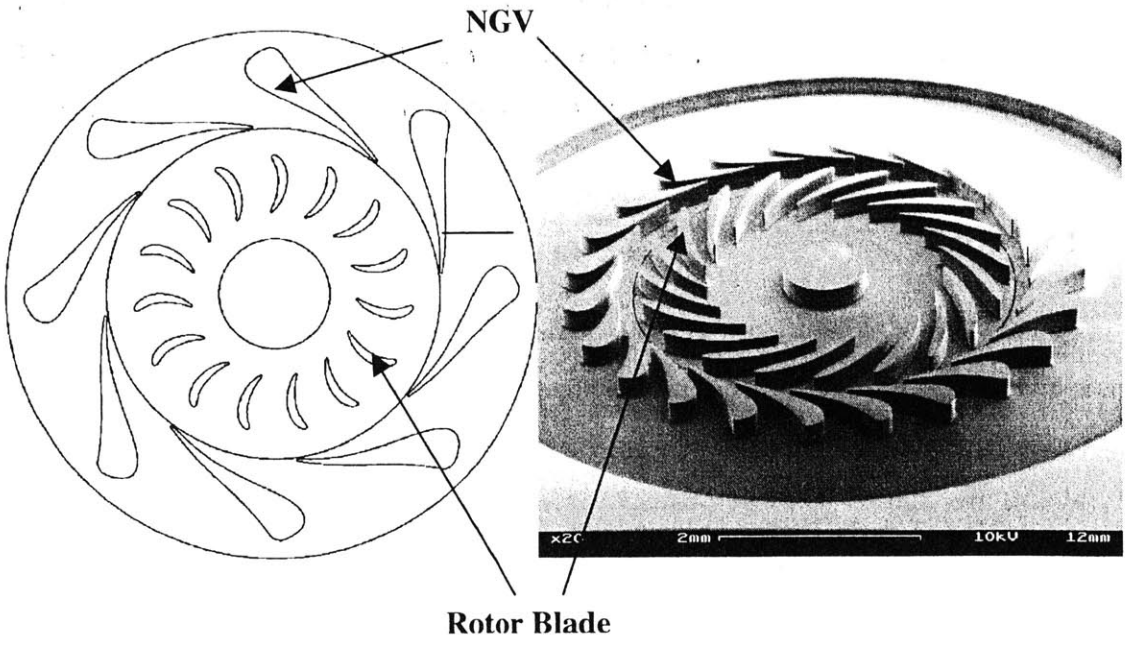


**Figure 5.1—Geometric configuration of the baseline micro gas turbine design**

Recently, the MIT micro engine group redesigned a turbine stage for the micro gas turbine engine, by adopting a new methodology. Figure 5.2 shows the geometry configuration of the new turbine design. This configuration has thinner and more rotor blades and a bigger nozzle guide vane (NGV) exit angle to improve the flow of the working fluid. According to the simulation result, it has better performance over the baseline design on stage efficiency, pressure ratio as well as the ratio of turbine work output to the compressor work input. The parameters characterizing the baseline design and the new design and their selected performances are delineated and compared in Table 5.1 [2].

As can be seen from Table 5.1, the new design has a significant improvement of stage pressure ratio ($P_{in}/P_{out}$), and at the same time, the optimal stage efficiency increases from 59% to 70%.

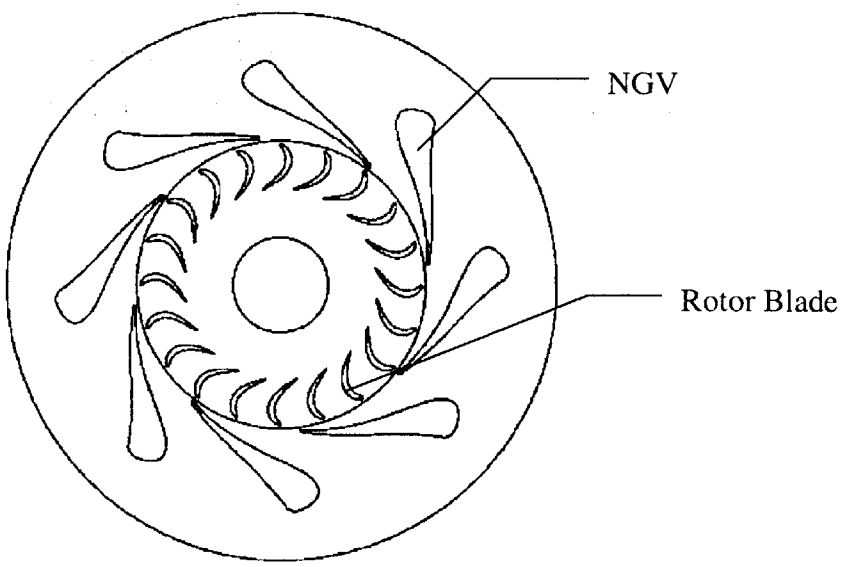


**Figure 5.2—Geometric configuration of the new turbine design**

| Metrics | Parameters/Performance | | Change % |
|---|---|---|---|
| | Baseline Design | New Design | |
| NGV exit angle | 74° | 77° | -- |
| Rotor inlet radius | 2.5 mm | 2.96 mm | +18.4% |
| Rotor exit radius | 1.5 mm | 2 mm | +33.3% |
| No. of rotor blades | 15 | 21 | -- |
| Stage pressure ratio | 1.65 | 2.1 | +27.3% |
| Mass flow rate | 0.23 g/s | 0.29 g/s | +26.1% |
| Stage efficiency | 0.59 | 0.70 | +18.6% |

**Table 5.1—Parameters and performance of the baseline and the new turbine design**

**2. Micro Compression Systems**

In the MIT micro gas turbine engine and rocket projects, two types of compression systems have been developed. The first is a centrifugal flow compressor for air and the second is a centrifugal pump for water (or liquids). The inherent simplicity of the centrifugal-type machines (they do not require inlet and discharge valves) combined with their high power density makes them the choice for the Rankine-based systems.

The motor-compressor designed by the MIT micro engine group is an example of the centrifugal flow compressor. This single-stage compressor has 6 impeller blades and a rotor diameter of 4 mm. Figure 5.3 shows the 2-D and 3-D views of the baseline motor-compressor and Table 5.2 lists the specifications of the various motor-compressor configurations [3].

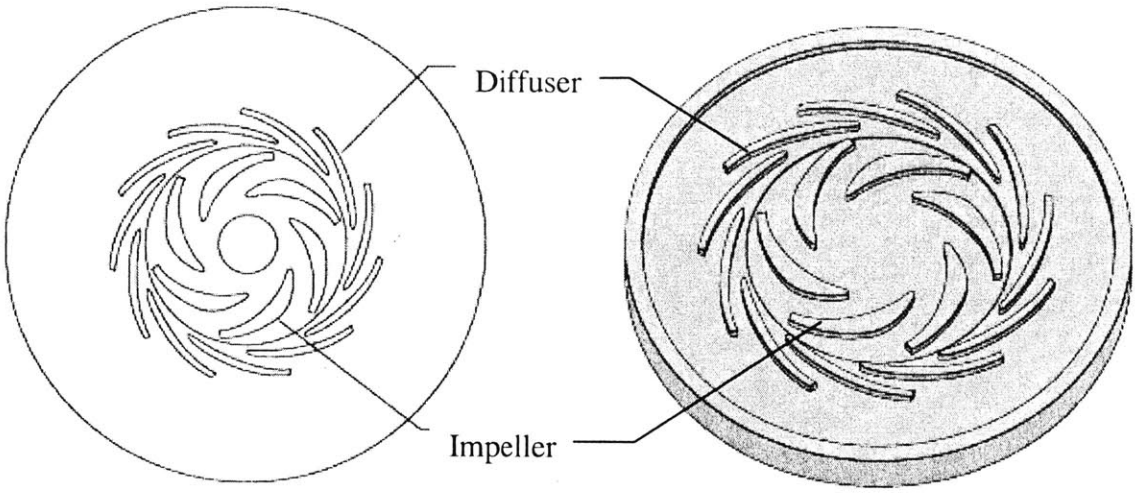


**Figure 5.3—Geometric configuration of the micro motor-driven compressor design**

| | Demonstration | Micro Blower | Micro Compressor |
|---|---|---|---|
| **Airflow** | 0.05 g/s | 0.33 g/s | 0.11 g/s |
| **Pressure rise** | 1.02:1 | 1.06:1 | 2:1 |
| **Device size** | 15×15×2.5 mm | 20×20×1.5 mm | 20×20×3.0 mm |
| **Inlet pressure** | 1 atm | 1 atm | 1 atm |
| **Compressor power** | 0.3 W | 2.5 W | 12 W |

**Table 5.2—Motor-compressor configurations and expected performance**

In the MIT micro rocket project, a micro turbopump is designed for pumping liquid propellants (fuel: JP7 and oxidizer: $H_2O_2$ currently) into the micro rocket engines. In the rocket system, this pump "compresses" the liquid propellant to high pressure. The liquid is then vaporized and passed through the pump's turbine, providing power to the pump, before the propellant is injected into the rocket's combustion chamber. In the demonstration turbopump (the "demo" turbopump) the compressed liquid is water. The demo turbopump is a centrifugal design for a 30 atm pressure rise. Figure 5.4 shows impeller blade profiles for the demo turbopump and Table 5.3 lists the turbopump specifications (the design data in Table 5.3 was obtained from reference [2]; the experimental data was from internal presentation in 2003).

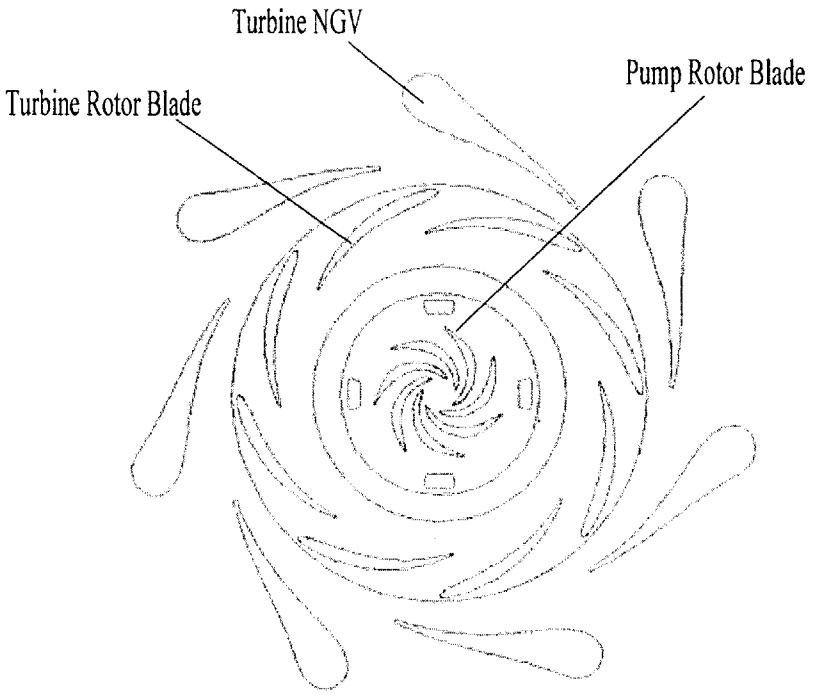


**Figure 5.4—A 2-D geometric configuration of the micro turbopump design**

| | Design Parameters | Experimental Data |
|---|---|---|
| **Working Fluid** | Propellant | $H_2O$ |
| **Airflow for calculation** | 2.5 g/s | 0.15 g/s |
| **Pressure rise** | 30 atm | 0.68 atm |
| **Pump rotor outer diameter** | 2 mm | 2 mm |
| **Efficiency expected** | 30% | -- |
| **Shaft power** | 36 W | -- |

**Table 5.3—Micro turbopump configurations and performance**

### 5.1.2 Turbomachinery Design in the Rankine-Based Machines

The previous section has been a review of the state-of-the-art of various devices that are relevant to the design of a micro-Rankine cycle device. In what follows, the turbomachinery required for a micro-Rankine bottoming cycle (more specifically, the "Max-Power Design" —$T_7$ = 420 K in Chapter 2) and a waste-heat driven micro heat pump ("Design III" in Chapter 4) are discussed in detail.

**1. Turbine**

The turbine in both the micro-Rankine bottoming cycle and the waste-heat-driven micro heat pump is used to provide mechanical energy to all the other components of the cycle. The specifications for the turbine for the Max-Power Design of Rankine cycle and the Design III are shown in Table 5.4.

As can be seen from Table 5.4, the turbine pressure ratios required for these cycles are substantially higher than those imposed on the gas turbines described in the previous section. (The Rankine-based power machine and the Waste-Heat-Driven Cooler require pressure ratios of 9.15 and 3.57 respectively versus a gas turbine pressure ratio of about two.)

| | **Rankine power machine** | **Waste-heat-driven cooler** |
|---|---|---|
| **Air mass flow rate** | 0.15 g/s | 0.21 g/s |
| **Pressure ratio** | 9.15 | 3.57 |
| **Pressure decrease** | 3.56 MPa | 7.9 MPa |
| **Efficiency assumed** | 50% | 50% |
| **Typical** $\dot{W}_{turbine}$ | 44 W | 39 W |

**Table 5.4—Requirements to the micro turbines in the Rankine-based machines**

The net power of a turbine can be increased by increasing the hot air inlet temperature or by increasing the pressure ratio across the turbine. In the bottoming Rankine machines, the inlet temperature of the vapor entering the turbine is limited by either the temperature of the hot gases entering the high temperature heat exchanger (< 800 K) or by the thermal properties of the working fluid. With this limit, the power output of the turbine can only be improved by increasing the pressure ratio across the turbine.

Rankine-cycle turbines may be operated under conditions not seen by Brayton-cycle turbines. The Rankine-cycle turbine exhaust conditions may be in the two-phase region where the liquid phase begins to appear in the working fluid. This can lead to the spalling of the surfaces of the turbine blades. It has been shown that low surface roughness of a silicon rotor is critical to the rotor's strength and ability to operate at high speed; therefore, the existence of liquid particles in the fluid passing through the rotor may result in its failure. It is prudent, then, to use a Rankine cycle so that the turbine exhaust conditions are not in the two-phase region. There has been another approach in macro-scale turbines that are designed to be tolerant of small liquid particles in the discharge stream. It may be possible to design a micro-scale liquid-particle-tolerant turbine.

The micro engines are built on silicon wafers; and consequently, the properties of silicon limit the highest operating temperature of those engines. Silicon creeps for temperatures above 900 K, and it melts at 1683 K. In the micro gas turbine engine, the highest temperature exists in the combustor, where flame-combustion or non-flame-combustion process occurs. Currently, with cooling mechanism, the actual temperature of the micro combustor walls reached by MIT micro engine group is no higher than 1,000 K and the total pressure of the air-fuel mixture is about 3 atmospheres in the combustor. In the micro rocket engine project, the pressure in the rocket chamber in experiment is currently up to 19 atmospheres [2][19].

In the Rankine-based devices, the highest temperatures seen by solid components are in hot heat exchanger walls between the high temperature air stream and the Rankine cycle's

working fluid. The high-temperature turbine also sees very high temperatures as well as being under high rotationally induced stresses. Because of the combined thermal and mechanical stresses the high temperature turbine is likely to be the most critical part in the cycle. The design of a Rankine turbine in a bottoming cycle application will probably be less challenging than a Brayton cycle turbine, since the topping (Brayton) cycle turbine will necessarily be operating at temperatures much higher (>900 K) than the bottoming (Rankine) cycle turbine. In stand-alone applications, where a combustor can supply very high temperature gases (>900 K) to the Rankine machine's HTHEX, the designs of the Rankine turbine will need to embrace many of the innovations now being explored for the gas-turbine cycle turbines such as SiC, composite structure and film cooling.

In the low turbine pressure ratio design ($\pi_{turbine} = 2$), which conforms with the current turbine pressure ratio expected in the gas turbine engine, the mass flow rates in the Rankine power machine discussed in Chapter 2 have typical mass flow circulation rates of ~0.01 g/s. Unfortunately, the mass flow rates of current turbine designs are appropriate for steam mass flows rates of the order of 1 g/s under the assumed turbine inlet conditions. Designing smaller turbines to match the requirements of the Rankine device designs is likely to result in higher losses. In addition, smaller turbines must operate at still higher rotation rates possibly introducing further challenges in bearing designs.

Increasing the mass flow rate in the Rankine machines to match the turbines available will have its challenges. The mass flow rate of the combined Rankine machine working fluid is limited by the mass flow rate and temperature of the air entering the HTHEX. For example, in the bottoming Rankine power machine discussed in Chapter 2, the exhaust mass flow rate from the gas turbine engine assumed was 0.1 g/s and the exhaust temperature was 770 K. The mass flow rate in the matching Rankine (bottoming) cycle design is adjusted to provide the proper superheat temperature (in this work, 750 K) to the fluid entering the Rankine turbine. If the air mass flow rate is increased then larger mass flow rates in the Rankine cycle are possible. This could be done, for example, by

ganging several gas turbines with one Rankine machine. This will come at a cost of a larger high temperature heat exchanger to contend with the larger air and water/steam flows.

The low temperature side of the Rankine cycle also puts limitations on the mass flow rate. Larger steam mass flow rates result in larger heat fluxes though the low temperature heat exchanger. If the temperature drops across the heat exchanger are to be maintained at their original design levels, the area of the heat exchanger and the mass flow rate of the cooling air must be increased. If the low temperature heat exchanger area (and possibly its footprint) is not increased, the blower power requirements will outstrip the additional power produced by the turbine. It is likely that a successful bottoming Rankine cycle design will combine smaller turbine designs with larger heat exchanger designs.

**2. Blower**

In both the Rankine bottoming cycle machine and the waste heat cooler blowers are used to enhance heat transfer between the ambient air and the working fluid. The adoption of forced flow in these heat exchangers was driven by the need to minimize the footprint of these devices.

| | **Rankine power machine** | **Waste-heat-driven cooler** |
|---|---|---|
| **Air mass flow rate** | 3.15 g/s | 12 g/s |
| **Inlet Pressure** | 1 atm | 1 atm |
| **Pressure ratio** | 1.03 | 1.01 |
| **Pressure rise** | 2.93 kPa | 1.02 kPa |
| **Efficiency assumed** | 50% | 50% |
| **Typical** $\dot{W}_{blower}$ | 17 W | 20 W |
| **Type of heat exchanger** | Fin-type | Hole-type |

**Table 5.5—Requirements to the micro blowers in the Rankine-based machines**

The blower performance for the Max-Power Design Bottoming Cycle and the Design III Waste Heat Driven Cooler are shown in Table 5.5. The pressure ratios needed for the Max Power Design (1.03) and the Design III Waste Heat Driven Cooler (1.01) have already been exceeded experimentally by a micro-gas turbine compressor (1.2) [3]. (This micro gas turbine engine compressor's 100% design tip speed was 400 m/s, with a design pressure ratio of 2:1. At 42% design tip speed, the measured pressure ratio was 1.2.) The MIT micro engine project team has generated blower designs not specific to these Rankine-based machines. These machines have been discussed earlier and their predicted performance is summarized in Table 5.2. The design pressure ratios of these machines (1.06) compares well with the required pressure ratios for the Max Power Design (1.03) and the Design III Waste Heat Driven Cooler (1.01). However, the mass flow rates for these blowers (0.33 g/s) is substantially less than what is required in the Max Power Design (3.15 g/s) and the Design III Waste Heat Driven Cooler (0.85 g/s). Consequently, the current designs will need to be upgraded to allow for the larger mass flows required by the Rankine machines.

### 3. Compressor

Compressor is only needed in the Waste-Heat-Driven Cooler (heat pump). Table 5.6 lists selected design parameters for the compressor of the Waste-Heat-Driven Cooler (based on "Design III" in Chapter 4).

| | **Waste-heat-driven cooler** |
|---|---|
| **Air mass flow rate** | 0.026 g/s |
| **Pressure ratio** | 4.7 |
| **Pressure rise** | 2.4 MPa |
| **Efficiency assumed** | 50% |
| **Typical** $\dot{W}_{compressor}$ | 12.1 W |

**Table 5.6—Requirements to the micro compressor in the waste heat cooler**

Contrary to the requirements to the blower, mass flow rate of the vapor compression cycle is lower than the typical compressor design mass flow rate by the micro engine group (0.026 g/s vs. 0.11 g/s). The heat pump also requires a higher pressure rise (4.7 vs. 2). As a result, the compressor in the heat pump will need much more power input from the turbine than the blower (12.1W vs. 1.5W respectively). The high pressure ratio makes it likely that the compressor will be multi-stage (2-3 stages).

**4. Pump**

Micro feedpumps are used in both the Rankine power machine and the waste heat cooler, to increase the pressure of the liquid working fluid. It requires the same absolute value of pressure change and mass flow as turbine. Table 5.7 lists the characteristics required for pumps in the Max-Power Design and Design III in the Rankine power machine and the waste heat cooler.

The turbopump discussed earlier (Figure 5.4 and Table 5.3) has a design mass flow rate of 3.5 g/s versus ~ 0.01 g/s and ~0.2 g/s required for the bottoming devices discussed here. Experimentally, $H_2O$ was used for the demo pump with a mass flow rate of 0.15 g/s and measured to-date pressure rise is 0.68 atm, lower than the required pressure rise for the combined cycles. Therefore, a feedpump with higher pressure rise and wider range of mass flow rates needs to be designed to fit into the micro Rankine machines.

| | **Rankine power machine** | **Waste-heat-driven cooler** |
|---|---|---|
| **Working fluid mass flow** | 0.15 g/s | 0.21 g/s |
| **Pressure ratio** | 9.15 | 3.57 |
| **Pressure rise** | 3.56 MPa | 7.9 MPa |
| **Efficiency** | 50% | 50% |
| **Typical pump power** | 1.17 W | 6.14 W |

**Table 5.7—Cycle requirements to micro feedpump**

Comparing the above component parameters with those being built or designed, there is no perfect match available. Therefore, turbomachinery scaling is needed to adjust the component performances to fit the cycle designs. The adjustment could include inner/outer diameter, height of blades, and blade span, etc. to achieve the desired mass flow rate tolerance, pressure ratios and power. Whereas, for some of the components, such as the compressor, improved design has to be made in order to build a successful waste heat cooler.

### 5.1.3 Turbomachinery Scaling Issues

It is apparent from the previous discussions that combined cycles require turbomachinery that is substantially different from those found in the micro gas turbine engine. Presumably, the turbomachinery developed for the gas turbine engine can be scaled for the different fluid mass flow rates, pressure ratios and operating temperatures required by these combined cycles. This section explores how the dimension variations of micro-scale turbomachinery designs fit the micro-scale Rankine cycle and refrigeration cycle requirements. In the design and fabrication, there are many more complexities in turbomachinery than in heat exchangers, because static fluid channels of the heat exchangers have relatively simple structure and fluid dynamics: their performance can be improved by simply adjusting the dimensions and number of channels. Turbomachinery design is more difficult in that there are rotating parts in which fluid dynamics is complicated, and in addition, operating conditions, performance requirements and fabrication capability need to be strictly integrated.

In the micro scale, the ultimate achievable pressure ratio is restricted by component diameter (design requirement), blade height (etching techniques), and the number of stages (fabrication technologies). To avoid excessive complexity, it is desirable to minimize the number of stages in a pump, compressor or turbine. With this limitation then, the design process is limited to the diameter of the rotor and the size and the configuration of the blades.

For this sizing study, the turbine blade geometry is the baseline turbine design, shown in Figure 5.1 and Table 5.1. Candidate designs were evaluated using simulations. The code programmed by the MIT micro engine research group is used to estimate $\dot{m}$, $\dot{W}$ and turbomachinery efficiency for given design parameters (inlet temperature and pressure and outlet pressure). In the case of a micro-turbine design, the working fluid vapor is assumed to be an ideal gas. The procedure is:

1. Assume the turbine inlet temperature (superheat temperature of the working fluid). This parameter is obtained from basic assumptions of combined cycle and single cycle respectively. Gaseous working fluid's properties vary with different superheat temperatures, and thus the performance of turbines.
2. Assume a pressure ratio for the turbine and inlet pressure of working fluid (assumed in the cycle design).
3. Assume turbine dimensions (inlet and outlet diameters, blade height, blade span) and rotating speed of the turbine.
4. An estimation of mass flow rate through the turbine, turbine work output and stage efficiency can be derived using the programmed code.

Table 5.8 shows several results of several turbine designs and their performance. The temperature and pressure of the steam entering the turbine are assumed to be 900 K and 4 MPa. (This temperature is high for the bottoming cycle but might be realized in a combustor driven Rankine power cycle.)

| TURBINES FOR STEAM CYCLE | | | | | | | |
|---|---|---|---|---|---|---|---|
| Design | pressure ratio | mass-flow | efficiency | W out | RPM | R in | R out |
| 1 | 5.0 | 5.9 g/s | 40% | 1280 W | 1.2 M | 3000 um | 2000 um |
| 2 | 3.6 | 3.0 g/s | 51% | 730 W | 1.2 M | 3000 um | 2000 um |
| 3 | 3.5 | 0.28 g/s | 50% | 63 W | 7.2 M | 500 um | 200 um |
| 4 | 3.5 | 0.19 g/s | 53% | 46 W | 10.3 M | 350 um | 150 um |

**Table 5.8—Various turbine designs for the steam cycle**

**Turbine inlet temperature and pressure are assumed to be 900 K and 4 MPa respectively.**

The simulation suggests that turbine pressure ratios between 3.5 and 5 are achievable in the micro scale with turbine efficiencies from 40% to 50%. Mass flow rates as low as 0.19 g/s can be realized in a small (0.7 mm) diameter turbine spinning at 10.3 million rpm.

The first two entries of the table are for a turbine of the same geometry and operating at the same angular velocity. The mass flow rate through the turbine is strongly dependent on the pressure ratio imposed across the turbine. (A pressure ratio of 5 yields a mass flow rate of 5.9 g/s whereas a pressure ratio of 3.6 yields a mass flow rate of 3 g/s.)

The mass flow rate can be reduced, holding the pressure ratio constant, by reducing the size of turbine (i.e. flow path cross-sectional area "$A_c$"). This effect can be seen in the latter two entries of Table 5.8 where the diameter of the turbine is reduced from 1mm to 0.7 mm resulting in a mass flow reduction from 0.28 g/s to 0.19 g/s.

For other turbomachinery components, a similar process can be used to adapt current designs to the Rankine-cycle engine's requirements. For example, the blower needed for the Rankine bottoming cycle has a pressure ratio similar to the pressure ratio achieved in the micro-blower project (shown in Table 5.2) but requires a much higher mass flow rate (3.15 g/s vs. 0.33 g/s). Nevertheless, the sizing of the turbomachinery for the combined cycle remains one of the major challenges for realizing a working device.

## 5.2 Turbomachinery Arrangement Discussion

Arrangement of the turbomachinery depends on the number of components, their respective power requirements, their rotational speeds and fabrication capability considerations. Schematic layouts for the bottoming cycle and refrigeration cycle are shown in Chapter 2 (Figure 2.3 and 2.4) and Chapter 4 (Figure 4.5, 4.6) respectively. In the micro gas turbine engine, the compressor is physically built back-to-back with turbine so that both of them rotate at the same rotational speed. In the combined cycles, there will be one (a feedpump in the Rankine power machine) or two (a feedpump and a

compressor in the waste heat cooler) additional rotating components powered by a single turbine. Each of these devices needs a high-pressure-ratio turbine and a low-pressure-ratio blower with relatively high air mass flow rates. This adds complexity for the turbomachinery matching, if same rotating speed is desired. (Micro gearboxes to change rotational speeds would significantly add to the complexity of the device.) Besides, the turbine still needs to power the pump. Therefore, turbomachinery arrangement an issue will require much attention.

The MIT micro engine group has used two approaches to mechanically connect a turbine to a compressor and a pump impeller. In the turbopump project, the pump blades was placed on the same side of the rotor as the turbine blades (as shown in Figure 5.4). Whereas in the micro gas turbine engine, the compressor was placed back-to-back with the turbine. The former design requires a single-wafer rotor and the latter design requires 2 or 3 wafers. Consequently, in the bottoming Rankine power machine it is possible to arrange the turbine and the feedpump on the same side, and put the compressor back-to-back with the turbine and feedpump.

There are other possible options besides a direct mechanical connection between rotating components. For example, generator-motor sets can be used to electrically transfer power from one rotating component to another. The MIT micro engine group is studying and developing electromechanical energy conversion devices. The system consists of three primary components: an electromagnetic machine, its power electronics and its controller as shown in Figure 5.5. The system can convert mechanical energy to electrical energy and can convert electrical energy back to mechanical energy. To convert mechanical energy to electrical energy, the electromagnetic machine becomes a generator (in the direction from left to right as shown in the figure). To convert electrical energy to mechanical energy, the machine becomes a motor (in the direction from right to left as shown in the figure). If this electromechanical energy conversion system is used in the combined cycles, the turbine can power one of the rotating components by direct physical connection and the other/others by a two-way energy conversion process: mechanical-

electrical-mechanical. By adopting this energy conversion system, power distribution can be controlled to allow each component rotating at different speeds.

MIT micro engine group has built its first functional magnetic induction machine: a tethered motor. Figure 5.6 is a drawing of the motor design [2][19]. The motor has a 4-mm active outer diameter, a 2-mm active inner diameter, and a 25-μm rotor-stator gap.

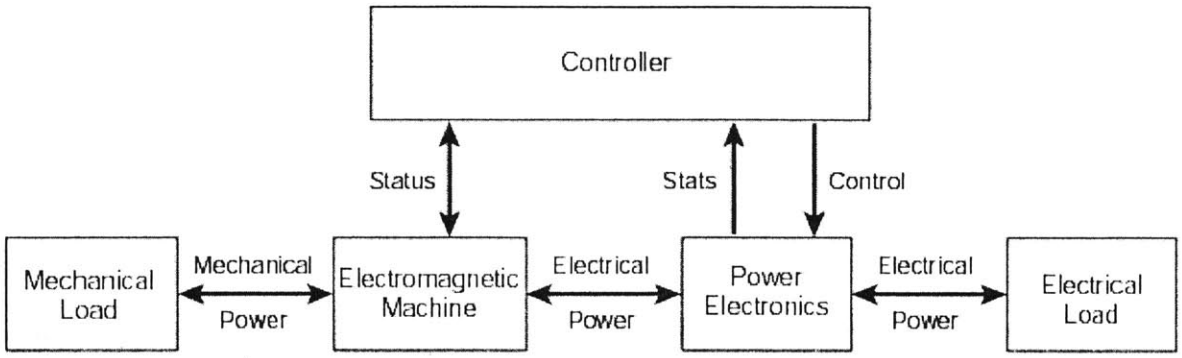


**Figure 5.5—Electromechanical energy conversion subsystem**

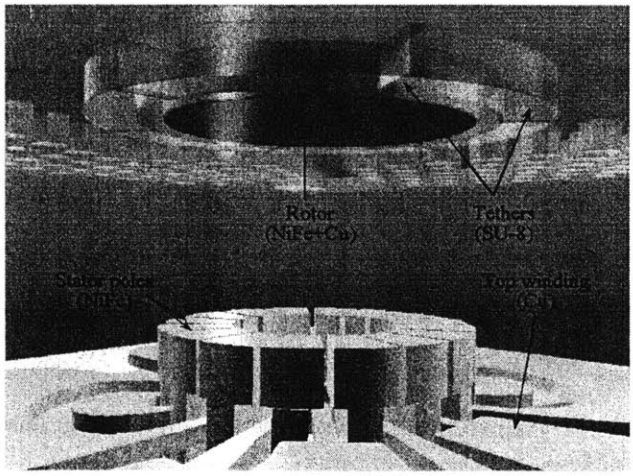


**Figure 5.6—Rotor design of the electromechanical energy conversion subsystem**

Unfortunately, the energy conversion efficiency for this magnetic induction machine is very low. The efficiency of this machine is predicted to be 50 % for each electro-mechanical conversion, which would mean that the overall conversion efficiency of a generator-motor set is 25 %. Hence, these devices can be considered for the micro combined cycles only if their energy conversion efficiency is significantly improved.

Another approach could be directly using the fixed magnets. The idea is to attach magnets directly onto the turbine and blower rotors in the areas facing each other. The magnet poles need to be arranged N-S-N-S alternatively on both components. The magnets act as a magnetic gear set. Once the turbine starts to rotate, the magnetic force pushes the blower to rotate too. The maximum torques that can be achieved and whether these torques are sufficient for this application remains to be determined.

Still another concept would be to use an induction type coupling between the turbine rotor and the blower rotor. A conductive coating could be placed on one rotor and the magnets arranged on the other. The motion of the magnets relative to the conductive coating would induce eddie currents in the conductive film. These currents interact with fields to induce a torque between the rotors. The specifics of this type of coupling scheme remain to be determined.

## 5.3 Concerns and Comments on Micro Turbomachinery

Improvements on turbomachinery are desired in order to realize both the combined and single micro Rankine cycles. First of all, turbomachinery designs with high pressure ratios are desired. The new designs could be of smaller diameter, with re-designed blade configurations and/or better fluid dynamics based on the improvement of MEMS fabrication technologies. Multi-stage turbines/compressors could also be considered to satisfy higher pressure ratio requirements. Secondly, higher turbomachinery efficiency is also desired, from which the performance of the cycles would be greatly improved (shown in Figure 4.12 for the waste-heat-driven cooler).

In the previous calculations, the rotating components were assumed as adiabatic, which means heat flow among turbomachinery components not being considered. In the micro gas turbine engine baseline design, the heat flow between gas turbine and compressor is about 50-60 W, which is counterproductive to the overall performance of the engine. Some approaches are being considered to reduce the heat transfer between turbine and compressor including spiral and hollow axis design, new blade design, etc. [2][19].

MEMS fabrication improvement is a key to the success of the micro engine components. Deep etching, bonding more wafers in a row, better surface roughness and future 3-D blade design could make the individual component, as well as cycle performance much better. At last, turbomachinery matching and arrangement are key issues for realizing the combined cycle based devices.

# Chapter 6 Summary and Future Work

The design and feasibility of adopting Ranking-cycle-based machines in the micro scale has been assessed on a theoretical level in this work. These machines can be combined with micro gas turbine engines to improve the overall energy performance by increasing the useful power output of the system and/or by adding additional functionalities (cooling, water production) to the system.

## *6.1 Micro Rankine-Based Bottoming Machine*

The concept of a Rankine bottoming power machine for micro gas turbine engine was discussed in Chapter 2. Theoretical design and analysis of the cycle operating parameters and heat exchangers were conducted by implementing general thermodynamics and heat transfer correlations as well as analytical methods. The model can be used to design both bottoming cycles and stand-alone Rankine cycles.

Initial calculations used water as the working fluid with a goal of an optimized design having a footprint of one inch by one inch. The analysis showed that the cycle's low temperature heat exchanger would require forced flow cooling to achieve acceptable performance. The result shows that this bottoming machine can be designed to generate as high as 41 W of useful power.

The use of water as working fluid requires large pressure ratios across the turbine and feed-water pump to achieve this performance (turbine pressure ratios of nine are assumed). To date, micro turbines of pressure ratios of two to three have been made. The Rankine cycle discussed above would probably require multi-stage turbomachinery.

If a micro Rankine machine is built with a single stage turbine with the currently available low pressure ratio (2 ~ 3), the temperature of the steam entering the turbine must be increased to achieve a net positive power output. Unfortunately, this temperature (900 K ~ 1000 K) is above the assumed micro gas turbine exhaust temperature (770 K). Consequently, such a Rankine device would have to be driven by a higher temperature air stream that could be provided by a combustor.

Current micro turbine is too large for the water mass flow rates found in the above Rankine cycle. The mass flow rates for the Rankine cycle are set by the size of the heat exchangers (the footprint of the device) and the latent heat of the working fluid. With a one-inch-by-one-inch footprint the water mass flow rate required is in the order of 0.01 g/s, which should be compared to the order of 1 g/s for the current gas turbine designs. In order to match current turbomachinery (pressure ratio of two and matched volumetric flow rate), the footprint of the device would have to be enlarged beyond $10^2$ $cm^2$.

The choice of another working fluid can result in a cycle that matches the heat exchanger footprint restriction to the currently available turbomachinery sizes. Several substances were considered. The criteria for choosing the appropriate working fluid included temperature, latent heat, heat capacity and the availability of thermal property data. A benzene-based Rankine cycle was chosen for further analysis resulting in a cycle that could provide 20 W useful power with a 4 cm x 6 cm footprint. The turbine for this cycle is comparable in size to the current turbines being used in the MIT micro engine project and has a pressure ratio of two which is achievable with current MIT micro turbine designs.

## *6.2 Micro Waste-Heat-Driven Cooler (Heat Pump)*

The concept of a micro Rankine-cycle-based heat pump combined with micro gas turbine engine was discussed in Chapter 4. This device could provide air-conditioning as well as condensed water under appropriate ambient conditions. Detailed design and analysis of the device were done based on general thermodynamics and heat transfer correlations.

In the calculation, ammonia was used as the working fluid and the device was designed to provide zero shaft power in addition to the cooling power for air-conditioning and water condensation. With a footprint of ~ 6 cm by 6 cm the cooling power is about 25 W (sum of power for air-conditioning and power for water condensation) while effective cooling power (for air conditioning) and water condensation rate vary depending on the ambient temperature and humidity. For example, at ambient temperature of 300 K and relative humidity of 90%, the effective cooling power is about 9 W and water production rate is 20 ml/hr when the machine is combined with a gas turbine engine generating air exhaust at a rate of 1 g/s at 760 K.

In this device, a new hole-type heat exchanger design was adopted, in which the channels are normal to the surface of the silicon wafers (parallel to stacking direction of the wafers). This design not only makes full use of the footprint area of the silicon wafer but also reduces the pressure drop by a factor of ten compared to the fin-type heat exchanger design. Albeit this heat pump still requires a blower to drive the ambient air into its heat exchanger channels.

This calculation assumed a universal turbomachinery efficiency of 50%. If the efficiency were to be improved from 50% to 100%, the cooling power could be improved by a factor of seven with the other parameters unchanged.

## 6.3 Micro Heat Exchangers

Micro heat exchanger designs for the Rankine-based devices were discussed in Chapter 3. The counter-flow type heat exchanger was chosen in the low temperature heat exchanger design (LTHEX) for the Rankine power machine in order to reduce the complexity of working fluid and cooling air's flow paths in the micro Rankine machines. The heat rejection heat exchanger (HRHEX) and the cold heat exchanger (CHEX) were cross-flow type because of this is determined by the low-pressure-drop hole-type heat exchanger design. The high temperature heat exchanger design (HTHEX) in both devices was counter-flow design because of its inherent high thermodynamic efficiency.

As mentioned above, there are two micro heat exchanger designs studied in this work—the fin-type heat exchanger and the hole-type heat exchanger. The fin-type micro heat exchanger design was used for the HTHEX in both the Rankine-engine and the waste heat cooler as well as the LTHEX in the Rankine engine. The HTHEX design is a two stack silicon wafer design; whereas, due to more demanding heat transfer requirements, the LTHEX is a three-stack design. In these heat exchangers, high aspect ratio (deep) channels are desired in that they incur less pressure drop throughout the flow path, which results in a reduction of the required blower power. Unfortunately, the ultimate channel aspect ratio is restricted by MEMS fabrication limitations.

The hole-type heat exchanger design was used in the HRHEX and the CHEX in the waste heat cooler. This new design renders a pressure drop of about one order of magnitude less than the traditional fin-type heat exchangers, within a similar footprint. Theoretically, the fabrication of this type of heat exchanger should be no more complicated than fin-type heat exchangers.

## 6.4 Turbomachinery

Current progress of micro turbomachinery developed by MIT micro engine research group was introduced and compared with the specific requirements by the Rankine engine and waste heat cooler in Chapter 5. Because of the nature of the different working fluids (air in the gas turbine engine and water/ammonia in the Rankine-cycle machines) and operating conditions (temperatures and pressures), there are few micro-gas-turbine-engine turbomachinery components that match the requirements for the Rankine devices (pressure ratio, pressure rise, mass flow rate, etc). There are two solutions to this problem: one is to redesign the turbomachinery and the other is to scale up or down those components that have already been manufactured and/or tested.

There are additional mechanical complexities associated with a blower that sits outside the working fluid loop. The Rankine-based prime mover discussed here requires more turbomachinery components (turbine, pump and blower) than the gas turbine engine (turbine and compressor). Designs that make the mechanical connections necessary to

connect the turbine, pump and blower in the Rankine engine are apparent. Using hybrid geometries that draw from the MIT micro turbopump and the micro gas turbine designs, the turbine and pump could be mounted on the one face of the rotor disk and the blower connection could be mounted on the other face of the rotor. In the waste heat cooler, the complexity increases still further because of the existence of an additional compressor. Much of the complexity of these Rankine cycle machines can be mitigated if the heat exchangers used natural convection instead of forced convection which will be discussed further in Section 6.5. There are also two other possible solutions by using an electro-magnetic connection: one is to adopt a generator-motor approach, i.e. converting mechanical energy to electrical energy and to mechanical energy again. The major hurdle of this approach would be its low energy conversion efficiency. Another approach is to imbed magnets into the turbomachinery components. The magnets in adjacent rotors would act as magnetic gears, locking the motion of those rotors together. Another possibility is to use magnets to inductively couple to a film on an adjacent rotor. The interactions of the magnets with the induced eddie currents in the film result in a torque between the two rotors. These latter two options have not yet been examined in detail.

## 6.5 Challenges and Future Work

The major hurdle to bring the micro combined cycles into reality is how to match turbomachinery to the cycle parameters and to each other. Therefore, new designs of turbines and compressors with higher pressure ratios, higher efficiencies while being able to sustain smaller mass flow rate are desired.

The second issue is that the heat transfer between the turbomachinery components was not taken into account in this work. There are several choices for the arrangement of the turbomachinery. Methods to reduce the heat transfer between the turbine and other components by redesigning and/or innovative arrangement need to be developed.

Improvement of MEMS fabrication techniques is key to most of the problems associated with the micro Rankine machines as well as micro gas turbine engines. Improved

methods for deep etching, bonding of more silicon wafers, and improved surface roughness of heat exchanger channels are all needed.

For the heat exchangers, the feasibility of the new hole-type design needs to be demonstrated. In order to ensure the working fluid to be in 100% liquid phase, sub-cooling might be desired in the LTHEX and HRHEX in the Rankine power machine and the micro heat pump respectively.

In the Rankine designs presented here, the blower consumes a major part of the turbine power (~40% for the single-Rankine machine and ~50% for the waste heat cooler). Since additional turbomachinery components unavoidably increase the complexity of the whole device, it is worth examining the possibilities of removing the blower:

(1) Natural convection:
Is it possible to adopt natural convection instead of forced convection as to avoid using the blower? A rough estimation of the device dimensions was conducted. Equation (6.1) shows the correlation of heat transfer rate $\dot{Q}$ vs. the cycle and the heat exchanger parameters [7]:

$$\dot{Q} = \overline{h}_c (T_h - T_c) \times A \tag{6.1}$$

where $\overline{h}_c$ is the average heat transfer coefficient and $T_h$ and $T_c$ are the temperatures of the cold and hot fluids. The channel configuration was determined by the criterion of Ra > 1000 (where natural convection occurs), and the calculation shows that in order to achieve the typical heat transfer rate of 400W for the Rankine-based engine, the LTHEX should be at least 25 cm by 25 cm.

(2) Another approach could be connecting the LTHEX cooling air outlet to the inlet of the micro gas turbine engine so that the gas-turbine compressor intakes the exhausted cooling air from the Rankine machine. The compressor of the gas turbine engine generates a large suction force to meet the requirement of the blower pressure ratio in the Rankine machine. Therefore, if the cooling air outlet is connected with the inlet of the

gas turbine engine, the blower could be removed. This will impose the pressure rise required to the blower onto the compressor. The ambient-air heat exchanger have pressure drops of ~3 kPa in the Rankine-based machine and ~1 kPa in the waste heat cooler and the blower power are both about 20 W. Although this is an additional burden to the gas turbine, the combined-cycle could still generate a similar amount of power. Also note that this approach requires the same or similar airflow rates of the gas turbine engine and ambient air going into the Rankine-based machine.

(3) All of the previous micro Rankine cycle designs are closed cycle. The third idea is to use a vessel containing the working fluid at high-pressure and in the liquid-phase. The working fluid is fed into the cycle through a control valve. Figure 6.1 shows the schematic diagram of this open-cycle machine. This design obviates the need for a blower, a LTHEX and a feedpump, improving the useful power output, reducing the system complexity, and possibly decreases the dimensions of the machine. The high constant pressure of working fluid could be achieved by using a piston separating a high-pressure gas (in a large volume) and the liquid to be pumped into the HTHEX. The gas acts as a gas spring that maintains a high pressure on the liquid as the liquid drains out of the volume into the HTHEX which is shown in Figure 6.1. The tradeoff of this approach would be that additional working fluid (and gas for pressure control) would have to be carried with the Rankine engine. For example, for a gas turbine engine supplying $\dot{m}_{hotair}$ = 0.1 g/s, the Rankine power machine needs about 0.01 g/s of water. The gas turbine engine fuel consumption is 16g/hr, and if we assume the machine is supposed to sustain 2 hours, the water needed to be carried is about 80 g, vs. the fuel about 32 g.

Finally, if a stand-alone (rather than a combined) micro power system is desired, an independent energy source should be considered. A micro combustor can provide heat source of much higher temperature than the combined cycle, which, thus could possibly improve the cycle performance. Although the improvement still depends on the performance of the turbomachinery, the Rankine-based engines are still less sensitive to the turbomachinery performance compared to the gas turbine engines.

In sum, the Rankine-based bottoming machine and the heat pump combined with the micro gas turbine engine will improve the overall cycle performance and provide additional functionalities. And these Rankine systems can also act as independent machines for power generation, refrigeration and water condensation.

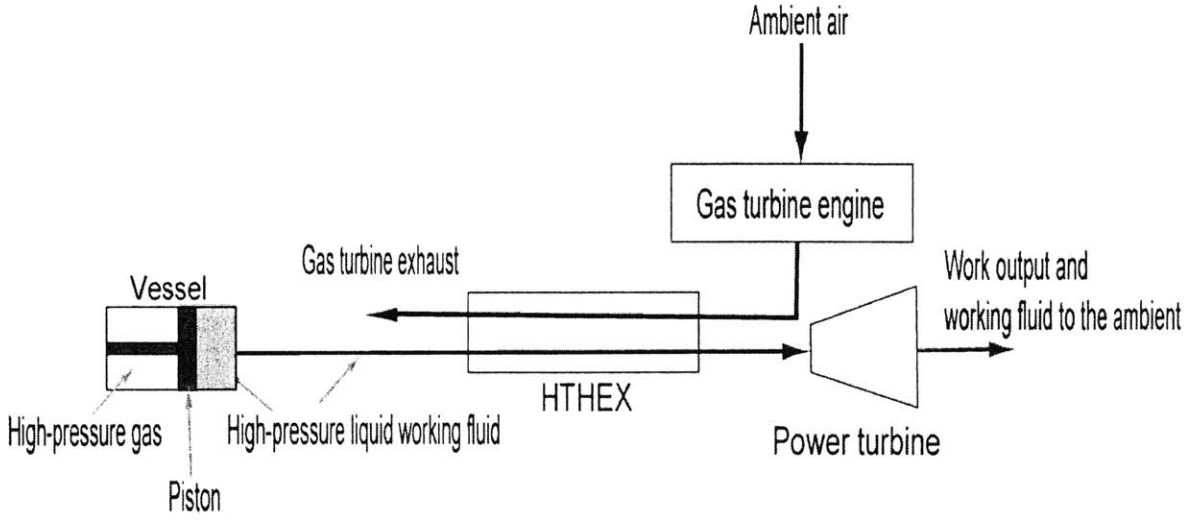


**Figure 6.1— A Schematic diagram of the open Rankine-based engine**

# Appendix I—Calculation Procedures of the Waste-Heat-Driven Cooler

Performances of the heat exchangers can be obtained from their inlet and outlet enthalpy [19]:

$$\dot{Q}_{HTHEX} = \dot{m}_{upperammonia} \times (h_4 - h_1) \quad \text{(A1.1)}$$

$$\dot{Q}_{HRHEX} = \dot{m}_{totalammonia} \times (h_6 - h_7) \quad \text{(A1.2)}$$

$$\dot{Q}_{CHEX} = \dot{m}_{lowerammonia} \times (h_9 - h_8) \quad \text{(A1.3)}$$

where $\dot{Q}$ [W] denotes the heat transfer rate of the heat exchangers; $\dot{m}_{upperammonia}$, $\dot{m}_{lowerammonia}$ and $\dot{m}_{totalammonia}$ [kg/s] are the ammonia mass flow rates in the Rankine cycle, vapor compression cycle and the whole cycle in Figure 4.14 respectively. $h_x$ represents the enthalpy in the corresponding states. $\dot{Q}_{CHEX}$ is also referred to as the refrigeration capacity.

Assuming no heat transfer to or from among the individual turbomachinery components, the mass and energy rate balances for control volumes give the power output/consumption of the turbomachinery:

$$\dot{W}_{turbine} = \dot{m}_{upperammonia} \times (h_4 - h_5) \quad \text{(A1.4)}$$

$$\dot{W}_{pump} = \dot{m}_{upperammonia} \times (h_1 - h_7) \quad \text{(A1.5)}$$

$$\dot{W}_{blower} = \dot{W}_{blower-upper} + \dot{W}_{blower-lower} \quad \text{(A1.6)}$$

where $$\dot{W}_{blower-upper} = \frac{\dot{m}_{coolingair} \times \Delta P_{coolingair}}{\eta_{blower}} \quad \text{(A1.7)}$$

and

$$\dot{W}_{blower-lower} = \frac{\dot{m}_{airlowercircle} \times \Delta P_{airlowercircle}}{\eta_{blower}} \quad \text{(A1.8)}$$

$$\dot{W}_{compressor} = \dot{m}_{lowerammonia} \times (h_{10} - h_9) \quad \text{(A1.9)}$$

$$\dot{W}_{net} = \dot{W}_{turbine} - \dot{W}_{pump} - \dot{W}_{blower} - \dot{W}_{compressor} \quad \text{(A1.10)}$$

where $\Delta P$ is the pressure drop of the ambient air along the channels in the corresponding heat exchangers:

$$\Delta P = \frac{1}{2}\frac{L}{D_{hole}} f \rho_{air} u^2 \quad \text{(A1.11)}$$

where $L$ is the length of the holes (air channels), $D_{hole}$ is the diameter (equals to hydraulic diameter) of the holes, $u$ represents the velocity of the fluid, and $f$ is a friction factor corresponding to the value of Reynolds number and geometry of fluid channels, which were defined in Equation (2.9) and (2.10). $u$ can be obtained from Equation (2.11). Therefore, the pressure drop along the heat exchanger air passages can be expressed as the following:

$$\Delta P_{air} = \frac{\mu L n \dot{m}_{air}}{2 D_{hole}^{\ 2} \rho A} \quad \text{(A1.12)}$$

Thus power consumption of the blower can be derived from (A1.6), (A1.7), (A1.8) and (A1.12).

Calculation process (Corresponding to the T-s diagram shown in Figure A1.1):

1. Assume the hot air mass flow, inlet and outlet temperature;
2. $\dot{Q}_{hot\ air} = C_{p\ hot\ air} \times \dot{m}_{hot\ air} \times (T_{inlet} - T_{outlet})$;
3. $\dot{Q}_{HTHEX} = \dot{Q}_{hot\ air}$;
4. Assume STATE 4: $T_{superheat\ ammonia}$ ($T_4$) and $P_{superheat\ ammonia}$ ($P_4$), $\rightarrow h_4$ and $s_4$;
5. Assume STATE 7: Saturated liquid: $T_7$, $\rightarrow P_7$, $h_7$ and $s_7$;
6. $P_{1R} = P_4$, $s_{1R} = s_7$, $\rightarrow h_{1R}$ and $T_{1R}$--STATE 1R;

7. Assume STATE 9: Saturated vapor: $T_9$ ($T_{low\ operation}$) =285 K, $\rightarrow P_9$, $h_9$, $s_9$;
8. $T_8=T_9$, $P_8=P_9$, $h_8=h_7$ (throttling process), $\rightarrow x=(h_8-h_{sat.\ liquid})/h_{sat.vapor}-h_{sat.liquid}$ (vapor%)–STATE 8;
9. Assume $\eta_{feedpump}$, $h_1=h_7+(h_{1R}-h_7)/\eta_{feedpump}$, $P_1=P_4$, $\rightarrow T_1$ –STATE 1;
10. $P_7=P_{10R}$ ($=P_{10}=P_5=P_6=P_{5R}$), $s_{10R}=s_9$, $\rightarrow h_{10R}$ and $T_{10R}$—STATE 10R;
11. Assume $\eta_{compressor}$, $h_{10}=h_9+(h_{10R}-h_9)/\eta_{compressor}$, $P_{10}=P_7$, $\rightarrow T_{10}$ –STATE 10;
12. $P_{5R}=P_7$, $s_{5R}=s_4$, $\rightarrow h_{5R}$ and $T_{5R}$--STATE 5R;
13. Assume $\eta_{turbine}$, $h_5=h_4-\eta_{turbine}\times(h_4-h_{5R})$, $P_5=P_7$, $\rightarrow T_5$ –STATE 5;
14. $\dot{m}_{upperammonia}=\dfrac{\dot{Q}_{HTHEX}}{(h_4-h_1)}$; (i.e. $\dot{m}_5$, $\dot{m}_{5R}$, $\dot{m}_1$, $\dot{m}_{1R}$, $\dot{m}_4$)
15. Assume $\dot{m}_{lowerammonia}$ ($\dot{m}_9$, $\dot{m}_{10}$, $\dot{m}_{10R}$, $\dot{m}_8$);
16. $\dot{W}_{compressor}=\dot{m}_{10}\times(h_{10}-h_9)$;
17. Design the LTHEX; calculate UA, $\varepsilon$, and $\dot{Q}_{LTHEX\ max}$.
18. The heat rejected by moist air can be separated to 4 parts: cooling dried air, cooling vapor to dew point, condensing vapor to water, cooling water from dew point to final state:
    a. $\dot{Q}_{LTHEX\ max}=\dot{m}_{dryair}\times Cp_{hotgas}(T_{LTHEXin}-T_{lowerammonia})+\dot{m}_{water}[(h_{vapor,in}-h_{vapor,dew})+h_{fg}+Cp_{water}(T_{dew}-T_{ammonia})]$

       where dew point temperature is obtained from $P_{vapor,\ in}$,
    b. $\dot{Q}_{LTHEX\ actual}=\dot{Q}_{LTHEX\ max}\times\varepsilon$;
    c. Find $\dot{m}_{moist\ air}$ from heat exchanger and cycle design;
    d. Assume an air outlet temperature, and use $\dot{Q}_{LTHEX\ actual}$ ($=\dot{Q}_{lowerammonia}$) to calculate the mass flow rates of air cooled and water condensed.
    e. Sum up the mass flow rates in (d) and get $\dot{m}_{moist\ air}$. Change the assumed air outlet temperature, to make $\dot{Q}_{LTHEX\ actual}$ in (d) equal to that in (b);
    f. Get $\omega_{out}$, $\rightarrow \dot{m}_{dry\ air}$ and $\dot{m}_{water}\rightarrow \dot{W}_{blower}$;
19. Change $\dot{m}_{lowerammonia}$, make $\dot{W}_{blower}+\dot{W}_{feedpump}+\dot{W}_{compressor}\leq\dot{W}_{turbine}$.

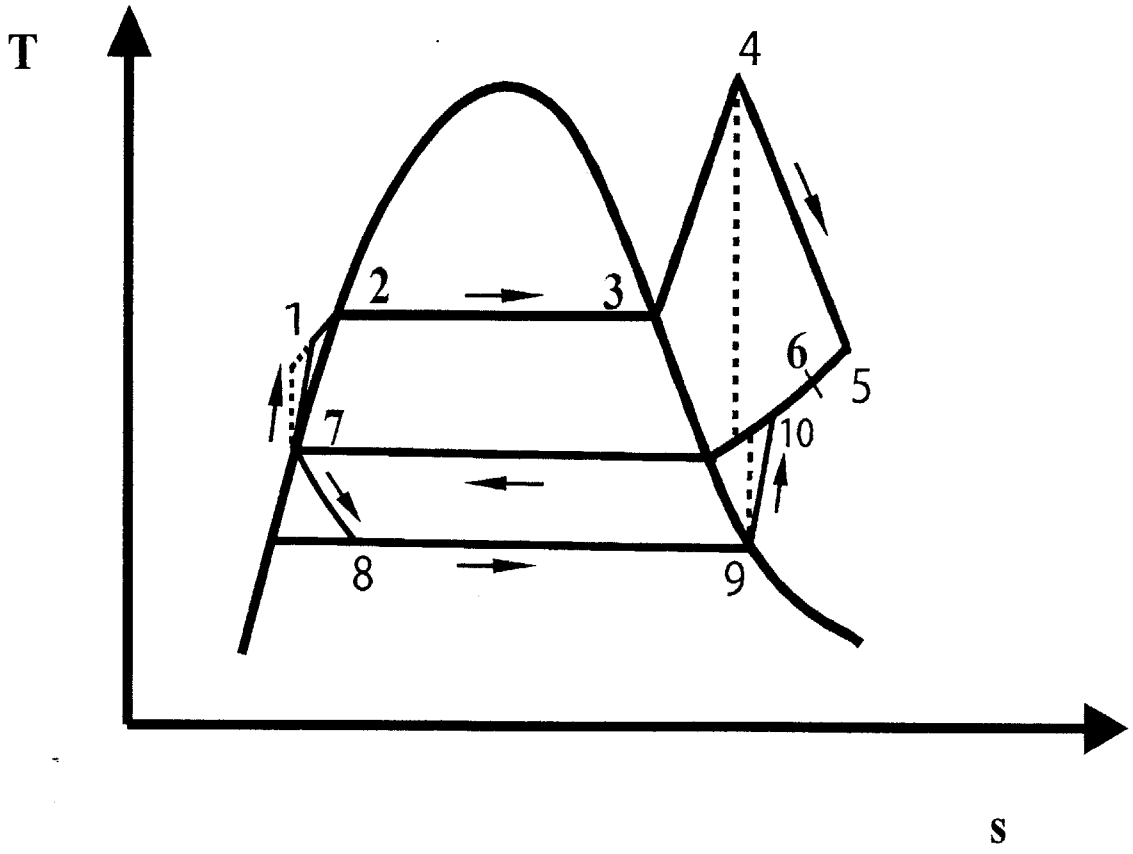


**Figure A.1.1— Combined waste heat cooler T-s diagram**

## References:

[1] Martin A. Schmidt, 2003, "Portable MEMS power sources", Digest of Technical Papers - IEEE International Solid-State Circuits Conference, Institute of Electrical and Electronics Engineers Inc.

[2] MIT Micro Engine Group, 2001, "The MIT Micro Engine Project Annual Technical Report" (distribution restricted to U.S. government agencies), Gas Turbine Lab, Department of Aeronautics and Astronautics, MIT, Cambridge, MA.

[3] Luc G. Fréchette, 2000, "Development of A Microfabricated Silicon Motor-Driven Compression System", Ph.D. thesis, Department of Aeronautics and Astronautics, MIT, Cambridge, MA.

[4] Shaun Sullivan, 2001, "Development and Testing of Microscale Silicon Heat Exchangers for the MIT Micro Gas-Turbine Engine", Master of Science thesis, Department of Mechanical Engineering, MIT, Cambridge, MA.

[5] N. Miki, X. Zhang, r. Khanna, A.A. Ayón, D. Ward, S.M. Spearing, 2003, "Multi-stack Silicon-direct Wafer Bonding for 3D MEMS Manufacturing", *Sensors and Actuators* A 103 194-201.

[6] Antoine Deux, 2001, "Design of a Silicon Microfabricated Rocket Engine Turbopump", Ph.D. thesis, Department of Aeronautics and Astronautics, MIT, Cambridge, MA.

[7] A. F. Mills, 1999, "Heat Transfer (Second Edition)", Prentice Hall, Upper Saddle River, NJ.

[8] P. X. Jiang, M. H. Fan, G. S. Si, Z. P. Ren, "Thermal-hydraulic Performance of Small Scale Micro-channel and Porous-media Heat-exchangers", *Int. Journal of Heat and Mass Transfer* 44 (2001) pp.1039-1051.

[9] Gh. M. Mala, D. Q. Li, "Flow Characteristics of Water In Microtubes", *Int. J. Heat Fluid Flow* 20 (1) (1999) pp.142-148

[10] David R. Lide, Henry V. Kehiaian "CRC Handbook of thermophysical and thermochemical data" 1994

[11] Frank P. Incropera, David P. DeWitt, 2002, "Fundamentals of Heat and Mass Transfer (Fifth Edition)", John Wiley & Sons, Inc., Appendix A.

[12] George M. Harpole and James E. Eninger, 1991, "Micro-channel Heat Exchanger Optimization", *Seventh IEEE Semi-Therm Symposium*, pp.59-63.

[13] Samalam, V. J., 1989, "Convective Heat Transfer in Microchannels", *Journal of Electronic Materials*, Vol. 18, No. 5, pp.611-618.

[14] Phillips, R. J., 1987, "Forced convection, liquid cooled microchannel heat sinks," Master's Thesis, Massachusetts Institute of Technology, Cambridge, MA.

[15] T. M. Harms, M. J. Kazmierczak, F. M. Gerner, "Developing Convective Heat Transfer In Deep Rectangular Microchannels", *Int. J. Heat Fluid Flow* 20 (1) (1999) pp.149-157.

[16] Online database of National Institute of Standards and Technology: webbook.nist.gov/chemistry/fluid/

[17] Michael J. Moran, "Fundamentals of Engineering Thermodynamics" 5th edition, New York John Wiley 2004

[18] Michael J. Moran, Howard N. Shapiro, 2000 "Fundamentals of Engineering Thermodynamics (fourth edition)", Wiley, NY

[19] MIT Micro Engine Group, 2000, "The MIT Micro Engine Project Annual Technical Report" (distribution restricted to U.S. government agencies), Gas Turbine Lab, Department of Aeronautics and Astronautics, MIT.